Liver cancer in a dish: modelling hepato-cellular carcinoma using patient-derived tumor organoids

Inauguraldissertation
zur
Erlangung der Würde eines Doktors der Philosophie
vorgelegt der
Philosophisch-Naturwissenschaftlichen Fakultät
der Universität Basel

von

Sandro Nuciforo
aus Basel, Basel-Stadt

Basel, 2019

Genehmigt von der Philosophisch-Naturwissenschaftlichen Fakultät
auf Antrag von

Prof. Dr. Markus H. Heim
Prof. Dr. Markus Affolter

Basel, den 11. Dezember 2018

Prof. Dr. Martin Spiess
Dekan

ACKNOWLEDGEMENTS

First, I would like to express my sincere gratitude to my advisor Prof. Dr. Markus Heim for giving me the opportunity to perform my PhD studies in his research lab. I would like to thank him for the great mentoring, all the advices and crucial scientific inputs that helped me to improve my scientific thinking.

Besides my advisor, I would like to thank the rest of my PhD thesis committee: Prof. Dr. Markus Affolter and Prof. Dr. Rolf Zeller, for their helpful comments and encouragement during our yearly meetings.

My sincere thanks go to Dr. Isabel Fofana for her support in the initiation of this project, her constant positive mindset, and the enthusiasm for scientific writing that helped me in the finalization of our manuscript and this thesis. I would also like to thank all other colleagues and friends of the lab, in particular Dr. Diego Calabrese for his immense help with all aspects of histology, all the discussions about science and life, and for the important instructions on how to “survive” a PhD. I will never forget. I appreciated the great scientific knowledge of Dr. Stefan Wieland and all his helpful insights. I truly valued our common passion for aviation. Special thanks to: Dr. Tanja Blumer for her long-lasting friendship, all the nice moments in the lab, and for always joining the weekly dodgeball class; Dr. Mairene Coto for the nice atmosphere in the lab and the never-ending jokes. Thanks to Sylvia Ketterer for her help and for keeping our lab in perfect condition at all times. Many thanks to Dr. Tujana Boldanova for her help with the clinical data; Xueya Wang for the immense support with the animal experiments; Qian Chen for sharing the ups and downs of HCC research; Aleksei Suslov for trying to convince me to go running; Alexandra Gnann for her support with organoid culture; Marie-Anne Meier for joining the organoid team; Dr. Daniela Di Blasi for the insights into immunology and our hiking attempts that never took place; and last but not least, Dr. François Duong, Ilona Krol and Dr. Benedetta Campana.

Further, I am very grateful for the collaboration with the Institute of Pathology. I highly enjoyed working with Prof. Dr. Luigi Terracciano and Dr. Matthias Matter. I had the great opportunity to learn a lot about the various fascinating aspects of liver pathology. Thanks to Petra Hirschmann for the immunohistochemical staining. I’m indebted

to Dr. Salvatore Piscuoglio and Dr. Charlotte Ng for their immense help with the genomic data analysis of our HCC organoids.

The establishment of organoid cultures in our lab would not have been possible without the help of Prof. Dr. Gerald Schwank and Femke Ringnalda.

During my PhD studies I also had the great opportunity to be a member of the steering committee of the PhD Club. I truly enjoyed all the meetings, scientific retreats, career days, BBQ events, dinners. Therefore, special thanks to all Club members, Nicole, Simon, Lukas, Sabine, Daria, Claudia, Milica, and Madeleine.

Finally, I want to express my gratitude to my parents and my sister for their outstanding support and for always encouraging me. And thank you, Josipa for your support, endless patience and everything else.

TABLE OF CONTENTS

1. SUMMARY

Hepatocellular carcinoma (HCC) is the most common primary liver cancer and the second most frequent cause of cancer-related mortality worldwide. HCC predominantly arises in cirrhotic livers as a consequence of underlying chronic diseases including viral hepatitis, alcoholic liver disease and non-alcoholic steatohepatitis. Treatment options for advanced HCC are limited. Sorafenib (Nexavar®) has been the only approved drug for the management of advanced HCC for the past ten years. Recently, additional multikinase inhibitors entered the clinic, however, without significantly improving overall survival as compared to sorafenib. Major advancements are expected to be achieved with the introduction of immune checkpoint inhibitors such as nivolumab (Opdivo®), but biomarkers to identify patients who may benefit from the treatment are currently missing. Moreover, several additional drugs have failed to meet clinical end points in large phase III trials, indicating a need for new drug discovery for HCC.

A major obstacle for the development of new therapies is the lack of suitable preclinical animal models or cell culture systems that allow a faithful translation of basic research findings into the clinical setting. This thesis describes the generation of organoids derived from needle biopsies of HCCs. The use of tumor biopsies instead of surgically resected HCC specimens is important because it allows to generate organoids from all tumor stages, whereas surgical resection of HCCs is limited to a minority of patients with small, early stage tumors. These tumors are typically not treated with systemic therapies, and material derived from them might have limited value for developing new treatments for advanced HCCs.

Because of the very limited amount of tissue that can be obtained with a needle biopsy, generation of HCC organoids was technically challenging. A key to our success was the immediate sample processing. The biobank of tumor organoids described in this study encompasses different etiologies and, most importantly, all clinical tumor stages. Our study design also allowed to compare the organoids with the originating tumor biopsies. We found that HCC organoids preserve the morphological characteristics and tumor marker expression of their originating tumors. Moreover, a comprehensive analysis of the genetic landscape in both, primary tumors and corresponding organoids, revealed a high concordance of the molecular alterations and the genetic heterogeneity, confirming that the organoids are a genuine representation of the originating tumors. In addition, tumor organoids can be successfully transplanted and propagated in immunodeficient mice to generate xenografts. Finally, in a proof of concept study, we show that tumor organoids can be used to test sensitivities to clinically-relevant drugs and provide a promising novel tool for developing tailored therapies.

2. ABBREVIATIONS

AASLD	American association for the study of liver diseases
ADH	alcohol dehydrogenase
AFB1	aflatoxin B1
AFP	alpha-fetoprotein
ALD	alcoholic liver disease
aSC	adult stem cell
BCLC	Barcelona clinic liver cancer
CCC	cholangiocellular carcinoma
CCF	cancer cell fraction
CCLE	cancer cell line encyclopedia
CHB	chronic hepatitis B
CHC	chronic hepatitis C
CLD	chronic liver disease
CRC	colorectal cancer
CT	computer tomography
DAA	direct-acting antivirals
DNA	deoxyribonucleic acid
DM	differentiation medium
EASL	European association for the study of the liver
ECM	extracellular matrix
EM	expansion medium
ESC	embryonic stem cell
EtOH	ethanol
FA	fatty acid
g	g-force
H&E	hematoxylin and eosin
HBV	hepatitis B virus
HCC	hepatocellular carcinoma
HCV	hepatitis C virus
HH	hereditary haemochromatosis
HLC	hepatocyte-like cell
IM	isolation medium
iPSC	induced pluripotent stem cell

kb	kilobase
MRI	magnetic resonance imaging
NAFLD	non-alcoholic fatty liver disease
NASH	non-alcoholic steatohepatitis
NGS	next generation sequencing
ORF	open reading frame
PBS	phosphate-buffered saline
PDO	patient-derived organoid
PDX	patient-derived xenograft
PLC	primary liver cancer
RFTA	radiofrequency thermal ablation
RNA	ribonucleic acid
RNA-seq	RNA sequencing
RT	room temperature
SIRT	selective internal radiation therapy
TACE	transcatheter arterial chemoembolization
TERT	telomerase reverse transcriptase
US	ultrasound
WES	whole exome sequencing

3. INTRODUCTION

3.1. The human liver

The liver is one of the largest and micro-anatomically most complex organs of the human body given its numerous functions required for maintaining whole-body homeostasis. Liver function can be summarized in five classes: (I) uptake of nutrients derived from the intestines, supplied by the portal vein; (II) metabolic biosynthesis, conversion, and degradation of endogenous compounds; (III) detoxification of exogenous compounds; (IV) supply of the body with essential metabolites and nutrients; and (V) excretion of compounds with the bile[1,2]. All these functions are carried out by the main cell type in the liver, the hepatocyte. An estimate of 2.4×10^{11} hepatocytes are present in the liver, accounting for ~80% of its total mass[3]. Cholangiocytes or bile duct cells build up the whole intra- and extrahepatic biliary tree and represent the second most frequent cell type in the liver, accounting for ~3% of the total cell number[4]. Bile produced by the hepatocytes is transported via the bile ducts to the gallbladder where it is stored until its controlled release during digestion[1]. Kupffer cells represent the macrophages of the liver and function as scavengers of foreign as well as endogenous material[4]. The hepatic stellate cells only account for ~1.4% of the total cell number in the liver but play a central role in the maintenance of the extracellular matrix (ECM) and the regenerative response upon liver injury (discussed below)[4].

The functional unit of the liver is the liver lobule[2,4]. The rough shape of a lobule is hexagonal with every corner harboring a portal triad, consisting of one hepatic artery, one portal vein, and one bile duct, respectively (Figure 1). The lobule is constituted of hepatocytes lined towards the center where a central vein is located. The hepatocytes within a lobule can be divided into three zones from the portal space towards the central space. Liver zonation is based on the spatial distribution of different metabolic enzymes along the three zones due to oxygen- and nutrient gradients from the periportal to the pericentral space[2,5] (Figure 1). Nutrient-rich blood from the intestine and oxygen-rich blood enter the liver through the portal vein and hepatic artery, respectively. From each portal triad, the blood flows through the hepatocyte plates in so-called sinusoids towards the central vein (Figure 1). During its flow, the blood comes in close contact with the hepatocytes thanks to the fenestrated endothelium of the sinusoids[4]. On the other hand, bile acids and salts are released into bile canaliculi — formed between adjacent hepatocytes — and flow in retrograde direction into

the bile duct of the portal triad for further transport into the gallbladder (Figure 1). The three-dimensional architecture of the liver lobule is central to liver function but also important for the regenerative responses followed by various hepatocyte insults.

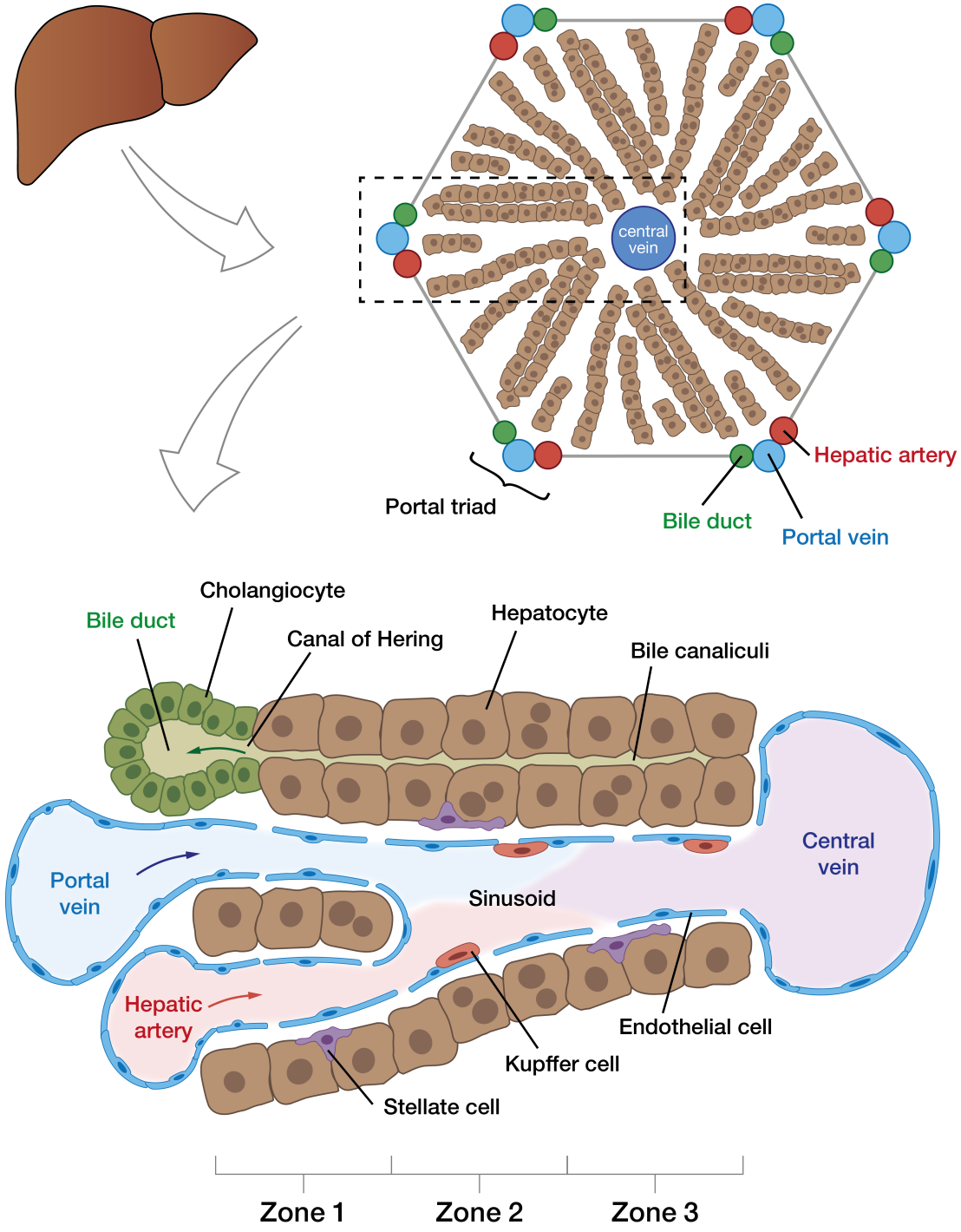

Figure 1. Architecture of the liver lobule and the basic organization of the periportal-to-pericentral axis. Nutrient-rich, mildly-oxygenated blood enters the liver through the portal vein and flows towards the central vein. Oxygen-rich blood enters the liver through the hepatic artery and flows in the same direction where it mixes with portal blood inside the sinusoids. Bile produced by the hepatocyte flows in the retrograde direction towards the bile duct. The portal vein contributes to 80% of the total blood flow entering the liver, the remaining 20% are supplied by the hepatic artery.

3.1.1. Liver development

Knowledge about the mechanisms underlying the development of an organ is fundamental for the understanding of its maintenance and regeneration in the adult stage. Like all the other organs of the digestive tract, the liver is formed from cells arising from the endodermal germ layer (Figure 2A)[6,7]. The definitive endoderm — initially a monolayer of cells at the ventral side of the developing embryo — forms a tube that is patterned into three different regions: foregut, midgut, and hindgut[2,8]. The foregut endoderm will later give rise to the liver, specifically to hepatocytes and cholangiocytes (Figure 2A)[8].

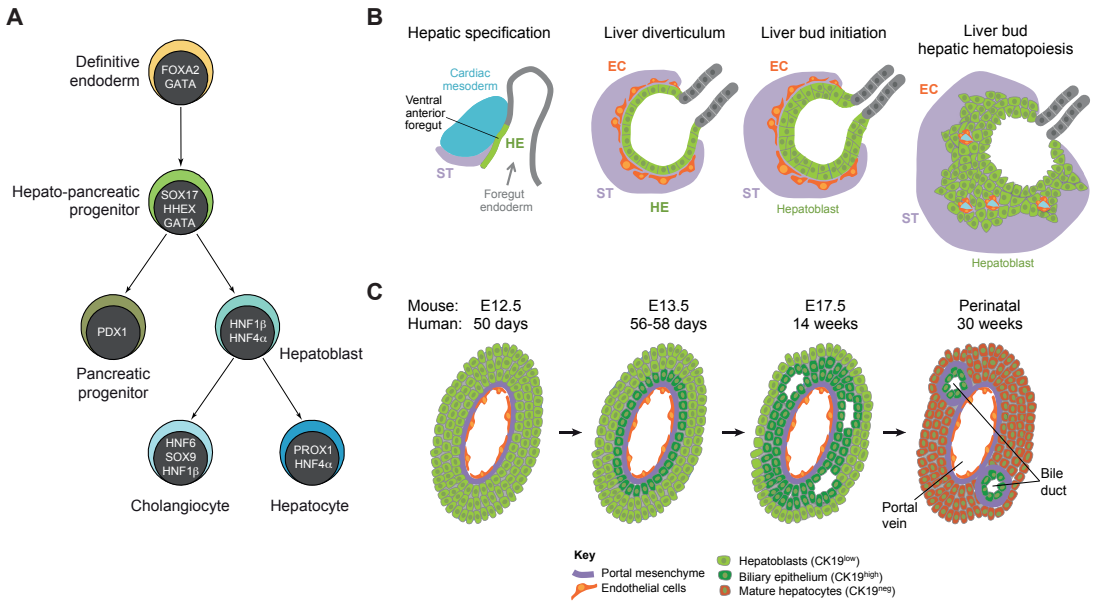

Figure 2. Schematic representation of fetal liver development. (**A**) Schematic lineage from definitive endoderm to hepatocytes and cholangiocytes. The factors indicated within the cells are needed for the transition in that specific developmental stage. (**B**) Liver diverticulum and bud formation. (**C**) Hepatoblast maturation into hepatocytes and cholangiocytes. Abbreviations: ST: septum transversum; EC: endothelial cell; HE: hepatic endoderm. Figure obtained and modified from Gordillo et al.[8]

Liver development is initiated with the formation of a diverticulum that is followed by the outgrowth of the liver bud (Figure 2B)[8,9]. These tissue remodeling steps are precisely coordinated by surrounding cells of the septum transversum and cardiac mesoderm that both provide the required morphogens such as Bone Morphogenetic Proteins (BMPs) and Fibroblast Growth Factor (FGF)[8,9]. The transition from diverticulum to liver bud consists in the differentiation of foregut endodermal cells into bipotent hepatoblasts, the progenitor cells of hepatocytes and cholangiocytes[8,9]. Hepatoblasts are marked by the expression of two specific hepatic transcription factors, Hepatocyte Nuclear Factor 1β and 4α (HNF1β and HNF4α, respectively), as well as Alpha-

Fetoprotein (AFP), the most abundant plasma protein in the fetus[8]. With continuing embryonic growth, the hepatoblasts increase in number and start to differentiate into hepatocytes, that will exclusively express HNF4α, and cholangiocytes, that will exclusively express HNF1β[8]. The generation of hepatocytes and cholangiocytes from hepatoblasts is spatially regulated by the portal mesenchyme (Figure 2C). Hepatoblasts that are close to the portal mesenchyme will differentiate into cholangiocytes, in particular under the influence of the NOTCH- and Transforming Growth Factor β (TGFβ) signaling pathways, while the hepatoblasts located further away will differentiate into hepatocytes[2,8,9].

3.1.2. Facultative stem cells and liver regeneration

The regenerating capability of the liver is by far its most intriguing feature that has fascinated researchers for decades. As for every other organ, the liver also needs to maintain and repair its tissue to endure for long time intervals. Under homeostatic conditions the proliferation rate of hepatocytes is very low and they usually persist for weeks to months without cell division[10]. However, upon tissue injury, e.g. due to toxins, viruses, or physical damage, the liver is able to initiate a potent proliferative program that replenishes the lost cell pool within a very short time frame. Since decades, partial hepatectomy — a procedure by which up to two thirds of the liver mass are surgically removed — has been the most widely used model to study liver regeneration[10]. This type of experiments, already performed in the rat model decades ago, highlight the massive regenerative potential because the missing liver mass is recovered within only a week after surgery[11].

The source of regenerating hepatocytes following liver injury is a controversial topic and not completely understood. Some organs, such as the small intestine, harbor a very well established and characterized stem cell niche[12]. The short-lived epithelium of the small intestine is constantly replenished by the rapidly proliferating stem cells residing in the crypts[13]. Regarding the liver, two main ideas dominate the field of liver regeneration: (i) the presence of facultative stem cells that repopulate the liver upon injury, and (ii) the proliferation of pre-existing hepatocytes re-entering the cell cycle. The truth lays in between. Depending on the type of injury, pre-existing hepatocytes are able to re-enter the cell cycle and rapidly replenish the missing cell pool[14-16]. This type of proliferative response is mostly observed in partial hepatectomy-based injury models. On the other hand, several groups reported the injury-mediated emergence of a facultative stem cell population that replenishes the organ[10]. These facultative

stem cells share some phenotypic characteristics of bile duct cells and were initially referred to as “oval cells” because of their atypical appearance compared to the actual ductal cells[10]. Oval cells were described to appear following toxin-mediated liver injury and to reside at the interface between hepatocytes and cholangiocytes within the *Canal of Hering*[10,17] (Figure 1). They display bipotential progenitor features because of their ability to differentiate into hepatocytes as well as cholangiocytes, analogous to hepatoblasts during embryonic liver development[14]. Recently, increasing number of research groups refined the definition of oval cells or proposed new concepts of liver regeneration: generation of hepatocytes from $SOX9^+$ bile duct cells[18], later refuted by another study[19]; generation of hepatocytes from bile duct-derived “buds” in cirrhotic livers[20]; proliferative ducts derived from dedifferentiated chronically-injured hepatocytes[21]; bipotent progenitors of biliary origin that repopulate hepatocytes and cholangiocyte pools[22]; hybrid hepatocytes with ductal features[23]; and direct lineage conversion of bile duct cells into hepatocytes[24]. The above-mentioned studies all share one characteristic: the facultative stem cell pool resides at the periportal side of the liver lobule (i.e. adjacent to the portal triad). Facultative because all the described putative stem cells only appear after injury. Only one study so far described a putative liver stem cell population residing at the pericentral (i.e. adjacent to the central vein) side[25], however, the stem cell features attributed to these cells are most probably shared by all hepatocytes independently of their zonal position within the liver lobule[15].

In conclusion, liver regeneration is a very robust process and includes different programs of cell cycle reactivation. Whether this is occurring in terminally differentiated hepatocytes or bipotent progenitors may depend on the type of injury and/or the insulted cell type.

3.2. Hepatocellular carcinoma

Cancer is a major global health burden and a leading cause of death worldwide. In 2016, 8.9 million people died of cancer worldwide, with primary liver cancer (PLC) representing the fourth most common cause of cancer-related deaths[26]. Of all PLCs, hepatocellular carcinoma (HCC) accounts for about 75%–85% of the cases, whereas 10%–15% are intrahepatic cholangiocellular carcinomas (CCC)[27]. Each year about 1’000’000 people are diagnosed with HCC and about 830’000 people die as a consequence[26]. The incidence increases with age, reaching a peak at 70 years[28]. Moreover, the prevalence is four times higher in men compared to women[26]. In the past

25 years, the incidence of HCC doubled and was paralleled by increasing mortality rates[26,29]. A recent projection of the worldwide HCC incidence rate until 2030 using age-period-cohort models, revealed that the overall incidence is predicted to rise in both sexes, however, geographical exceptions are expected[27]. For Asian countries like China, Japan and Singapore — currently accounting for over 50% of HCC cases worldwide — the incidence rates are predicted to decline due to better control of the related underlying risk factors, mostly hepatitis B and C virus infections[27]. On the other side, HCCs associated with obesity and its metabolic complications are predicted to increase, in particular in the United States and western European countries[27]. A better understanding of the factors and pathogenic mechanisms contributing to HCC development is therefore of crucial importance for improving disease control rates and reducing the growing incidence and mortality rates.

3.2.1. Etiologies and risk factors

Chronic liver disease (CLD) is closely associated with the development of HCC. About 90% of HCCs occur in the background of CLD[30]. The risk factors leading to CLD, and consequently the same responsible for HCC development, are well defined: hepatitis B virus (HBV) infection, hepatitis C virus (HCV) infection, alcoholic liver disease (ALD), non-alcoholic fatty liver disease (NAFLD), exposure to aflatoxin B1 (AFB1) and to a minor extent genetic disorders such as Morbus Wilson and hereditary haemochromatosis[31].

Geographic area	AAIR	Risk factors		Alcohol	Others
	M/F	HCV (%)	HBV (%)	(%)	(%)
Europe	6.7/2.3	60-70	10-15	20	10
Southern	10.5/3.3				
Northern	4.1/1.8				
North America	6.8/2.3	50-60	20	20	10 (NASH)
Asia and Africa		20	70	10	10 (Aflatoxin)
Asia	21.6/8.2				
China	23/9.6				
Japan	20.5/7.8	70	10-20	10	10
Africa	1.6/5.3				
WORLD	16/6	31	54	15	

Table 1. Geographical distribution of the main risk factors of HCC. AAIR: Age-adjusted incidence rate. Table obtained from the EASL-EORTC clinical practice guidelines[30].

Most of these risk factors lead to liver cirrhosis, present in 90% of all HCCs[32]. Worldwide, the incidence of HCC is heterogeneous because of the geographical variation in the prevalence of the various risk factors (Table 1; Figure 3). Most of the HCC cases occur in eastern Asia and sub-Saharan Africa, where HBV infection and afla-

toxin B1 represent the major risk factors. In contrast, the main cause of HCC in Western Europe and the United States is attributed to HCV infection and alcohol abuse[30,33] (Table 1). In developed countries, NAFLD and its more advanced and severe form NASH (non-alcoholic steatohepatitis) are emerging causes of HCC commonly associated with the metabolic syndrome in obese and/or diabetic individuals[33,34].

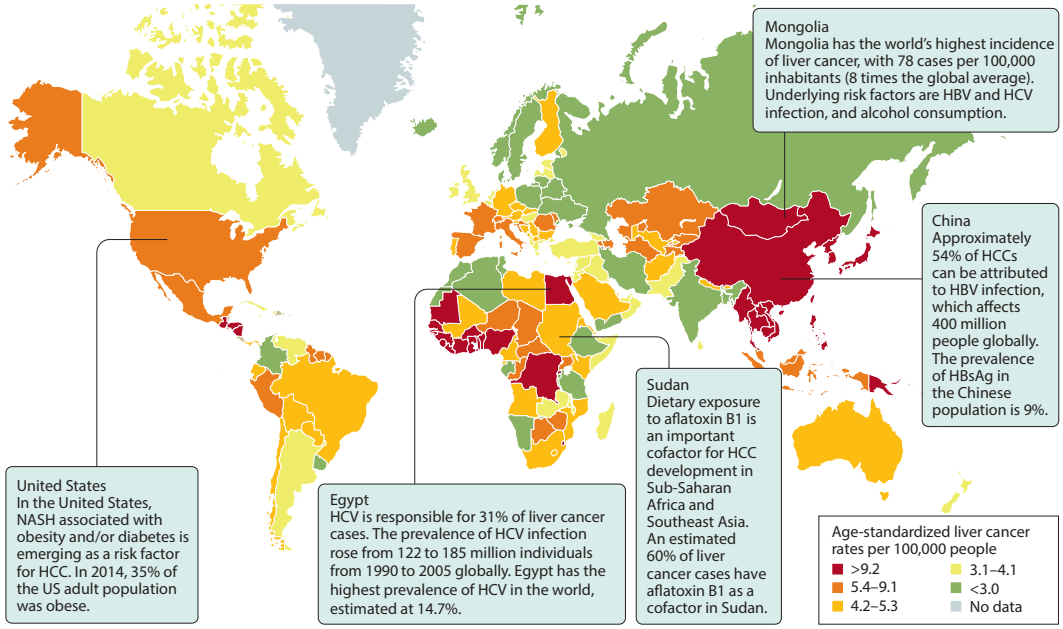

Figure 3. Age-standardized global incidence of HCC. Figure obtained from Llovet et al.[33]

Hepatitis B virus. Chronic hepatitis B (CHB) infection, occurring in 5-10% of infected individuals, is the major risk factor for the development of HCC, accounting for 54% of all cases worldwide[30]. The highest prevalence of CHB can be found in Asian and sub-Saharan countries[33,35] (Figure 3), although the incidence is decreasing due to improved socioeconomic status and the implementation of broad vaccination programs[36].

HBV belongs to the Hepadnaviridae family of DNA viruses and harbors a partially double-stranded circular genome with a total size of 3.2 kb[37]. Upon hepatocyte entry through the Sodium Taurocholate Cotransporting Polypeptide (NTCP) receptor, the viral genome is converted to covalently closed circular DNA (cccDNA) that serves as template for the transcription of viral RNA from its four open reading frames (ORF)[37,38]. The virus replicates itself through a pre-genomic RNA intermediate. The four proteins encoded by HBV are the surface envelope protein S (HBs); the core protein C (HBc, forming the viral capsid); the viral polymerase P; and the X protein

(HBx)[37,38]. The latter was shown to alter several of the host's cellular processes, but the exact function and its presumed direct carcinogenic properties have been a matter of debate for years[39].

The molecular pathogenesis underlying HBV-associated HCC development can be divided into direct and indirect mechanisms. Direct carcinogenesis can be a result of insertional mutagenesis and/or the alteration of cellular pathways by HBV-encoded proteins. Because of its DNA nature, HBV can integrate into the host genome and potentially alter (cancer) gene expression[40,41]. The fact that HBV integration events were initially detected in HCC tissues of HBV-infected patients and HCC cancer cell lines lead to the initial hypothesis that virus integration was the cause of HCC tumorigenesis[42-45]. However, whole genome sequencing of HCCs from HBV-positive patients revealed a random HBV integration pattern at many different sites in the genome with only a few recurrent hotspots[46]. This notion, therefore, does not fully support a classic *cis*-acting insertional mutagenic mechanism as the main driving event of HCC[47,48]. On the other hand, viral proteins — expressed from integrated or non-integrated HBV — were shown to contribute to HCC carcinogenesis by directly affecting oncogenic pathways in the host cell[41,49]. The most acclaimed one, HBx, has been shown to alter gene expression, increase proliferation and prevent apoptosis, however, direct evidence from human tissue samples is missing since most of these observations were made in cell culture and/or animal models[39,41,49].

Indirect mechanisms of HBV-induced HCC pathogenesis are generally immune mediated. The immune response to HBV-infected cells results in hepatocyte death and inflammation of the surrounding tissue[38,49]. Thus, chronicity of hepatitis B, leads to persistent inflammation that combined with increased hepatocyte proliferation can contribute to cirrhosis and accumulation of oncogenic mutations ultimately leading to HCC[49,50].

Hepatitis C virus. HCV is the second most frequent risk factor of HCC, accounting for 31% of all cases[30]. Chronic hepatitis C (CHC) infection is the leading cause of HCC development in Japan, Western Europe and North America[30]. The recent introduction of highly effective direct-acting antivirals (DAA) markedly improved HCV treatment outcome which may, in principle, result in complete eradication of the disease[51-53].

HCV belongs to the Flaviviridae family of RNA viruses and harbors a 9.6 kb long, positive sense, single-stranded genome encoding a large polyprotein from one single

ORF[52]. The ORF is flanked by untranslated regions on both ends, which function as regulatory units for the synthesis of viral RNA and proteins. The polyprotein is co- and post translationally modified by host cellular and viral proteases to yield structural proteins such as viral capsid and envelope, and non-structural proteins such as viral proteases and RNA polymerase[52].

The pathogenesis of HCCs associated with HCV is also based on direct and indirect mechanisms. Compared to HBV and its progression to CHB, HCV results in chronic infection in a much larger proportion of infected individuals, with 60%–80% of all patients developing chronic disease[38].

Direct carcinogenic mechanisms are mainly a result of altered cellular processes, such as activation of oncogenic signaling pathways, interaction with tumor suppressors like TP53 and/or RB, interference with the DNA damage repair machinery, induction of oxidative stress and inhibition of apoptosis[49].

As for CHB, indirect mechanisms of CHC-associated HCC carcinogenesis are mediated by the host immune system[49]. The immune response to chronic infection leads to liver inflammation and, as a result, increased hepatocyte proliferation that elevates the risk to accumulate oncogenic mutations eventually leading to HCC development[49,50].

Alcoholic liver disease. Heavy use of alcohol for prolonged time is a frequent risk factor for HCC development[28,33]. Depending on the geographic area, 10%–20% of HCCs can be attributed to alcohol abuse and its consequences[30]. Daily alcohol consumption in the range of 40–80 g ethanol (EtOH) intake is a strong predictor of ALD, however, only 35% of heavy drinkers will eventually display a severe disease course that includes hepatitis, fibrosis and cirrhosis[54,55].

The expression of enzymes involved in EtOH detoxification, most importantly Alcohol Dehydrogenase (ADH) and Cytochrome P450 2E1 (CYP2E1), are highest in hepatocytes[54]. EtOH breakdown generates byproducts that deregulate the intracellular redox potential and favors the generation of fatty acids (FA)[54,56]. Increased amounts of FA are deposited as triglycerides within lipid droplets and contribute to the progression to alcoholic steatosis[54,56]. The further pathogenic mechanisms leading to progression from alcoholic steatosis towards hepatitis, fibrosis, cirrhosis and eventually HCC, are associated with immune cell-mediated liver inflammation[50,54,56]. As in the case of chronic viral hepatitis, the permanently inflamed tissue results in an environment that favors carcinogenesis[50].

Non-alcoholic fatty liver disease and non-alcoholic steatohepatitis. Several large-scale cohort studies showed that the risk to develop cancer, including HCC, is higher in overweight/obese individuals[57]. NAFLD is an emerging cause of HCC development related to obesity, diabetes and the metabolic syndrome. The disease presents as non-physiological, increased fat accumulation in the hepatocytes that, in a subset of the cases, can progress to a hepatitis and cause NASH[34,57]. In a recent European study, nearly all (= 94%) obese patients were found to have NAFLD, and about 25% had NASH[57]. Moreover, because of the rising prevalence of obese individuals, NAFLD is close to become the main risk factor for HCC development in the United States and Europe, offsetting the reduction of CHC-related HCC mortality reached with year-long global public health programs[34,57,58].

NAFLD-associated HCCs might be the exception of the general rule that HCC is generally associated with advanced fibrosis or cirrhosis[57]. Indeed, different groups reported that up to ~50% of patients with NAFLD or NASH did not have a background of cirrhosis[34,59,60]. The pathophysiology of the progression from NAFLD to NASH, cirrhosis and eventually HCC is a result of tissue inflammation and oxidative stress mediated by lipid accumulation[34,57]. For NAFLD patients that progress to HCC without cirrhosis development, the pathophysiologic mechanisms are less clear but likewise involve insulin resistance associated with oxidative stress and inflammation of the liver parenchyma[34,57,61].

Aflatoxin B1. AFB1 is a toxin produced mainly by two fungal species, *Aspergillus flavus* and *Aspergillus parasiticus*[62]. Unproperly stored food may cause fungal growth and contamination by their toxins. Most HCC cases associated with AFB1 can be found in sub-Saharan Africa and southeast Asia, because of the local climatic conditions that favor the growth of fungal species[63]. In Africa, particularly in Sudan, AFB1 is a frequent cofactor in HBV-induced HCCs[33,63,64].

The pathogenicity of AFB1-induced carcinogenesis can be explained by the toxin's ability to produce DNA adducts and therefore induce DNA damage, strand break and ultimately mutations[63]. Moreover, the specific liver toxicity is due to the biotransformation and conversion of AFB1 to a reactive compound by Cytochrome P450, which is highly expressed in hepatocytes[63]. The most common mutation associated with AFB1 intoxication is the R249S substitution in the *TP53* gene[63].

Inherited diseases. Together with extrinsic (HBV, HCV, EtOH, AFB1) and intrinsic (e.g. lipids in NAFLD and NASH) etiological agents, inherited disorders that cause liver fibrosis, cirrhosis or inflammation can also potentially lead to the development of HCC.

Hereditary haemochromatosis (HH), an autosomal recessive condition that results in iron overload within hepatocytes, increases the risk to develop HCC[65,66]. The increased amount of intracellular iron favors the formation of free radicals and oxidative stress that consequently damage the tissue and lead to inflammation that does not necessarily culminate in the development of fibrosis or cirrhosis[65,66].

Morbus Wilson is an autosomal recessive disease that manifests with hepatic and neurologic symptoms due to excessive copper depositions in liver and brain of affected individuals, as a result of abnormal copper metabolism in hepatocytes[67]. The association between Morbus Wilson and HCC is not very firm because of the very low number of cases[66,68]. The mechanisms leading to HCC development in patients with Morbus Wilson can be attributed to persistent liver damage as a consequence of copper overload within the hepatocytes and the associated cycles of regeneration that may lead to fibrosis and cirrhosis in the long-term[66,68]. As a summary, these and other rarely occurring hereditary disorders account for less than 10% of all HCC cases worldwide[30,33].

3.2.2. The conceptual framework of HCC pathogenesis

The etiological factors described above share common ground on how they contribute to the progression from a diseased liver to HCC development. As outlined before, most of the HCCs occur on the setting of chronic liver disease, that can develop because of different agents such as viruses, toxins, ethanol or hereditary diseases. In the majority of cases, the risk factors culminate in the development of cirrhosis, a process taking several years to decades, explaining why HCC typically occurs in older patients[50]. The pathophysiology of HCC can be summarized in a conceptual framework involving the progressive gain of cancer hallmarks[69]. The progression from a healthy liver to HCC starts with hepatocyte injury by the etiological agent followed by hepatocyte death and regeneration[33,50] (Figure 4). Sustained hepatocyte injury due to chronic liver disease and persistence of the etiological factors results in repetitive cycles of hepatocellular necrosis and compensatory proliferation[33,50]. This process is accompanied by an increment of tissue inflammation mediated by the innate and adaptive immune system[33,50]. Year-long liver damage reduces the hepato-

cyte's regenerative potential and leads to tissue scarring through excessive collagen deposition, eventually resulting in the progression from fibrotic scars to complete cirrhosis[33,50]. Throughout this process, somatic mutations and epigenetic modifications in driver and passenger genes are acquired and selected, resulting in a stepwise sequence from initially low-grade dysplastic nodules to high-grade dysplastic nodules and ultimately HCC[33,50].

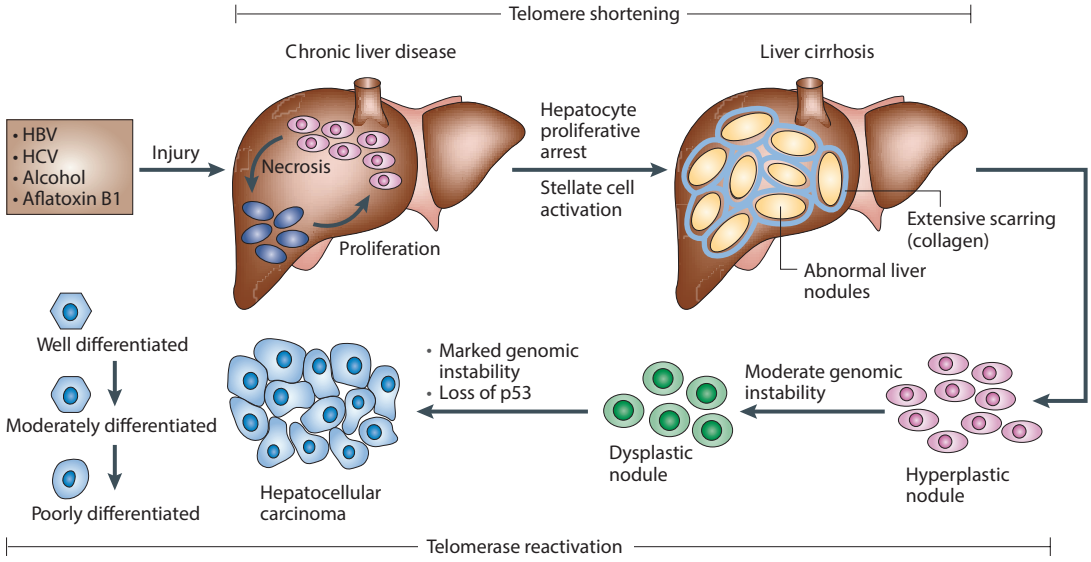

Figure 4. Pathogenesis of HCC development. Despite different insults such as viruses or toxins, the pathophysiology of HCC is comparably similar. Chronic hepatocyte damage results in compensatory proliferation and tissue scarring followed by genetic and epigenetic alterations that induce cancer formation. Figure obtained from Farazi et al.[50]

3.2.3. Prevention – Diagnosis – Treatment

In the past years most of the progress in the HCC field was made in its prevention, diagnosis and treatment. The following sections recapitulate the most important aspects.

Prevention. HCC belongs to those cancers for which prevention is possible. As previously described, patients with CLD display high risks to develop HCC, and therefore, controlling the progress to CLD could prevent HCC tumorigenesis[28]. The best example is the vaccination program against HBV that reduced the incidence of HCC in countries with high prevalence of HBV-infected individuals[33,70]. Furthermore, interferon- and/or DAA-based therapies against HCV infection can lead to the cure of CHC, however, when patients already progressed to cirrhosis before virus eradication, the risk to develop HCC remains[70,71]. Finally, promoting a healthy lifestyle and a

moderate alcohol intake, can contribute to reduce the risk to develop diabetes, NAFLD and ALD respectively[72].

Surveillance and diagnosis. Beside the prevention of HCC, by avoiding the risk factors, or by early treatment of the underlying liver diseases, surveillance of patients affected by CLD plays an equal central role in reducing HCC-related morbidity. HCC typically causes symptoms only in patients with advanced disease. At this progressed stage, patients usually can't undergo curative treatments anymore. However, because HCCs have relatively long sub-clinical incubation periods, patients with known CLD can be included in surveillance programs that aim at detecting HCCs at early-stage. In general, both the American- and European Associations for the Study of the Liver (AASLD and EASL, respectively) recommend the surveillance of patients with cirrhosis, owing to any cause, because previous studies clearly demonstrated improved survival rates[73,74]. Both associations also recommend the surveillance in patients with HBV or HCV infections associated with advanced fibrosis or cirrhosis, or in a subset of HBV patients without cirrhosis but with specific ethnical characterstics[73,74]. Currently, patients with ALD or NAFLD/NASH are included in surveillance programs only in cases with associated cirrhosis[73,74]. Generally, surveillance consists of ultra-sound (US) alone or in combination with serum AFP measurements, a common biomarker of HCC, whose expression normally restricts to the fetal developmental stage[73,74].

Once a nodule is detected in the liver of a patient with CLD by US modality, two main diagnostic procedures can be used to confirm the finding, (i) non-invasive radiological imaging, such as contrast-enhanced computer tomography (CT) or magnetic resonance imaging (MRI) — with or without complementary AFP measurements — and (ii) tissue biopsy collection.

Radiological diagnosis can be of high specificity and sensitivity in patients with cirrhosis[73,74]. This is due to the dual blood supply of the liver and the particular vascular profile of HCCs. The majority of the blood in the liver enters through the portal vein, that carries nutrient-rich and oxygen-poor blood, while the remaining minority is supplied by the hepatic artery that provides oxygen-rich blood[75]. HCCs are predominantly vascularized through neoangiogenesis from the hepatic artery because of the high oxygen demand by tumor cells[75]. This feature can be used to specifically recognize an HCC nodule due to its dense contrast enhancement in the arterial phase, i.e. indi-

cating arterial blood supply, followed by a decreased signal in the portal venous phase[75]. However, not every HCC nodule can be diagnosed with this procedure. In such cases, especially in non-cirrhotic patients, tumor biopsies represent the diagnostic standard[33,70]. Histological diagnosis requires examination by experienced pathologists, particularly for early-stage HCCs that usually don't present many visible tumorigenic abnormalities. Nevertheless, the use of specific markers (see below) and the comparison of tumor biopsies with those of adjacent non-tumor liver tissue can increase the specificity and ensure a precise diagnosis[76].

Treatment. After confirmed diagnosis of a HCC, the tumor is staged according to the Barcelona Clinic Liver Cancer (BCLC) classification[77] (Figure 5).

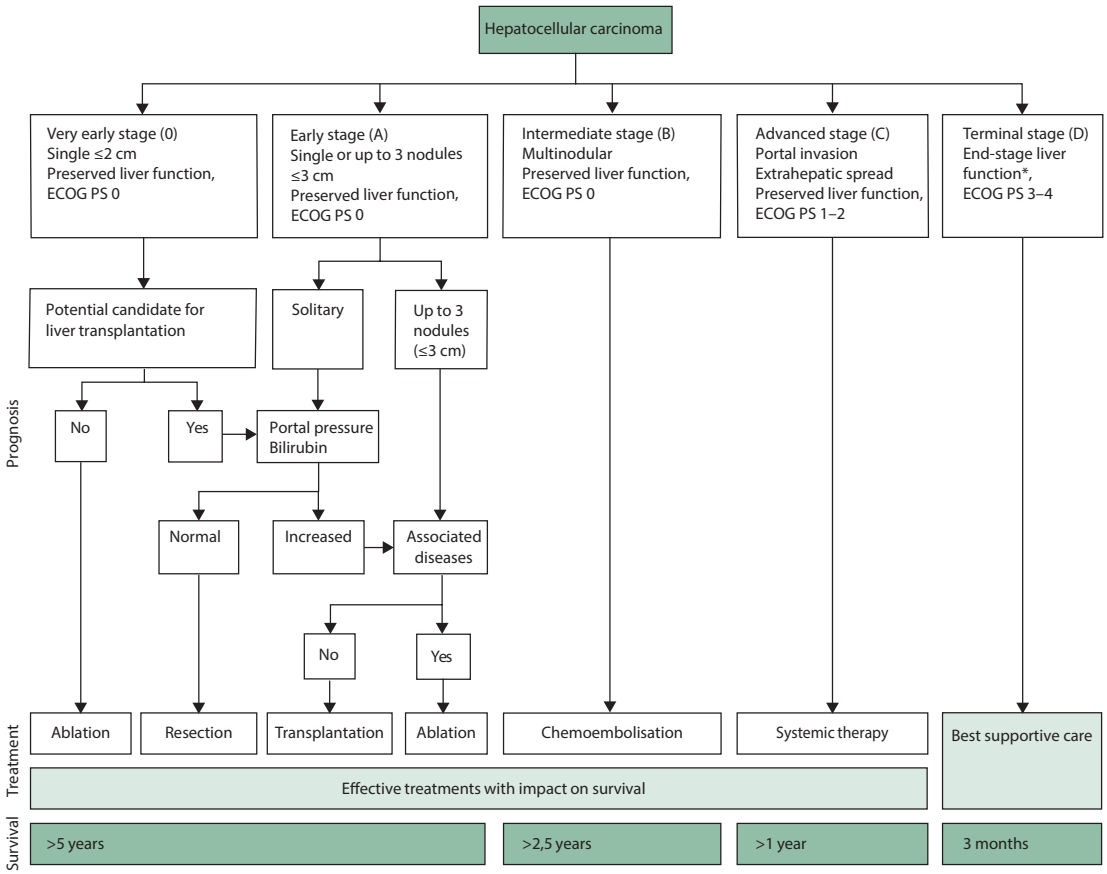

Figure 5. The BCLC classification system. Figure obtained from Forner et al.[70]

The BCLC staging system links tumor stage with appropriate treatment options and provides an evidence-based guide for the management of HCCs. HCC patients can be stratified into five different groups according to their disease stage: BCLC 0; A; B; C; and D[77]. Treatment modalities differ according to the disease stage.

Very early- to early-stage disease patients, i.e. BCLC 0 and A respectively, benefit from potentially curative treatments such as surgical resection of the tumor or liver transplantation (Figure 5). The requirements for these treatment options however, are a well-preserved liver function, e.g. no cirrhosis; and the absence of portal hypertension[70,77]. Because several HCCs are detected at later stages and/or with underlying CLD, only a minority of patients are surgically treated. This important circumstance is also a major limitation for the collection of tumor tissue for research purposes (discussed in more detail below). Patients with early-stage HCCs that don't meet the criteria for surgery, are then usually treated with thermal ablation, either with radiofrequency thermal ablation (RFTA) or more recently with microwave-mediated ablation[33,70,77].

Tumors of patients with intermediate-stage disease, i.e. BCLC B, are predominantly treated with transcatheter arterial chemoembolization (TACE, Figure 5). Treatment consists of small beads loaded with a chemotherapeutic agent, typically doxorubicin, that are administered through the main tumor-supplying artery, resulting in the embolization of the tumor by obstruction of the vessels combined with local release of the drug[33,70]. Alternatively, patients can be treated with selective internal radiation therapy (SIRT), whereby the beads are loaded with compounds containing β-radiation-emitting isotopes such as yttrium-90[33,70].

Patients with advanced-stage disease, i.e. BCLC C, receive systemic treatments in the form of targeted therapies[33,70,78] (Figure 5). Sorafenib (Nexavar®), a multikinase inhibitor targeting cancer cells as well as angiogenesis[79], was shown to increase survival from 7.9 months in the control group to 10.7 months in the treated group in a landmark clinical trial taking place ten years ago[80]. The survival benefit in sorafenib-treated patients is obviously marginal and the efficacy is limited due to side effects and the occurrence of drug resistance. Nevertheless, sorafenib is still the primary choice for the first-line treatment of HCC patients, given the fact that for ten years following its approval no additional targeted therapy met the desired clinical endpoint[81]. Very recently, lenvatinib (Lenvima®) resulted non-inferior to sorafenib in the first-line setting[82], while four additional drugs — regorafenib (Stivarga®)[83]; cabozantinib (Cabometyx®)[84]; ramucirumab (Cyramza®)[85]; and nivolumab (Opdivo®)[86] — improved the clinical outcome as second-line treatments in patients progressing under sorafenib. However, the manageability of advanced HCCs using these new therapies will require further evaluation in the daily clinical setting.

Lastly, patients with end-stage disease, i.e. BCLC D, have very short life expectancy

and are supported with palliative care[33,70] (Figure 5).

3.2.4. Histopathological features of HCC

Heterogeneity is a known feature of HCCs, either at the molecular level (discussed below) as well as at the histological level. The pathological evaluation of HCC biopsies or surgically-resected tumor specimen includes the determination of the growth pattern; differentiation grade; presence of immune cell infiltrates; necrosis; and other important histopathological features that can strongly differ between patients.

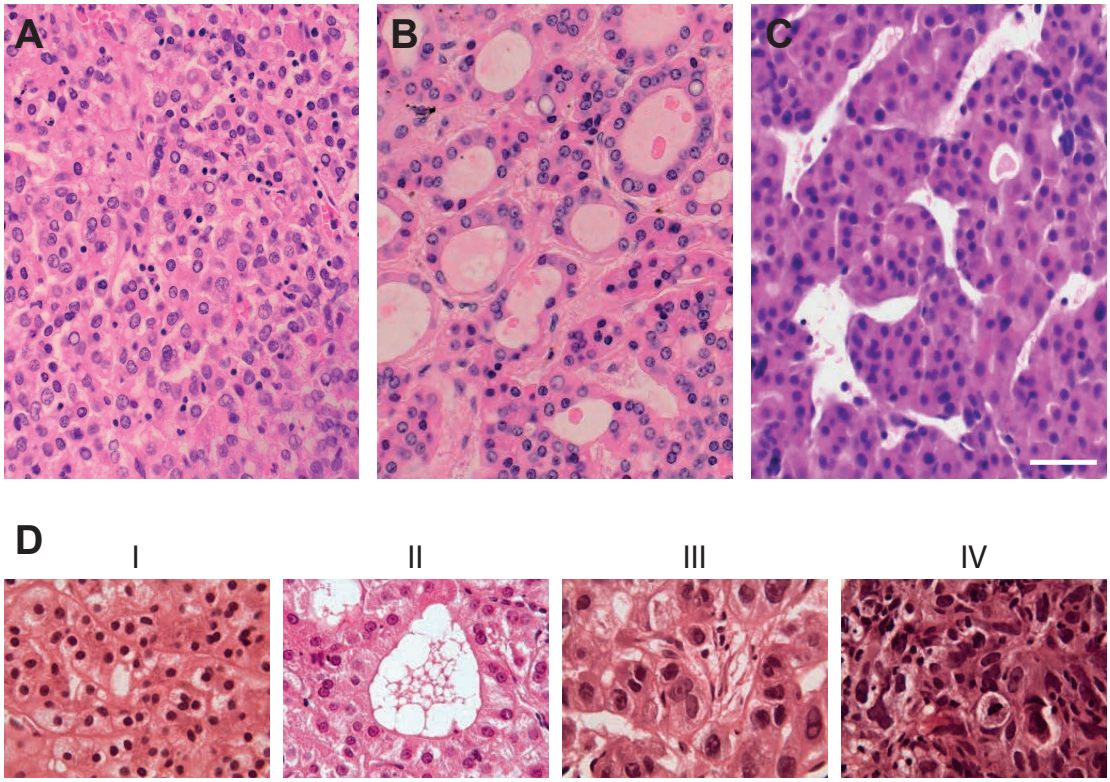

Figure 6. The three main morphological growth patterns of HCC. (**A**) solid growth pattern; (**B**) pseudoglandular growth pattern; and (**C**) trabecular growth pattern. Scale bar: 50 μM. (**D**) Micrographs displaying the four differentiation grades according to Edmondson and Steiner. Micrographs obtained and adapted from Iavarone et al.[87].

HCCs can display different growth patterns that emphasize their heterogeneity. The most common are: solid; pseudoglandular or acinar; and trabecular[88] (Figure 6 A-C). The differentiation or histologic grade describes the degree of abnormality between tumor and normal cells. Tumor cells within a low-grade tumor display few histologic abnormalities and closely resemble the normal tissue. The most common grading system for HCC was developed by Edmondson and Steiner in 1954[89]. The Edmondson grading comprises a four-scale system from grade I to IV (Figure 6D)[89]. Grade I HCCs are difficult to diagnose because of their high similarity to normal hepatocytes.

Grade II HCCs show more nuclear irregularity and pronounced nucleoli. Grade III HCCs display more variability in cellular size and shape compared to grade II and can harbor angulated nuclei. Grade IV HCCs show the highest degree of cellular variability and in some cases can contain anaplastic giant cells. In cases of low-grade, difficult to recognize HCCs, a combination of immunohistochemical markers — Glypican-3; Glutamine Synthetase; and Heat Shock Protein 70 — was shown to increase the specificity of diagnosis and helping in discriminating low-grade HCCs from benign dysplastic nodules[76].

3.2.5. The molecular landscape of HCC

The development of HCC involves a long process of tumorigenesis typically starting from liver cirrhosis caused by different etiological factors. Cirrhotic nodules are non-neoplastic regenerative nodules surrounded by scar tissue, mostly collagen. These nodules can develop into low-grade dysplastic nodules followed by high-grade dysplastic nodules, finally giving rise to very early- to early-stage (BCLC 0 and A) HCCs[33] (Figure 7).

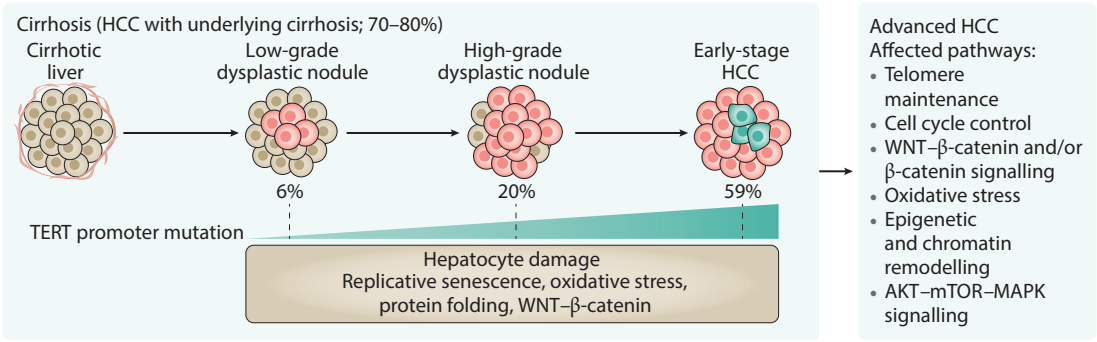

Figure 7. Progression of cirrhosis to early-stage HCC. *TERT* promoter mutations occur early during HCC carcinogenesis and are present in >50% of early-stage HCCs. Alterations in several pathways and cellular processes (right panel) occur during the progression from cirrhotic nodules to HCC. Figure obtained and modified from Llovet et al.[33].

This multistep process is accompanied by the accumulation of somatic genetic and epigenetic alterations that induce malignant transformation. HCCs contain between 40 and 100 somatic non-synonymous mutations[90], however, the number of mutated cancer driver genes within each tumor is typically ≤8[90,91]. The different combinations of driver gene mutations together with the various etiological routes to hepatocarcinogenesis, explains the complexity and heterogeneity of HCCs.

The early mechanism of malignant transformation of hepatocytes is likely based on the activation of the *Telomerase Reverse Transcriptase* (*TERT*) gene[92] (Figure 7)

resulting from mutations in the promoter region that lead to its constitutive expression[92]. These early mutations, already occurring within low- and high-grade dysplastic nodules, are required to initiate hepatocarcinogenesis by enabling unlimited proliferation of cirrhotic hepatocytes that would normally display a reduced regenerative potential or even replicative senescence. Indeed, *TERT* overexpression, either by promoter mutation or focal amplification, is observed in ~68% of HCCs[93].

In progressed HCC, the most commonly mutated genes are *TP53* and *CTNNB1* found in 31% and 27% of the cases, respectively[90] (Figure 8). Other frequently altered genes (also including gene amplifications and deletions) belong to members of the WNT pathway (*AXIN1* in 8% of the cases); the Retinoblastoma or cell cycle pathway (*RB1, CDKN2A* in 4% and 2% of the cases, respectively); and the family of chromatin remodelers (*ARID1A, ARID2* in 7% and 5% of the cases, respectively)[90]. Interestingly, inactivating mutations in the Albumin (*ALB*) and Apolipoprotein B (*APOB*) genes were found in 13% and 10% of the cases, respectively[90] (Figure 8). The hypothesized underlying rationale for mutations in the *ALB* and *APOB* genes is related to the fact that Albumin expression can account for up to 20% of cellular mRNA in hepatocytes and Very-low-density Lipoprotein (VLDL) secretion supported by APOB consumes great quantities of cellular energy[90]. Therefore, inactivating mutations in ALB and APOB results in an increase of the tumor cell's energetic resources. Finally, frequently detected amplifications on chromosome 11 result in the overexpression of *CCND1* and *FGF19*, that act as oncogenes by increasing cell growth and proliferation[90].

The analysis of transcriptomic data from large HCC cohorts revealed different molecular classifications of HCC[94-97]. Importantly however, none of the proposed molecular classifications could be translated to daily clinical practice so far. The classification systems reported by the different laboratories comprise distinct numbers of subclasses, from two to six, that don't share characteristics between each other. This is why no consensus molecular classification system could be established so far. Some of the published molecular classification systems[94,96] can be partially summarized into two main classes: the proliferation and the non-proliferation class[78,98]. The proliferation class is characterized by the activation of the RAS/MAPK-, mTOR-, NOTCH-, and IGF signaling pathways; the amplification of the *FGF19* locus; and the correlation with poor histologic differentiation and worse outcome[98]. On the other hand, the non-proliferation class is characterized by the activation of the WNT pathway and by

a correlation with better outcome[98]. However, as before, also this attempt to merge different transcriptomic studies did not result in their translation into clinical practice. One critical limitation of the above-mentioned transcriptomic-based classifications is the use of surgically resected HCCs as tissue source. As outlined in section 3.2.3, surgical resection is only an option for a minority of HCC patients that usually don't have cirrhosis. The bias introduced with this sample collection protocol might therefore be one reason why such classification systems could not find clinical utility so far.

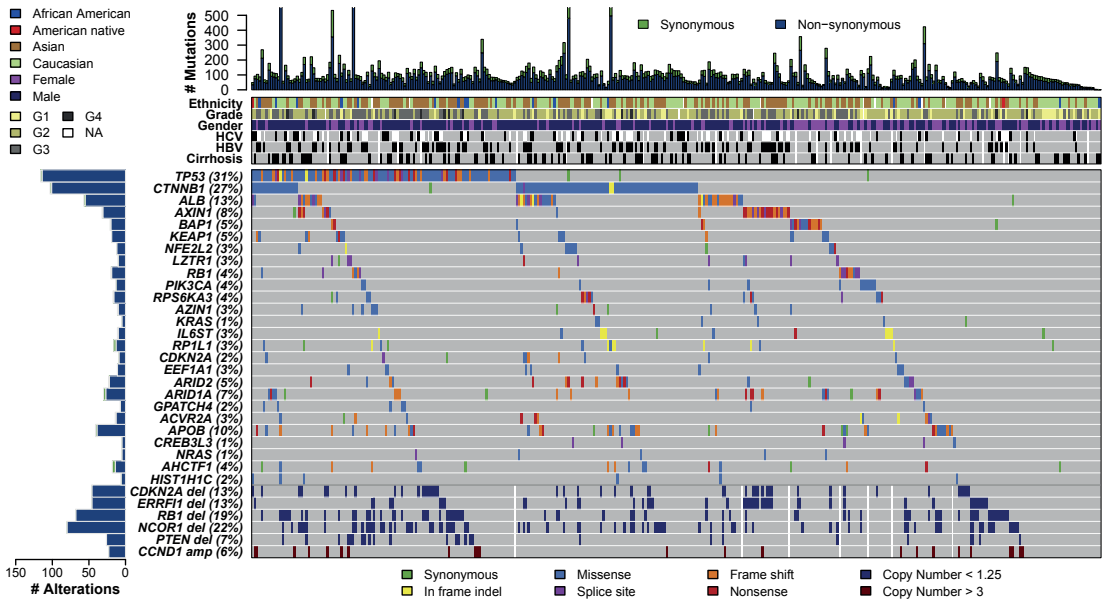

Figure 8. The mutational landscape of HCC. The top panel shows the mutation rate for each tumor (total: 363 patients). The middle panel includes information about ethnicity, tumor differentiation grade, gender, and the underlying liver disease. The bottom panel shows the significantly altered genes and copy number alterations. Figure obtained from the TCGA consortium[90].

In an attempt to generate a meaningful molecular classification, our lab established a classification for HCCs based on needle biopsy specimens[99]. The use of needle biopsies enabled the inclusion of a broad spectrum of HCCs in terms of disease stage, etiologies, and the presence and absence of cirrhosis. Paired non-tumor liver biopsies from each patient were used as control samples, in addition to a set of 5 normal liver biopsies from unrelated patients without history of HCC. The expected reduction of inter-individual variability with the use of paired biopsies as matched gene expression controls was not observed, yet the opposite happened as additional variations were introduced. Interestingly, when normalizing the HCC dataset to the 5 normal livers, the signature genes defining the different subclasses were equally differentially regulated independently of their original subclass. The same was true when apply-

ing the normalization protocol to previously published HCC classification systems. This observation led to the conclusion that the different subclasses in current classification systems are defined by expression level changes in a group of tumor-specific genes rather than subclass-defining genes. Finally, because of the heterogeneous nature of HCCs and the relatively low information content of single omics analyses, classification studies aiming at integrating different datasets (genomics, transcriptomics, phospho-proteomics, metabolomics, etc.) could potentially culminate in a clinically meaningful classification system.

3.2.6. Experimental models for the study of HCC

Despite the broad heterogeneity of HCCs within and between patients, the possibilities to study the biology of this cancer are currently limited to a variety of *in vivo* mouse models and a few frequently-used *in vitro* cancer cell lines as outlined below.

Animal models. As for most of the biomedical research fields, current animal models of HCC rely on the versatility of the mouse (*mus musculus*) model system. Mouse models of HCC can be derived by chemical induction through toxins; genetic engineering; and by xenotransplantation of tumor tissues[100-102].

HCCs in mice can be induced by different hepatotoxic/carcinogenic agents that are administered at young age. The underlying tumorigenic mechanism involves the hepatic metabolic conversion of such compounds into reactive metabolites that in turn exert their carcinogenic activity, usually by directly affecting DNA integrity[100-102]. The same mechanism underlies the development of aflatoxin B1-related HCCs in human patients as described above. The most commonly used compounds are carbon tetrachloride (CCl_4), diethylnitrosamine (DEN), and dimethylnitrosamine (DMN)[100-102].

Genetically-engineered mouse models offer the possibility to (partially) reproduce the molecular background of human HCCs in a tailored manner. The advancements in the field of genetic engineering, allowed the generation of hepatocyte-specific oncogene activation and tumor suppressor inactivation, respectively, e.g. by driving the Cre recombinase under the Albumin promoter[102]. So far, a large number of transgenic mouse models of HCC was generated by targeting cellular processes such as the cell cycle machinery (TP53; c-MYC; E2F-1; SV40 T-antigen) and a variety of cellular signaling pathways (WNT; PI3K/AKT; EGF; IGF; HGF)[102]. Another option to induce a carcinogenic process within hepatocytes consists in the overexpression of viral proteins originating from HBV and/or HCV that cause hepatocellular damage[100-102].

Despite the advantages offered by transgenic mouse models, the major drawback remains the inability to reflect the process of tumorigenesis from hepatocyte insult to fibrosis, cirrhosis and eventually HCC, as it is occurring in patients. On the other hand, chemically-induced tumors follow the common path of HCC tumorigenesis by inducing inflammation and fibrosis. However, they typically fail to reproduce the molecular background of human HCCs.

Patient-derived xenografts (PDX), are perhaps the closest *in vivo* models representing human cancer biology. To generate xenograft models, tissue fragments or cell lines derived from tumors are transplanted into immunodeficient mice, either subcutaneously or orthotopically[102,103]. Subcutaneous xenograft models facilitate tumor growth monitoring and measurement while orthotopic models might be necessary to enable growth of tumors with higher microenvironmental demands. Moreover, the use of primary tumor specimens rather than immortalized cancer cell lines allows to reproduce the complexity and heterogeneity of the primary tumor[103]. Therefore, PDX models have the potential to overcome the limitations of chemically-induced- and genetically-engineered mouse models. Indeed, several groups reported the generation of HCC-derived PDX mouse models, however, they were all generated using surgically-resected HCC specimens[104-108]. In our group, we recently generated a collection of PDX mouse models derived from needle biopsies of HCCs with different disease stages and from patients with different etiologies, thereby reflecting the broad spectrum of patients, and the histological features and molecular landscape of the primary tumors (unpublished data).

Current improvements in the PDX field aims at developing humanized PDX models that enable the generation of PDX mouse models with the presence of some components of the immune system, such as tumor-reactive T cells[103]. This will enable the study of the interactions between the tumor and the immune system and support the evaluation of novel immunotherapies.

Cell culture models. Cancer cell lines represent the workhorse of biomedical research and pre-clinical drug development. They are easy-to-handle, broadly applicable and generate low costs in terms of reagent usage, however, their generation is rather inefficient and requires selection and adaptation to 2D culture. About 30 HCC-derived cell lines are publicly-available to the research community and most of them were recently characterized at the genomic level within the frame of the Cancer Cell Line Encyclopedia (CCLE) project[109]. All these cell lines were derived from surgically

resected HCCs and thus suffer from the same drawbacks outlined above that limits their representability of the HCC patients' spectrum. Moreover, the most common cancer cell lines used in HCC research, HepG2 and HuH-7, were established decades ago, in 1979 and 1982, respectively[110-112]. A direct comparison of these cell lines to their primary tumors, especially in terms of genomic alterations, is therefore missing and the question how well they represent the original tumors remains unanswered. Importantly, the genetic evolution of these cell lines over time was not documented, thus, their original identity might have been remarkably altered since their establishment. Nevertheless, HuH-7 and HepG2 cells have demonstrated a remarkable broad utility in basic hepatological research due to the retention of several hepatocyte-specific features as, among others, the expression of a variety of metabolic enzymes, e.g. members of the Cytochrome P450 family, or the secretion of hepatocyte-specific proteins such as Albumin[112]. In addition, further adaptations and modifications to these cell lines rendered them permissive to infection with hepatotropic viruses such as HBV and HCV[112].

Recently, new cell lines were established, deeply characterized at the genomic and transcriptomic level, and compared to the primary tumor to evaluate the degree of representation[113]. Despite these efforts, they only partially represented the original tumor and their establishment did not add increasing value to the currently existing models. Most importantly, novel *in vitro* models will have to recapitulate the three-dimensional architecture and cellular and genetic heterogeneity to provide novel possibilities for a better understanding of HCC biology.

3.3. Organoid models in biomedical research

The term "organoid" first appeared half a century ago in the context of classical developmental biology experiments, that involved simple dissociation and reaggregation experiments to study the mechanisms of organogenesis[114]. After several years of "silence", the scientific community is now witnessing a revival of the organoid system[115]. However, the current definition of an organoid has changed from what developmental biologist initially described. An organoid — as recently defined by Lancaster and Knoblich — is a three-dimensional multicellular structure that, (i) contains multiple organ-specific cell types, (ii) recapitulates at least some of the organ-specific functions, and (iii) is spatially organized in a similar way as the original organ[114]. Organoids can be derived from pluripotent embryonic stem cells (ESCs); induced plu-

ripotent stem cells (iPSCs); and organ-restricted multipotent adult stem cells (aSCs)[114,116].

3.3.1. Stem cell- and multipotent progenitor cell-derived organoids

Back in 2007, Barker and colleagues succeeded in identifying and describing the stem cell niche of the small intestine and the colon[13]. The Wnt target gene Leucine-rich repeat-containing G-protein coupled receptor 5 (Lgr5) was shown to be specifically expressed at the surface of cells residing at the bottom of the intestinal crypt and, to mark rapidly-dividing cells that could give rise to all differentiated cell types of the intestinal epithelium[13]. This discovery paved the way for the development of the organoid culture system, as we know it nowadays.

Two years later, in an attempt to culture Lgr5$^+$ stem cells *in vitro*, Sato and colleagues described the first organoid culture protocol that was entirely derived from single adult stem cells[117]. The protocol involved the isolation of Lgr5$^+$ stem cells from the mouse intestine, their suspension in Matrigel droplets to allow 3D outgrowth and, importantly, the addition of a highly specialized growth factor-enriched culture medium[117] (Figure 9A). Alternatively, and more convenient, the culture can also be initiated by isolating single crypts, without the need to select for Lgr5$^+$ stem cells[117]. The growth factors in the culture medium recapitulate the signals provided by the stem cell niche. The most important ones among these are Wnt3a and the Wnt-agonist R-Spondin 1 (R-Spo1), two ligands that both drive the proliferation of stem cells in the intestine; Noggin, an inhibitor of BMP-mediated cell differentiation and cell cycle arrest; and Epidermal Growth Factor (EGF), a potent mitogen that activates the Mitogen-activated Protein Kinase (MAPK) pathway (Figure 9B). Interestingly, the molecular mechanisms of R-Spo1 activity were not known when the first organoid model was described but two years later the same group discovered that Lgr5 was actually the receptor of R-Spondins[118]. The organoid technology could be rapidly applied to other murine organs such as the liver[119], pancreas[120], stomach[121], prostate[122,123] and the esophagus[124]. Most of these organoid systems also rely on Lgr5$^+$ stem or Wnt-responsive multipotent progenitor cells and therefore, depending on the organ, the culture medium required only little modification, like for example the addition of single tissue-specific factors[116,125]. Remarkably, every organoid model described so far recapitulated some of the tissue-specific functions, e.g. albumin secretion and metabolic activity in liver organoids[119] or the expression of lysozyme and mucin in intestinal organoids[117]. The real breakthrough came with the protocol adaptations and modifi-

cations that allowed the culture of human aSC-derived organoids. Human prostate[122,123], intestine[126], colon[126], esophagus[126], liver[127], and pancreas[128] could be readily reproduced as mini-organs using refined culture media recipes. The utility of the organoid models was further demonstrated by their ability to model human diseases such as hepatic disorders[127], gastric bacterial infection[129], and cystic fibrosis[130]. These studies highlighted the potential of organoids to personalize patient treatment.

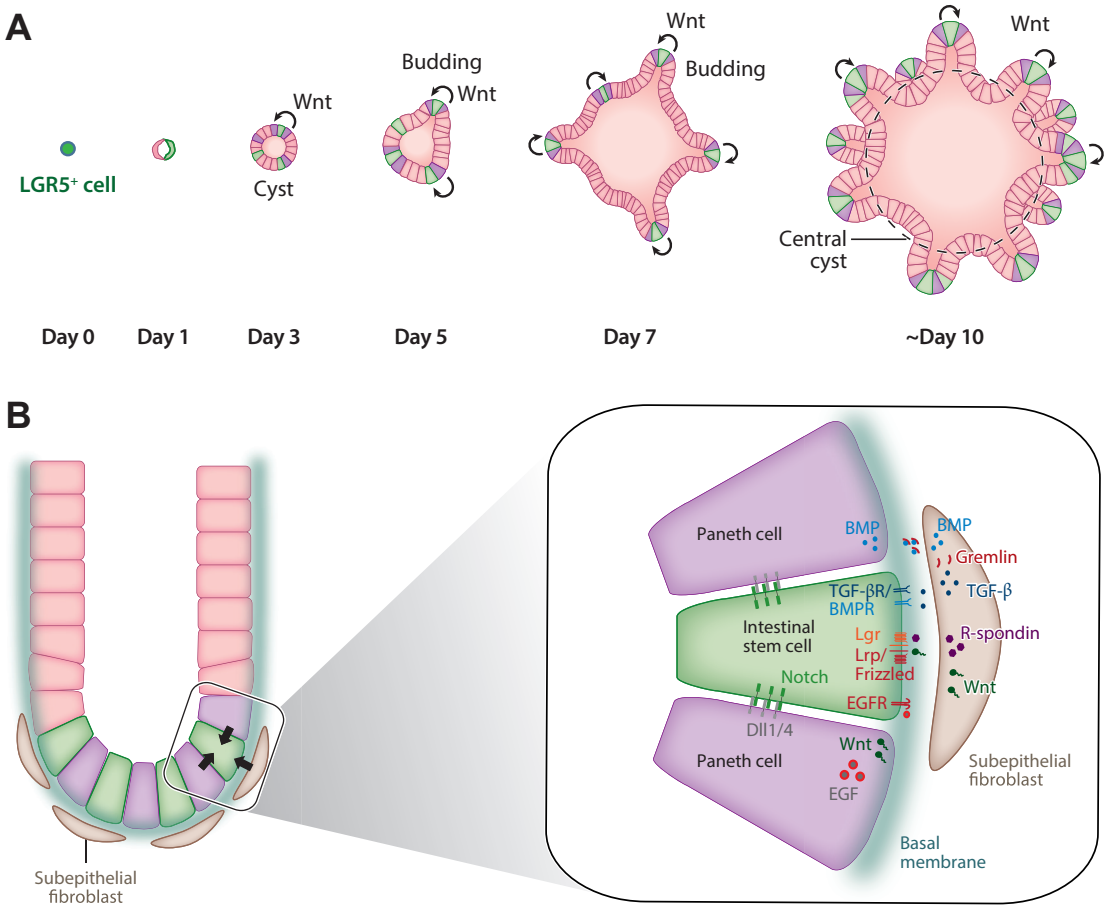

Figure 9. The intestinal organoid culture system. (**A**) Single Lgr5+ stem cells are embedded in Matrigel and overlaid with growth factor-enriched medium. Organoids form within one week and self-organize to resemble the *in vivo* epithelium with crypt and villus structure. (**B**) The crucial niche signals that are essential for the maintenance and expansion of Lgr5+ stem cells in vivo. Figure obtained and modified from Date et al.[131].

Importantly, because the growth of organoids relies on self-renewing stem- or progenitor cells, they can be stably maintained in culture for several months without loss of their proliferative potential. In addition, deep sequencing studies revealed a remarkable genetic stability, because only very few newly-acquired somatic mutations were detected in protein-coding genes[116,127].

As of today, all the organoid systems derived from aSCs — isolated from tissue biopsies — are of epithelial nature[116,125] and the current culture conditions do not allow the simultaneous expansion of other cell types present in the tissue biopsy, e.g. fibroblasts or immune cells[116,125]. This represents a current limitation of this *in vitro* system.

The majority of the organoid models can be derived from aSCs, however, the repertoire can be further expanded with the use of ES- or iPS cells as the cell of origin[116,125]. The culture workflow is more complex as it implies the initial differentiation of pluripotent stem cells into the required germ layer, followed by further differentiation steps into the desired tissue lineage[116,125,132]. Nevertheless, this procedure enabled the generation of highly complex and fascinating organoid models of the kidney[133] and the brain[134]. Importantly, there is currently no way to derive kidney or brain organoids directly from aSCs. The protocols to grow organoids from aSCs are (currently) only applicable for endoderm-derived organs as listed above, but not for mesoderm- (kidney) or ectoderm (brain)-derived organs[132].

3.3.2. Tumor-derived organoids

The observation that single stem cells isolated from biopsies of healthy tissues could give rise to organoids *in vitro* raised the question whether the technique would be also applicable to patient tumor tissues. However, one problem arising in tumor organoid cultures is their cellular heterogeneity, and in particular the presence of non-tumor tissue in a given tumor biopsy. Indeed, the initially-described organoid protocols allowed the growth of tumor cells but at the same time also of the normal, non-tumor tissue counterpart leading to mixed tumor/non-tumor cultures. For some tumor types this problem could be elegantly solved. In colorectal cancer (CRC) for example, about 90% of the tumors harbor mutations that aberrantly activate the Wnt pathway[135]. Because the growth of non-tumor organoids relies on the exogenous addition of Wnt and R-Spo1 ligands, removal of these components from the CRC organoid medium results in a pure tumor organoid culture[126,136]. This simple manipulation could be applied to additional tumor types and molecular alterations in a similar manner. The Mouse double minute 2 homolog (MDM2) inhibitor nutlin-3a for example can be used to positively selected tumor cells that harbor mutant TP53, while TP53 proficient cells are driven into apoptosis[137]. To date, as for CRC, the refinement of culture media recipes allowed the generation of patient-derived organoids (PDO)

from cancers of the pancreas[128], stomach[138], prostate[139], breast[137], bladder[140], and liver (this study)[141,142]. Importantly, the success rate of tumor organoid generation is currently between 15%–100% depending on the tumor type[143]. Moreover, the collection protocols for these organoid models were mostly based on tissues derived from surgical resections that, for some tumors, can have implications for the representability of the patient cohort. Nevertheless, the spectrum of tumor patients can be exceptionally represented as in the case of CRC[136,144].

When compared to the primary tumor, organoids markedly reproduced most of the histological features. Strikingly, several different histological tumor subtypes can be modeled in organoids[136,137]. However, because they are purely composed of tumor cells they consequently lack immune-, endothelial- and other stromal cells[143]. Nevertheless, recent reports described the first co-culture protocols that aimed to reproduce the tumor microenvironment by co-culturing tumor organoids with autologous cancer associated fibroblasts[145] or immune cells[146]. On the other hand, epithelial and mesenchymal organoid components can be directly obtained by culturing organoids at the air-liquid interface[147].

Beside the recapitulation of the primary tumors' histology, deep sequencing of tumor organoids and their primary tumor counterpart revealed a high degree of concordance in the number of genetic alterations such as mutations and copy number variations. Indeed, in all tumor organoid models, the vast majority of mutations in the primary tumors were maintained in the corresponding organoids[143]. Notably, analysis of the cancer cell fraction (CCF) revealed the presence of intratumor genetic heterogeneity, emphasizing the advantage of organoid cultures compared to typically clonal cancer cell lines[136,143]. Finally, the derivation of paired healthy organoids for each patient provides the ideal *in vitro* control tissue[143].

Despite the numerous advantages of PDOs given their robust recapitulation of the primary tumor, the ultimate proof of their utility for the clinical setting came from recent studies that correlated patients' response to therapy to the one observed in the corresponding organoids, providing evidence that PDOs can serve as a model to recapitulate but also possibly predict the clinical response to therapy[140,148].

Finally, the advancements in genome editing, especially with the rise of the CRISPR-Cas9 system and its broad applicability, allowed the simple manipulation of the genomes of cellular systems[149]. This methodology was recently used for the step-wise

generation of tumor organoids from initially non-tumor healthy organoids, thereby modeling the sequential accumulation of mutations, a process that is thought to occur in a similar manner in human patients[150,151]. Such studies are now possible without the need of artificially-transformed cell lines and will help in validating and identifying known as well as novel oncogenic mutations and defining new therapeutic targets[152].

4. AIMS OF THE PHD THESIS

Liver cancer research suffers from a lack of adequate *in vivo* and *in vitro* models that faithfully recapitulate the biology of hepatocellular- and cholangiocellular carcinomas. This circumstance is reflected by the scarcity of effective therapies for patients with advanced liver cancer. Therefore, new models that enable the translation of basic research findings to the pre-clinical and clinical setting would significantly advance the understanding as well as the clinical management of this malignancy.

Our laboratory follows a truly translational approach combining both, basic- and clinically-oriented research, aiming to better understand liver pathophysiology, with the ultimate goal of providing more effective treatments to patients. One of our approaches includes the collection of valuable primary tissue specimens from needle biopsies and their use for research purposes. Thanks to these precious samples, I was able to establish a protocol for the generation and characterization of a new patient-derived liver cancer model based on the organoid system.

The first part of this thesis focuses on the generation of liver organoid cultures from small biopsy fragments. Our starting material was much smaller than the resected specimens previously used for the establishment of the liver organoid protocol. Therefore, my first aim was to adapt the protocol to accommodate the isolation of organoid-initiating cells from biopsies, in particular by minimizing tissue loss due to the given specimen size. The resulting organoid cultures were then characterized in terms of hepatic markers and functional properties.
In the second part of this thesis, I describe my main PhD project, namely the generation of patient-derived organoid models obtained from needle biopsies of liver cancers. Because of my personal interest in cancer biology and the availability of tumor tissue it was obvious to apply the organoid technology also to biopsies derived from liver cancer patients. The aim was to comprehensively characterize the model (i) histologically, for the analysis of the phenotypic features, as well as (ii) molecularly, for the analysis of the genetic landscape and assessment of the genomic stability in culture. Importantly, these analyses were always conducted in comparison to the primary tissue biopsy to evaluate the degree of similarity between organoids and primary tumor. This approach resulted in the establishment of a biobank currently comprising more than 20 tumor organoid lines from hepatocellular carcinomas, cholangiocellular carcinomas and, to a smaller extent, from liver metastases of other primary tumors.

5. MATERIALS AND METHODS

5.1. Collection of human tissues and biopsy procedure

All human tissues used in this study were obtained from patients undergoing diagnostic liver biopsy at the Clinic of Gastroenterology and Hepatology of the University Hospital Basel. Written informed consent was obtained from all patients. The study was approved by the ethics committee of the north-western part of Switzerland (protocol number: EKNZ 2014-099). Biopsy collection was performed by Prof. Dr. Markus Heim and Dr. Tujana Boldanova. US-guided needle biopsies were obtained from tumor lesions with a coaxial liver biopsy technique that allows taking several biopsy samples through a single biopsy needle tract. After local anesthesia, the introducer needle was advanced 2-3 cm into the liver parenchyma. In case of a focal lesion, the needle was positioned precisely at the tumor border. The trocar of the introducer needle was removed, and up to five cylindrical biopsies of ~1 mm diameter and 10–30 mm in length were obtained with an automatic spring-loaded biopsy needle (Bio-Pince™). The introducer needle was kept in place during the entire procedure to ensure that all specimens came from the same area of the tumor. One cylinder was fixed in formalin and paraffin-embedded for diagnosis and staging by the pathologist. Additional cylinders were immediately snap-frozen in liquid nitrogen for later use in DNA and RNA extraction or embedded in O.C.T. (Tissue-Tek) and frozen using standard procedures. For organoid generation, biopsy pieces were placed in 1 ml advanced DMEM/F-12 (Gibco, Thermo Fisher Scientific) on ice. For control tissue, all patients that underwent US-guided HCC biopsy also got a biopsy of the liver parenchyma at a site distant from the tumor. Finally, the needle tract was filled with absorbable gelatin sponge before removal of the introducer needle. The biopsy collection procedure was identical for non-tumor patients.

5.2. Organoid culture

Tumor biopsy fragments designated for organoid generation typically measured ~1 mm in diameter and 5–10 mm length. All other (non-tumor) biopsies typically measured ~1 mm in diameter and 30 mm length. They were transported to the laboratory and further processed for organoid generation within 20 min after collection. The different media compositions used in the study are listed below:

- Isolation medium: advanced DMEM/F-12 supplemented with 1:50 B-27, 1:100 N-2, 10 mM Nicotinamide, 1.25 mM N-acetyl-L-cysteine, 10 nM [Leu^{15}]-Gastrin, 10 µM Forskolin, 5 µM A83-01, 50 ng/ml EGF, 100 ng/ml FGF10, 25 ng/ml HGF, 10% RSPO1-conditioned medium, 30% WNT3A-conditioned medium, 25 ng/ml NOGGIN and 10 µM Y-27632.

- Expansion medium: advanced DMEM/F-12 supplemented with 1:50 B-27, 1:100 N-2, 10 mM Nicotinamide, 1.25 mM N-acetyl-L-cysteine, 10 nM [Leu^{15}]-Gastrin, 10 µM Forskolin, 5 µM A83-01, 50 ng/ml EGF, 100 ng/ml FGF10, 25 ng/ml HGF, 10% RSPO1-conditioned medium.

- Differentiation medium: advanced DMEM/F-12 supplemented with 1:50 B-27, 1:100 N-2, 10 nM [Leu^{15}]-Gastrin, 500 nM A83-01, 50 ng/ml EGF, 100 ng/ml FGF19, 25 ng/ml HGF, 25 ng/ml BMP7, 10 µM DAPT and 30 µM Dexamethasone.

Commercial reagent sources: advanced DMEM/F-12, B27 and N-2 all from Gibco (Thermo Fisher Scientific); BMP7, EGF, FGF10, FGF19, HGF and NOGGIN all from Peprotech; DAPT, Dexamethasone, [Leu^{15}]-Gastrin, N-Acetyl-L-Cysteine, Nicotinamide and Y-27632 all from Sigma; A83-01 and Forskolin both from Tocris; RSPO-1 and WNT3A conditioned media were both homemade.

Non-tumor liver organoid generation and expansion. Organoid cultures from non-tumor liver biopsies of HCC patients or biopsies from non-tumor patients with other diseases (e.g. HBV, HCV, cirrhosis, NAFLD, ALD, genetic diseases) were generated with a previously-described, slightly modified protocol[127]. Briefly, biopsy tissue was minced to small pieces of ~1 mm^3 size and placed in 2 ml digestion solution (2.5 mg/ml collagenase D, 0.1 mg/ml DNase I in EBSS) in a water bath at 37°C for 10 min. Undigested tissue fragments were further disrupted by repetitive pipetting. The tube was filled with 10 ml DMEM+10%FBS and centrifuged at 400 × g for 4 min. This washing step was repeated twice. After the last washing, the supernatant was removed completely, and the tube pre-cooled on ice. The digested tissue was resuspended in the required amount of BME2 (Basement Membrane Extract, Type 2, Amsbio) and droplets of 15–50 µl (depending on the experiment) were pipetted on pre-warmed suspension cell culture plates (Greiner Bio-one). Plates were placed in a 37°C incubator for 20 min to allow the BME2 to polymerize before adding the required amount of pre-warmed organoid isolation medium (IM). After 3 days, isolation medium was switched to expansion medium (EM). Liver organoids were passaged

by mechanical dissociation through a fire-polished Pasteur-pipette or incubation in 0.25% Trypsin-EDTA (Gibco, Thermo Fisher Scientific) for 2 min. Disrupted or digested organoids were subsequently seeded in EM as described above. Cryovials were prepared by dissociating organoids and resuspending in Recovery Cell Culture Freezing Medium (Gibco, Thermo Fisher Scientific) prior to freezing. Presence of Mycoplasma contamination was regularly tested with the MycoAlert™ Mycoplasma Detection Kit (Lonza) according to the manufacturer's instructions.

Differentiation of liver organoids into hepatocyte-like cells. Liver organoids are composed of bipotent progenitors[127]. For differentiation into hepatocyte-like cells, organoids were first expanded as described above. To induce differentiation, EM was switched to differentiation medium (DM) and the organoids cultured for 11 days with medium changes every 3 days.

Tumor organoid generation and expansion. For tumor organoid generation, biopsies underwent a limited digestion to small cell clusters. Complete digestion into single cells was intentionally avoided because it has been reported that preservation of cell-cell contacts enhances derivation efficiency of tumor cultures[153]. Therefore, tumor tissue was minced and placed, for max. 2-4 min, in digestion solution (2.5 mg/ml collagenase D, 0.1 mg/ml DNase I in EBSS) at 37°C. The digestion step was completely skipped in case of very small and/or fragmented biopsy pieces. Instead the tissue was further disrupted by repetitive pipetting and washed with DMEM+10%FBS. The total yield of cells/cell clusters varied due to differences in the size of the tumor biopsy available for the generation of organoids and the variable content of viable tumor cells in the biopsies. This was different for each case and the result of variable degrees of necrotic areas in each tumor biopsy. Cells and cell clusters were seeded into BME2 as described above for non-tumor liver organoids. After polymerization of BME2, EM was added to the wells. Tumor organoids were passaged after dissociation with 0.25% Trypsin-EDTA (Gibco, Thermo Fisher Scientific). In the few cases for which enough biopsy material was available, we tried an adapted version of the culture medium in comparison to the standard one. The adapted medium lacked some of the original components reported to have a negative effect on HCC cell proliferation (i.e. Forskolin[154], N-Acetyl-L-Cysteine[155], Nicotinamide[156], HGF[157]) and contained FGF19 due to the frequent amplification of the *FGF19* gene detected in HCCs and its positive effect on proliferation of HCC cells[158].

However, these attempts did not result in the establishment of additional HCC organoid lines. Frozen stocks of early (≤P4) passages could be prepared as described for non-tumor liver organoids. All tumor organoid lines could be kept in long-term cultures with regular splitting for at least 1 year. Presence of Mycoplasma contamination was regularly tested with the MycoAlert™ Mycoplasma Detection Kit (Lonza) according to the manufacturer's instructions.

5.3. Generation of tumor organoid xenografts

All experiments involving organoid transplantations into mice were performed in strict accordance with Swiss law and were approved by the ethics committee of the northwestern part of Switzerland (protocol number: EKNZ 2014-099) and the animal care committee of the canton Basel-Stadt, Switzerland. Tumor organoids, corresponding to 1×10^6 cells, were released from BME2 by incubating in Cell Recovery Solution (Corning) or Dispase II solution (Sigma) for 30 min on ice or at 37°C respectively. After washing in DMEM+10%FBS, organoids were resuspended in 100 µl 50:50 (v/v) BME2:EM and injected subcutaneously into immunodeficient NOD scid gamma (NSG) mice (The Jackson Laboratory) at young age (6-8 weeks). Paired non-tumor liver organoids from the same patient were used as control. Tumor xenograft growth was measured every two weeks using a caliper. When tumors reached the size of at least 500 mm^3 (maximal volume allowed: 1'500 mm^3), mice were euthanized by CO_2 inhalation and tumors surgically excised. One half of the xenograft tissue was used for paraffin-embedding and further histological analysis, the other half was divided in equal parts that were snap-frozen in liquid nitrogen and embedded in O.C.T. (Tissue-Tek) respectively. Mice that did not show any sign of tumor growth 8 months after injection were euthanized and the xenografting considered unsuccessful.

5.4. Histology and immunohistochemistry

Biopsies from tumor and non-tumor tissue, as well as tumor organoid xenografts were fixed in 4% phosphate buffered formalin and embedded in paraffin using standard procedures. Tumor and non-tumor liver organoids were released from BME2 by incubating in Cell Recovery Solution (Corning) following the manufacturer's instructions or by incubating in Dispase II solution (Sigma). Organoids were then fixed in freshly prepared 4% formalin solution in PBS for 30 min at room temperature (RT) following dehydration and paraffin embedding. Sections were subjected to Hematoxylin and Eosin (H&E), Masson's Trichrome, Alcian Blue-PAS as well as immuno-

histochemical staining using standard procedures. Histopathological evaluation was assessed by two board-certified pathologists, Dr. Matthias S. Matter and Prof. Dr. Luigi M. Terracciano, at the Institute of Pathology of the University Hospital Basel. Tumors were classified based on architecture and cytological features and graded according to the Edmondson grading system[89].

For immunohistochemistry, the following primary antibodies were used for automated staining on a Benchmark XT device (Ventana Medical Systems, Inc.): Alpha-Fetoprotein (Ventana Cat. Nr. 760-2603), Glutamine Synthetase (Ventana Cat. Nr. 760-4898), Glypican 3 (Ventana Cat. Nr. 790-4564), Heat Shock Protein 70 (Biocare Medical CM407A), Keratin 7 (Ventana Cat. Nr. 790-4462), Keratin 19 (Ventana Cat. Nr. 760-4281), KI-67 (Ventana Cat. Nr. 760-4286).

5.5. Transmission electron microscopy (TEM)

For TEM, undifferentiated as well as differentiated organoids were fixed with 3% glutaraldehyde in PBS over night at 4°C. Organoids were then washed in PBS and fixed with 1% OsO_4 in PBS for 20 min at RT. After a dehydration series in 70%, 80%, 96% and 100% EtOH for 5 min each, the organoids were submerged in propylene oxide for 5 min, then in propylene oxide:epoxy resin (1:2) for 30 min and finally in propylene oxide:epoxy resin (1:3) for 4 hrs. Polymerization of the resin was carried out at 60°C for 48 hrs. Semi-thin sections (3 μm) were prepared for orientation purposes followed by ultra-thin (80 nm) sections that were placed on a copper grid. Contrasting was carried out with uranyl acetate and lead nitrate before acquisition.

5.6. Drug treatments

Drugs used in this study were dissolved in DMSO at 10 mM and stored in aliquots at -20°C. Sorafenib tosylate (Cat. Nr. S-8502) was purchased from LC Laboratories. For regular dose-response experiments with sorafenib, tumor organoids were plated at a density of 5×10^3 cells in 15 µl BME2 droplets in 300 µl EM. Medium was replaced with 250 µl fresh EM containing sorafenib or vehicle (=100% DMSO) after 6 days, when organoids were fully formed. All tumor organoid lines were subjected to a 7-point dilution series of sorafenib. The dose range was chosen based on pharmacodynamic data obtained from HCC patients[159]. Cell viability was measured after 6 days using CellTiter-Glo 3D reagent (Promega) according to the manufacturer's instructions. Luminescence was measured on a Synergy H1 Multi-Mode Reader (BioTek Instruments). Results were normalized to vehicle. Curve fitting was performed

using Prism (GraphPad) software and the nonlinear regression equation. All experiments were performed at least two times in duplicate. Results are shown as mean ± SEM.

5.7. Functional hepatocyte studies

Glycogen production and Albumin secretion were assessed on liver organoids at day 11 of the differentiation protocol. For glycogen production, organoids were embedded in paraffin and histological sections stained with Periodic Acid-Schiff (PAS, Sigma, Cat. Nr. 395B-1KT). One liver biopsy section was used as control. Albumin secretion was measured in the supernatant collected during the last day of differentiation. Protein measurement was carried out using a human Albumin-specific Sandwich ELISA kit (Assaypro, Cat. Nr. EA3201-1). Supernatant from HepG2 cells was used as control.

5.8. DNA and RNA extraction

Genomic DNA from organoids was extracted using the DNeasy Blood & Tissue kit (Qiagen) following the manufacturer's instructions, with the following modification of the protocol: Instead of using H_2O, DNA was eluted in 100 µl of a 5 mM Tris/HCl, pH 8.5 solution. Total RNA from organoids was extracted using Trizol® reagent (Invitrogen, Thermo Fisher Scientific) according to the manufacturer's instructions. Genomic DNA and total RNA from biopsies was extracted using the ZR-Duet DNA/RNA MiniPrep Plus kit (Zymo Research) following the manufacturer's instructions. Prior to extraction, biopsies were crushed in liquid nitrogen to facilitate lysis. For next generation sequencing (NGS) applications, the extracted DNA and RNA was quantified using the Qubit Fluorometer (Invitrogen).

5.9. Real-time quantitative PCR

Reverse transcription of 1 mg RNA was performed using M-MLV reverse transcriptase (Promega, Cat. Nr. M1701) following DNase I (Promega, Cat. Nr. M6101) treatment. RT qPCR was performed on 40 ng cDNA using FastStart Universal SYBR Green Master Mix (Roche, Cat. Nr. 04 913 850 001) and the ABI 7500 detection system (Applied Biosystems, Thermo Fisher Scientific). Primer sequences are listed below. Gene transcript expression levels were calculated using the ΔC_t method.

Gene	Forward primer (5' – 3')	Reverse primer (5' – 3')
ALB	TGCCAAAGTGTTCGATGAAT	AGCGCATTCTGGAATTTGTA
CYP3A4	TGTGCCTGAGAACACCAGAG	GTGGTGGAAATAGTCCCGTG
EpCAM	CGCAGCTCAGGAAGAATGTG	TGAAGTACACTGGCATTGACG
KRT19	CGCGGCGTATCCGTGTCCTC	AGCCTGTTCCGTCTCAAACTTGGT

Table 2. RT qPCR primer sequences.

5.10. Whole exome sequencing

DNA extracted from eight HCC biopsy-derived organoid lines (Patients 1, 2, 5-A, 5-B, 9, 12-I, 12-II and 25), three CCC biopsy-derived organoid lines (Patients 13, 16 and 20) the corresponding original biopsies and the control paired non-tumor biopsies were sequenced using whole-exome sequencing. The eight HCC biopsies were derived from six patients and for three of the biopsies, early and late passage organoids were profiled. The tumor biopsy sample corresponding to Patient 1 had to be excluded from further analyses because of low tumor cell content in the biopsy. Whole-exome capture was performed using the SureSelectXT Clinical Research Exome (Agilent) platform according to the manufacturer's guidelines. Sequencing was performed on an Illumina HiSeq 2500 at the Genomics Facility Basel according to the manufacturer's guidelines. Paired-end 101bp reads were generated.

5.11. Analysis of whole exome sequencing data

Sequence reads were aligned to the reference human genome GRCh37 using Burrows-Wheeler Aligner (BWA, v0.7.12)[160]. Local realignment, duplicate removal and base quality adjustment were performed using the Genome Analysis Toolkit (GATK, v3.6)[161] and Picard (http://broadinstitute.github.io/picard/). Somatic single nucleotide variants (SNVs) and small insertions and deletions (indels) were detected using MuTect (v1.1.4)[162] and Strelka (v1.0.15)[163], respectively. We filtered out SNVs and indels outside of the target regions, those with variant allelic fraction (VAF) of <1% and/or those supported by <3 reads. We excluded variants for which the tumor VAF was <5 times that of the paired non-tumor VAF, as well as those found at >5% global minor allele frequency of dbSNP (build 137). We further excluded variants identified in at least two of a panel of 123 non-tumor samples, including the 4 non-tumor samples included in the current study, captured and sequenced using the same protocols using the artifact detection mode of MuTect2 implemented in GATK. All indels were manually inspected using the Integrative Genomics Viewer[164]. To account for

the presence of somatic mutations that may be present below the limit of sensitivity of somatic mutation callers, we used GATK Unified Genotyper to interrogate the positions of all unique mutations in all samples from a given patient to define the presence of additional mutations.

Allele-specific copy number alterations (CNAs) were identified using FACETS (v0.5.5)[165] as previously described[166], which performs a joint segmentation of the total and allelic copy ratio and infers allele-specific copy number states. Somatic mutations associated with the loss of the wild-type allele (i.e. loss of heterozygosity, LOH) were identified as those where the lesser (minor) copy number state at the locus was 0. All mutations on chromosome X in male patients were considered to be associated with LOH. All gene amplifications and homozygous deletions were visually inspected using plots of raw Log2 and allelic copy ratios. Copy number states were collapsed to the gene-level based on the median values to coding gene resolution based all coding genes retrieved from the Ensembl (release GRCh37.p13).

The cancer cell fraction (CCF) of each mutation on the autosomes was inferred using the number of reads supporting the reference and the alternate alleles and the segmented Log_2 ratio from WES as input for ABSOLUTE (v1.0.6)[167]. Solutions from ABSOLUTE were manually reviewed as recommended[162,167]. A mutation was classified as clonal if its clonal probability, as defined by ABSOLUTE, was >50%, or if the upper bound of the 95% confidence interval of its CCF crosses 1. Mutations that did not meet the above criteria were considered subclonal.

Cancer genes were annotated according to the cancer gene lists described by Kandoth et al. (127 significantly mutated genes)[168], Lawrence et al., (Cancer5000-S gene set)[169], Fujimoto et al.[170] or the TCGA[90]. Mutations affecting hotspot residues[171,172] were annotated. Pathogenicity of missense mutations was predicted using CHASM (liver cancer predictor, viral or non-viral as appropriate)[173] and FATHMM (cancer predictor)[174].

Decomposition of the mutational signature was performed using deconstructSigs[175], based on the set of 30 mutational signatures (“signature.cosmic”, based on the signatures at http://cancer.sanger.ac.uk/cosmic/signatures[176,177]).

5.12. RNA sequencing

RNA extracted from all HCC biopsies (n=38) and the paired non-tumor biopsies were sequenced using RNA sequencing (RNA-seq). Tumor samples corresponding to Patients 1, 7-B (C959), 15-B and 29-A had to be excluded from further analyses because of low tumor cell content in the biopsy. 200 ng total RNA were used for RNA-seq library prep with the TruSeq Stranded Total RNA Library Prep Kit with Ribo-Zero Gold (Illumina) according to manufacturer's specifications. SR126 sequencing was performed on an Illumina HiSeq 2500 using v4 SBS chemistry at the Genomics Facility Basel according to the manufacturer's guidelines. Primary data analysis was performed with the Illumina RTA version 1.18.66.3.

5.13. Analysis of RNA sequencing data

Sequence reads were aligned to the human reference genome GRCh37 by STAR[178] using the two-pass approach. Transcript quantification was performed using RSEM[179]. For unsupervised cluster analysis, we retrieved the TCGA Liver dataset RNA-seq data ("V2_MapSpliceRSEM") from the Genomics Data Commons Data Portal[90]. We performed gene-level upper quartile normalization of the combined dataset to the fixed threshold 1000 as described in the TCGA study[90]. Genes whose expression was quantified to zero by RSEM in >75% of the samples were removed. RSEM values were subsequently log2-transformed, adding 0.5 to RSEM values prior to transformation. To identify genes with variable expression for clustering, genes with standard deviation <2 were excluded. Batch correction using the edgeR package[180] was performed to correct for systematic biases between the datasets. Cluster analysis was performed using hierarchical clustering using the Ward method and with a 1-Pearson correlation distance[90].

For the TCGA HCC cohort[90], images of diagnostic H&E slides were retrieved from the cbioportal (http://www.cbioportal.org; accessed December 2017)[181] and reviewed by two board-certified pathologists, Dr. Matthias S. Matter and Prof. Dr. Luigi M. Terracciano, according to the Edmondson grading system[89] for comparison purposes. Differential expression analysis between biopsies that yielded organoids and did not was performed using the edgeR package[180]. Specifically, genes with counts-per-million <1 in more than 5 HCC biopsies were removed. Normalization was performed using the "TMM" (weighted trimmed mean) method and differential expression was assessed using the quasi-likelihood F-test.

5.14. Statistical analysis

P values were calculated with Student's t-test, Fisher's exact test or Mann-Whitney test using Prism (GraphPad) software, as specified in the results section and in the figure legends.

6. RESULTS

6.1. Establishment of a patient-specific liver organoid biobank

The culture conditions to generate liver organoids from human tissue have been previously established with the use of surgically-resected liver specimens[127]. In our lab, we aimed to generate liver organoids from significantly smaller tissue pieces derived from needle biopsies. For this purpose, we modified the original protocol to avoid over-digestion and loss of tissue.

From March 2015 to June 2018, we established a biobank of liver organoids from patients undergoing diagnostic biopsy procedure. The biobank comprises more than 100 organoid lines encompassing all major liver disease backgrounds, namely, alcoholic liver disease (ALD), non-alcoholic fatty liver disease (NAFLD), hepatitis B virus (HBV) and hepatitis C virus (HCV) infections, primary biliary cirrhosis (PBC), drug-induced liver injury (DILI), and autoimmune hepatitis (AIH). In addition, we were able to generate organoids from two patients with Morbus Wilson, a rare genetic disease resulting in copper accumulation in liver and other organs. Among all liver organoids, some were obtained from the non-tumoral parenchyma of HCC patients[142] (see also section 6.2.).

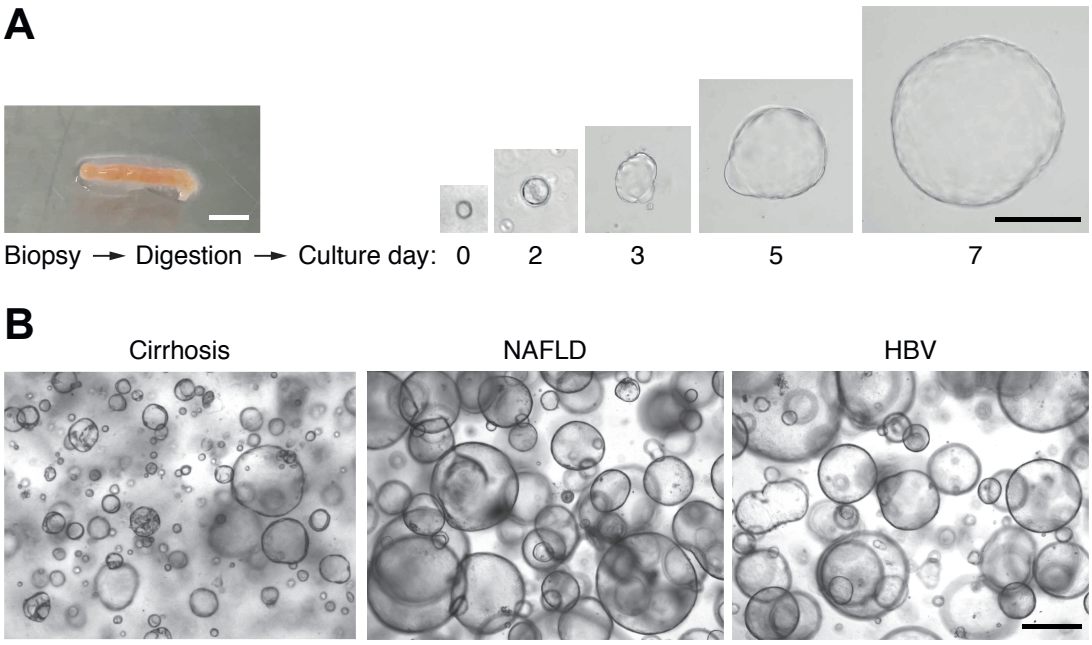

Figure 10. Generation of liver-derived organoids from needle biopsies. (**A**) Biopsy fragments are digested, and the resulting cell suspension embedded in BME2 as described in materials and methods (left side). Scale bar: 2 mm. Representative time-course of organoid growth from a single cell (right side). Scale bar: 200 μm (**B**) Representative images of organoids from patients with different disease backgrounds. Scale bar: 500 μm.

The success rate for generating liver organoids was 100%, and as expected they grew as single-cell layered cysts resembling the ductal epithelium when cultured in EM[127] that promotes their proliferation (Figure 10 and 11A). All liver-derived organoids are morphologically similar independently of their etiology.

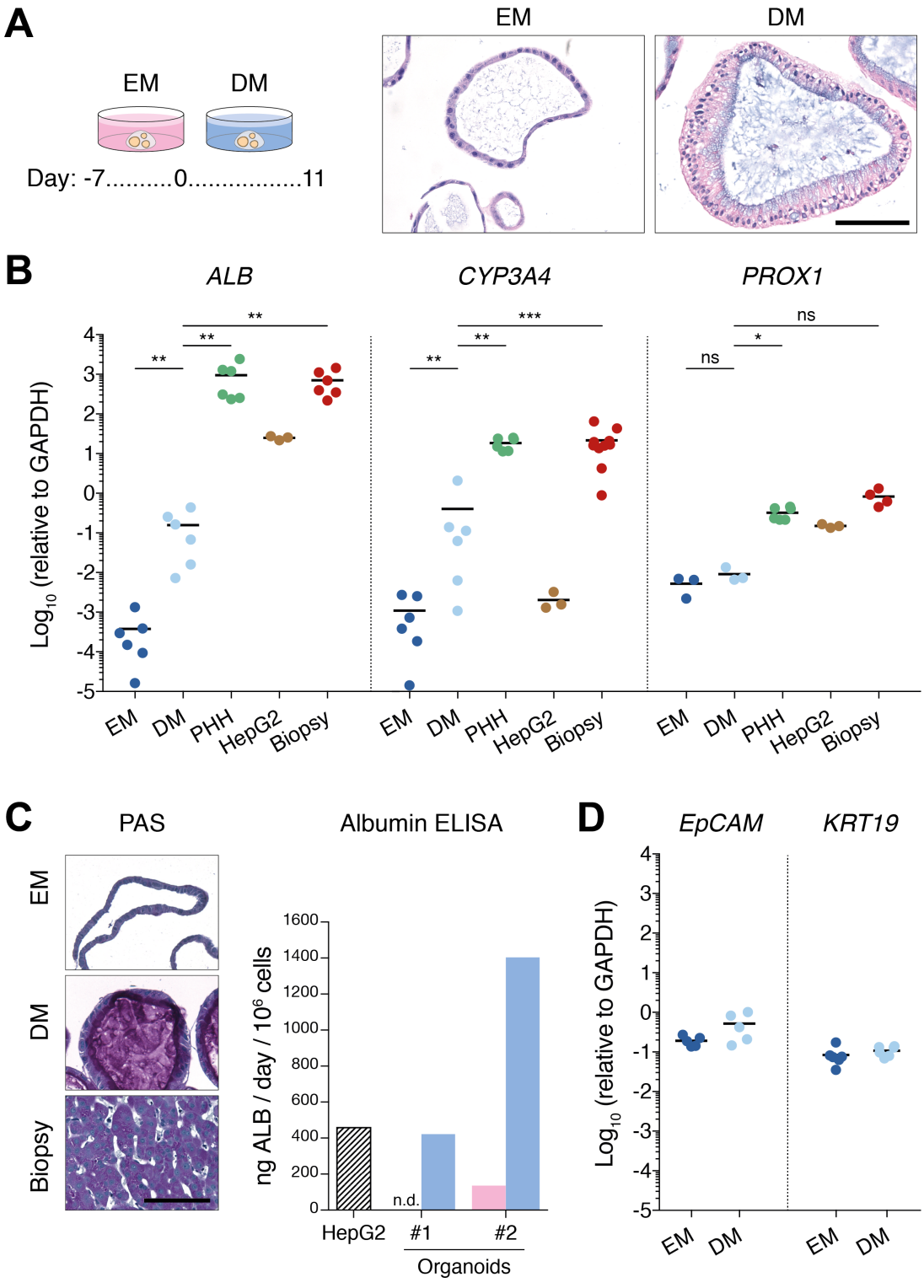

Figure 11. Differentiation of liver organoids into hepatocyte-like cells. (**A**) Left side: schematic representation of the differentiation protocol: organoids are cultured in EM supplemented with BMP7 for 7 days before switching to DM for

11 days. Right side: representative H&E images of undifferentiated (EM) and differentiated (DM) organoids. Scale bar: 100 μm. (**B**) RT qPCR analysis of common hepatocyte markers. EM: undifferentiated organoids; DM: differentiated organoids; PHH: primary human hepatocytes. Every dot represents one organoid line from a different patient, one biopsy, or biological replicate in case of HepG2 cells, respectively. (**C**) Glycogen production in undifferentiated and differentiated organoids assessed by Periodic Acid-Schiff (PAS) stain. Scale bar: 100 μm. Albumin secretion assessed by Sandwich ELISA in two different organoid lines (#1 and #2). (**D**) RT qPCR analysis of common cholangiocyte markers. n = 3–9 for RT qPCR experiments.

As described before, proliferating organoids are bipotent, since they can be differentiated into hepatocyte- and cholangiocyte-like cells. We used differentiation medium to direct the maturation of proliferating organoids into hepatocyte-like cells (HLCs)[127], a process that requires 11 days (Figure 11A). We then assessed the expression of hepatocyte-specific genes on proliferating, undifferentiated organoids and the corresponding differentiated organoids. Differentiated organoids were characterized by the induction of mature hepatocyte markers such as *ALB*, *PROX1* and *CYP3A4* (Figure 11B). Despite the strong upregulation, the expression levels of the different markers remained below the ones measured in PHH, liver biopsy or the HepG2 cell line, respectively. The strong upregulation of Albumin in differentiated organoids was further confirmed by measuring its secretion in the culture supernatant by sandwich ELISA. Interestingly, one organoid line secreted more Albumin than the HepG2 cells, despite the higher transcript expression levels measured by RT qPCR in the latter. We also detected glycogen synthesis in differentiated organoids (Figure 11C), another hallmark of hepatocyte function.

In the original report, liver-derived organoids were shown to originate from cells expressing EpCAM[127]. In the liver, only cholangiocytes express EpCAM implicating that liver organoids could originate from ductal cells or other cells within the biliary tree that have the ability to proliferate *in vitro* and differentiate into hepatocyte- or cholangiocyte-like cells, similarly to hepatoblasts during fetal liver development. We found a sustained expression of *EpCAM* even after differentiating organoids into the hepatocyte fate (Figure 11D). The same was true for another cholangiocyte marker, *KRT19*, suggesting that, despite the presence of liver-specific functions and expression of major hepatocyte markers, the differentiation efficiency of our current protocol for the hepatocyte fate is not optimal.

Because of the unique three-dimensional architecture of hepatocytes, we performed transmission electron microscopy (TEM) on undifferentiated as well as differentiated organoids to reveal microstructural details. We found common structural features between differentiated organoids and the originating liver tissue such as well-defined plasma membranes, tight junctions, desmosomes, rough endoplasmic reticulum, in-

tact mitochondria and the presence of microvilli (Figure 12). We could also detect glycogen, in line with the PAS staining. Interestingly, TEM revealed the presence of structures between adjacent cells that resembled bile canaliculi in the liver (Figure 12). These structures are only found between hepatocytes and this observation is in line with the detection of bile acid secretion by differentiated organoids as previously described[127]. In conclusion, we demonstrate the feasibility of deriving liver organoids from small biopsy specimens that retain similar characteristics of those derived from surgical resections.

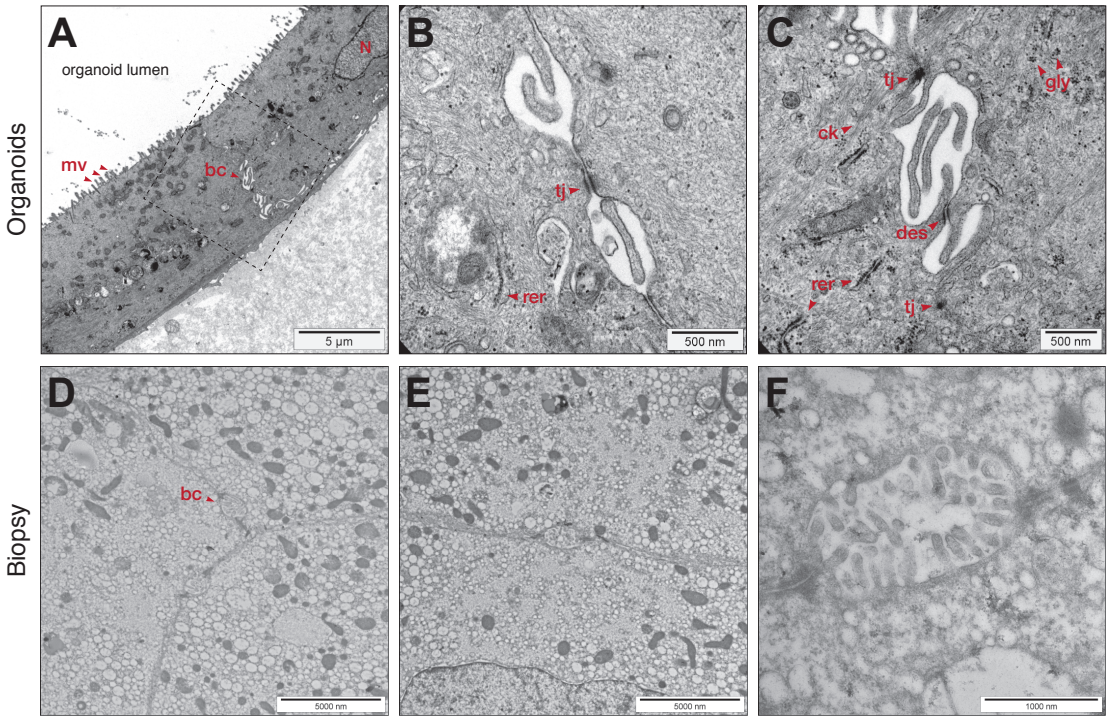

Figure 12. Transmission electron microscopy of liver organoids and primary liver tissue. (**A**) TEM images show the polarized organization of organoid-forming cells with microvilli facing the luminal side of the organoid cyst. (**B**) Undifferentiated- and (**C**) differentiated organoids form bile canaliculi-like structures between cells, morphologically similar to authentic bile canaliculi in liver tissue (**D-F**). Bc: bile canaliculi; ck: cytokeratin; des: desmosomes; gly: glycogen; mv: microvilli; N: nucleus; rer: rough endoplasmic reticulum; tj: tight junction.

6.2. Organoid models of liver cancers derived from tumor needle biopsies

The results for this part are presented in the following publication:

Nuciforo, S., Fofana, I., Matter, M.S., Blumer, T., Calabrese, D., Boldanova, T., Piscuoglio, S., Wieland, S., Ringnalda, F., Schwank, G., Terracciano, L.M., Ng, C.K.Y., Heim, M.H., 2018. Organoid Models of Human Liver Cancers Derived from Tumor Needle Biopsies. Cell Reports 24, 1363–1376.

Cell Reports
Resource

Organoid Models of Human Liver Cancers Derived from Tumor Needle Biopsies

Sandro Nuciforo,[1] Isabel Fofana,[1] Matthias S. Matter,[3] Tanja Blumer,[1] Diego Calabrese,[1] Tujana Boldanova,[1,2] Salvatore Piscuoglio,[3] Stefan Wieland,[1] Femke Ringnalda,[4] Gerald Schwank,[4] Luigi M. Terracciano,[3] Charlotte K.Y. Ng,[1,3] and Markus H. Heim[1,2,5,*]

[1]Department of Biomedicine, University Hospital Basel, University of Basel, 4031 Basel, Switzerland
[2]Clinic of Gastroenterology and Hepatology, University Hospital Basel, University of Basel, 4031 Basel, Switzerland
[3]Institute of Pathology, University Hospital Basel, University of Basel, 4031 Basel, Switzerland
[4]Institute of Molecular Health Sciences, ETH Zurich, Otto-Stern-Weg 7, HPL, 8093 Zürich, Switzerland
[5]Lead Contact
*Correspondence: markus.heim@unibas.ch
https://doi.org/10.1016/j.celrep.2018.07.001

SUMMARY

Hepatocellular carcinoma (HCC) is the most common primary liver cancer and the second most frequent cause of cancer-related mortality worldwide. The multikinase inhibitor sorafenib is the only treatment option for advanced HCC. Due to tumor heterogeneity, its efficacy greatly varies between patients and is limited due to adverse effects and drug resistance. Current *in vitro* models fail to recapitulate key features of HCCs. We report the generation of long-term organoid cultures from tumor needle biopsies of HCC patients with various etiologies and tumor stages. HCC organoids retain the morphology as well as the expression pattern of HCC tumor markers and preserve the genetic heterogeneity of the originating tumors. In a proof-of-principle study, we show that liver cancer organoids can be used to test sensitivity to sorafenib. In conclusion, organoid models can be derived from needle biopsies of liver cancers and provide a tool for developing tailored therapies.

INTRODUCTION

Hepatocellular carcinoma (HCC) is the most common primary liver cancer, accounting for 90% of all liver cancers, and is the second most frequent cause of cancer-related mortality worldwide (Marquardt et al., 2015). Main risk factors include infection with hepatitis B virus, hepatitis C virus, alcoholic liver disease, nonalcoholic fatty liver disease, and nonalcoholic steatohepatitis. Intrahepatic cholangiocellular carcinoma (CCC) represents the second most common primary liver cancer with main risk factors including primary sclerosing cholangitis, cysts of the biliary duct, and parasitic infection with liver flukes (Marquardt et al., 2015).

Currently available treatment options for HCC are unsatisfactory. In the past, conventional chemotherapies have been extensively tested, but none of them have improved survival (Chen et al., 2015). Major progress came with the introduction of the multikinase inhibitor sorafenib in 2008. In a landmark trial, sorafenib was found to significantly prolong median survival from 7.9 in the control group to 10.7 months in the sorafenib treatment group (Llovet et al., 2008). In the following years >10 additional targeted drugs were tested, but all failed to meet clinical endpoints in phase III trials (Llovet and Hernandez-Gea, 2014). More recently, the sorafenib derivative regorafenib (Bruix et al., 2017) and the immune-checkpoint inhibitor nivolumab (El-Khoueiry et al., 2017) showed efficacy in second-line treatments for advanced HCC. However, given the limited efficacy of current HCC treatment options, there is an urgent need for new therapies for HCC.

A major obstacle in preclinical drug development is the lack of appropriate cell culture model systems. Current *in vitro* cell culture models of HCC are based on conventional hepatoma and hepatocarcinoma cell lines that fail to recapitulate key features of tumor tissues such as three-dimensional tumor architecture, cellular heterogeneity, and cell-cell interactions. The recently developed organoid technology could overcome these limitations because it allows differentiation of tissue stem cells into functional organ-like structures (Clevers, 2016). Indeed, the generation of three-dimensional organoid cultures from patient-derived tumors has been a major breakthrough in cancer biology. Over the past 3 years, tumor-derived organoids have been described for prostate (Gao et al., 2014), pancreatic (Boj et al., 2015), colorectal (van de Wetering et al., 2015), breast (Sachs et al., 2018), and bladder cancers (Lee et al., 2018).

In this study, we report the successful generation of tumor organoid cultures from needle biopsies obtained from patients with HCC. We demonstrate that HCC organoids recapitulate the histological features of the originating tumor *in vitro*. Moreover, injection of HCC organoids into immunodeficient mice results in the formation of tumors that also recapitulate the histological features of the original biopsy. Additionally, we show that HCC organoids maintain the genomic features of their originating tumors during long-term culturing for up to 32 weeks. Finally, we demonstrate that HCC organoids respond to sorafenib treatment with variable sensitivity.

RESULTS

Establishment of HCC Organoid Cultures

We obtained tumor and non-tumor liver samples from patients undergoing diagnostic needle biopsies for suspected HCCs

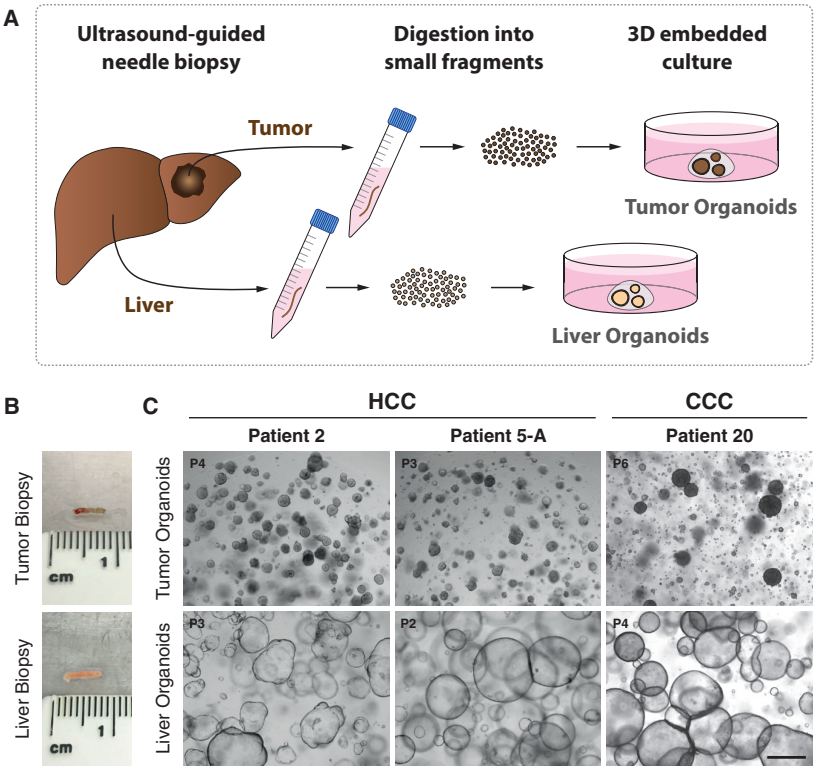

Figure 1. Establishment of Organoid Cultures from Needle Biopsies of Hepatocellular Carcinoma and Paired Non-tumor Liver Tissues

(A) Schematic workflow of organoid generation from needle biopsies.

(B) Representative biopsy pieces of tumor and liver tissue used for organoid generation.

(C) Representative bright-field images of tumor and paired non-tumor liver tissue organoids from three different patients. Tumor organoids form compact spheroids, whereas liver organoids from non-tumor liver tissue grow as cystic structures. Organoids were imaged at the indicated passage numbers. Scale bar: 500 μm.

(Figures 1A and 1B). Biopsies were performed under ultrasound guidance using a coaxial needle biopsy technique that allows for obtaining up to five samples from the same location in a tumor (described in the Experimental Procedures). This multiple sampling procedure allowed a comprehensive characterization of all samples by histopathology for clinical diagnosis and Edmondson staging (Edmondson and Steiner, 1954), by immunohistochemical staining to identify tumor markers, and by whole-exome sequencing and RNA sequencing (RNA-seq) for molecular analysis. In total, we established 10 HCC-derived organoid lines from eight patients (Table 1). For patient 5, we generated organoid lines from two different tumor nodules (5-A and 5-B). For patient 12, we established two tumor organoid lines from two different locations of the same large tumor nodule (12-I and 12-II; Table 1). We also established organoid cultures from non-tumor liver biopsies in all patients (Figures 1C and S1A; Table S1). HCC organoids present morphologically as compact spheroids without a lumen but occasionally forming pseudoglands (Figure 1C), whereas non-tumor liver-derived organoids, originating from cholangiocytes, grow as single-cell layered cysts resembling the ductal epithelium (Huch et al., 2015) (Figure S1A). The underlying disease spectrum of our patient cohort encompasses the major risk factors for HCC, viral hepatitis, nonalcoholic fatty liver disease (NAFLD), and alcoholic liver disease (ALD) (Table 1). Furthermore, the cohort represents all different clinical stages of HCC according to the Barcelona Clinic Liver Cancer (BCLC) staging system (Llovet et al., 1999) (Table 1).

The success rate for the generation of HCC organoids was 26% based on the number of cultured tumor biopsies (10 out of a total of 38 HCC biopsies). HCC organoids were obtained in 8 of the 24 HCC patients included in the study (33%) (Table S1). We did not find a correlation between a number of clinically relevant patient characteristics and the success or failure to generate HCC organoids from their tumors (Figure 2A). On the other side, there was a strong correlation with the histopathological grading of the HCCs: all HCC organoids are derived from poorly differentiated tumors (Edmondson grades III and IV) (Figure 2A; Table 1). Furthermore, KI-67 staining of tumor biopsies showed significantly higher cancer cell proliferation rates in samples that could be propagated as tumor organoids compared with samples that failed (Figures S2A and S2B).

The transcriptome data of the tumor biopsies were used to analyze the distribution of our samples within a reference set from The Cancer Genome Atlas (TCGA) (Cancer Genome Atlas Research Network, 2017) using an unsupervised hierarchical clustering analysis. Overall, our samples distributed evenly in the entire reference dataset, but the eight samples from which we could derive HCC organoids preferentially located in a subclass located at the left end of the clustering tree (Figure 2B). Because all of our HCC organoids originated from poorly differentiated HCCs (Edmondson grades III and IV), we also performed the clustering analysis using the subset of poorly differentiated HCCs from TCGA HCC database as a reference. In this analysis, our samples distributed over the entire spectrum of the tree (Figure 2C). We conclude that the organoid model system strongly selects for Edmondson grade III and IV HCCs, but within this group of poorly differentiated HCCs, there seems to be no further selection of a specific molecular subtype.

HCC Organoids Recapitulate the Histopathological Characteristics of the Originating Tumor

To investigate whether the histological characteristics of the originating tumors were preserved in the HCC organoids, two expert pathologists with expertise in hepatopathology

Table 1. HCC and CCC Patient Data Table

Patient	Biopsy ID	Sex	Age (Years)	Tumor	Liver Disease(s)	Cirrhosis	BCLC	Edmondson	Growth Pattern	AFP (IU/mL)
1	C655	male	55	HCC	HCV; ALD	no	C	III	trabecular-pseudoglandular	269
2	C798	male	73	HCC	NAFLD	no	C	III	solid-trabecular	20'377
5-A	C948	male	57	HCC	HCV; ALD	yes	C	III	trabecular	12′054
5-B	C949							III	trabecular	
9	C975	male	59	HCC	HCV; ALD	yes	B	III	solid	250
12-I	D045	male	69	HCC	HCV	no	A	III	solid-trabecular	7'852
12-II	D046							III	solid-trabecular	
13	D091	female	61	CCC	none	no	–	–	–	4.4
16	D141	male	59	LELCC	HBV	yes	–	–	–	2.1
20	D178	female	63	CCC	none	no	–	–	–	3.1
25	D324	male	58	HCC	HCV	yes	D	III	solid-trabecular	104'710
27	D359	male	86	HCC	NAFLD	no	A	III	trabecular	5'917
29-A	D386	male	80	HCC	ALD; NAFLD	no	A	IV	solid	49.8

Clinical staging was done according to the Barcelona Clinic Liver Cancer (BCLC) staging system (Llovet et al., 1999). Serum alpha-fetoprotein (AFP) concentrations were obtained from the clinical charts of the patients. Edmondson grade (Edmondson and Steiner, 1954) and the growth pattern were determined in each biopsy on H&E-stained sections by two experienced hepato-pathologists (M.S.M. and L.M.T.). All CCC tumors were poorly differentiated. AFP, alpha-fetoprotein; ALD, alcoholic liver disease; BCLC, Barcelona Clinic Liver Cancer; CCC, cholangiocellular carcinoma; HBV, hepatitis B virus; HCC, hepatocellular carcinoma; HCV, hepatitis C virus; LELCC, lymphoepithelioma-like cholangiocarcinoma; NAFLD, nonalcoholic fatty liver disease.

performed histological analysis and diagnostic evaluation on the original biopsies and their tumor organoids on paraffin-embedded sections. Notably, HCC organoids maintained the growth pattern and differentiation grade of the originating primary tumors (Figure 3A). For example, HCC organoids derived from patient 2 displayed a solid growth pattern with an Edmondson differentiation grade III as in the originating tumor (Figure 3A). Likewise, tumor organoids from patient 12 formed pseudoglands (Figure 3A), a feature that was also present in the original HCC of this patient. Importantly, long-term culturing up to 1 year did not alter the histological properties of the HCC organoids (Figure S1B). As expected, immune cell infiltrates and tumor stromal cells were not propagated in the organoids.

We next assessed whether the expression of alpha-fetoprotein (AFP), a tumor marker for HCC (Table 1), was maintained in the corresponding organoids. Immunohistochemical analysis revealed consistent distribution and expression intensity of AFP between organoids and their original tumor biopsy tissue (Figure 3B). The same was true for three additional biomarkers commonly used for histological HCC diagnosis, Glypican 3, glutamine synthetase, and heat shock protein 70 (GPC3, GS, and HSP70, respectively) (Di Tommaso et al., 2009) (Figure S1C). Some of the HCCs also stained positive for the biliary cell markers Keratin 7 (KRT7) and Keratin 19 (KRT19). Again, the expression of these markers was maintained in the organoids (Figure 3C). Taken together, these results demonstrate that HCC organoids retain the phenotypic characteristics of their originating tumors.

HCC Organoids Give Rise to Tumors upon Injection into Immunodeficient Mice

To assess whether HCC organoids retained the ability to form bona fide tumors in mice, we injected HCC organoids subcutaneously into immunodeficient mice. So far, 6 of the 10 HCC organoids could be stably propagated in mice (Figures 4A and 4D). Two organoids failed to grow despite repeated transplantations. Two organoids were injected recently and the outcome could not yet be determined (Figure 4D). Of note, all successfully transplanted organoids gave rise to xenograft tumors that recapitulated the histopathological features and the tumor marker expression (Figure 4B) of the originating organoids and the original tumors. In contrast, and as expected, none of the paired non-tumor liver organoids gave rise to neoplasms.

HCC Organoids Retain the Somatic Genetic Alterations of the Originating Tumor

To assess whether the HCC organoids recapitulate the genetic alterations of the originating tumor, we subjected DNA from seven HCC organoid lines, their originating tumor biopsies, as well as the paired non-tumor biopsies to whole-exome sequencing (WES). WES was performed to median depths of 85×, 95×, and 50× in the organoids, biopsies, and non-tumor counterparts, respectively (Table S2). The number of somatic mutations in organoids (median 165, range 117–180) did not significantly differ from that of the corresponding tumor biopsies (median 146, range 127–207; $p = 0.78$, Mann-Whitney U test; Table S3).

Of the total somatic and the subgroup of non-synonymous somatic mutations found in the HCC biopsies, a median of 88% and 90%, respectively, was observed in the corresponding HCC organoids at early passage of culturing (P3–P4) (Figures 5A, S3, and S4; Tables S3 and S4). Similar proportions (all somatic: 86%; non-synonymous somatic: 88%) were observed in three representative cases where late-passage HCC organoids ($\geq$P8) were profiled (Figures S3 and S7A; Tables S3 and S4). Nearly all non-synonymous somatic mutations in bona fide cancer genes, including all of those in *TP53* (p.Arg209fs in patient 2,

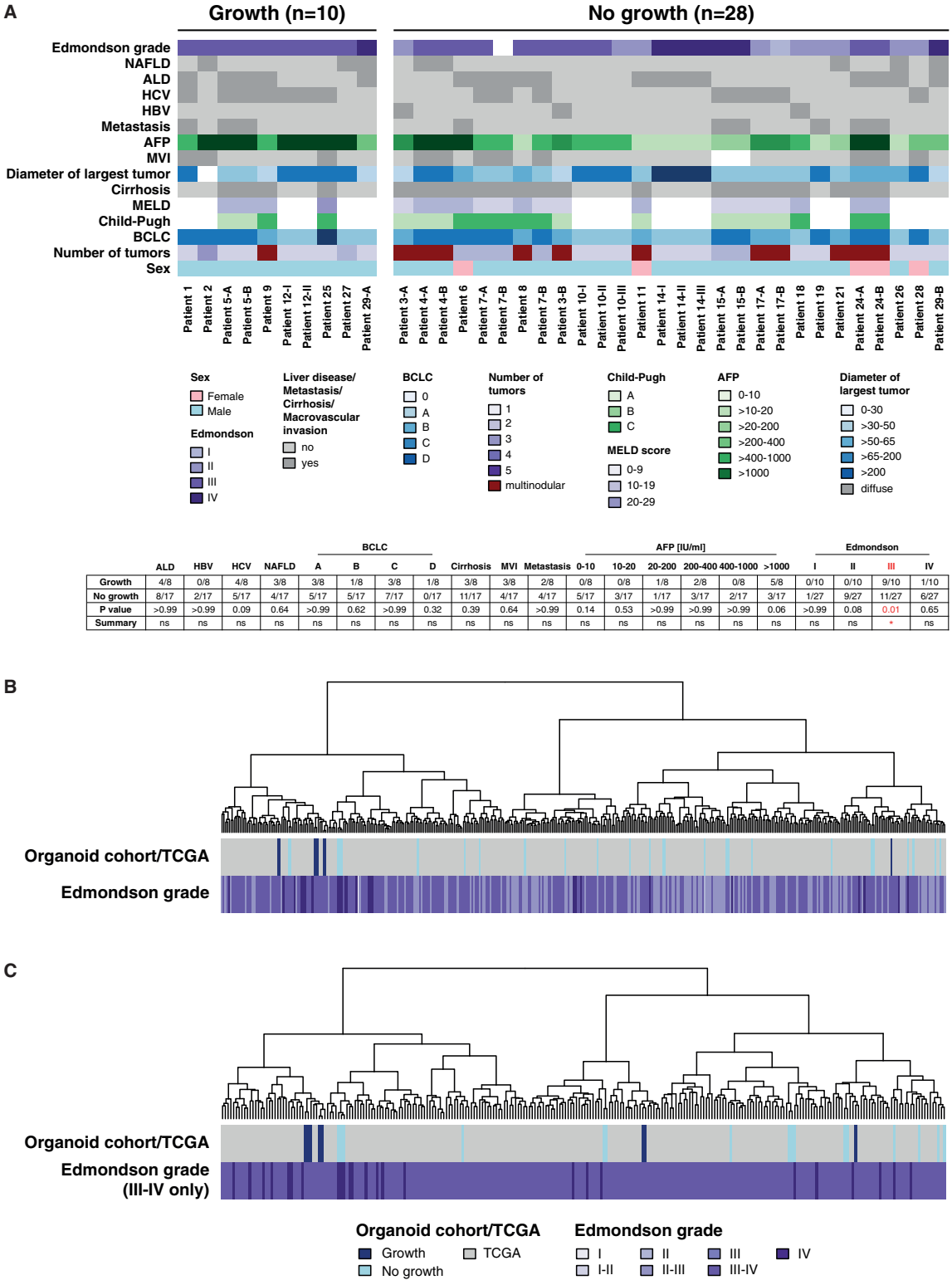

					BCLC								AFP [IU/ml]						Edmondson			
	ALD	HBV	HCV	NAFLD	A	B	C	D	Cirrhosis	MVI	Metastasis	0-10	10-20	20-200	200-400	400-1000	>1000	I	II	III	IV
Growth	4/8	0/8	4/8	3/8	3/8	1/8	3/8	1/8	3/8	3/8	2/8	0/8	0/8	1/8	2/8	0/8	5/8	0/10	0/10	9/10	1/10
No growth	8/17	2/17	5/17	4/17	5/17	5/17	7/17	0/17	11/17	4/17	4/17	5/17	3/17	1/17	3/17	2/17	3/17	1/27	9/27	11/27	6/27
P value	>0.99	>0.99	0.09	0.64	>0.99	0.62	>0.99	0.32	0.39	0.64	>0.99	0.14	0.53	>0.99	>0.99	>0.99	0.06	>0.99	0.08	0.01	0.65
Summary	ns	ns	ns	ns	ns	ns	ns	ns	ns	ns	ns	ns	ns	ns	ns	ns	ns	ns	ns	*	ns

(legend on next page)

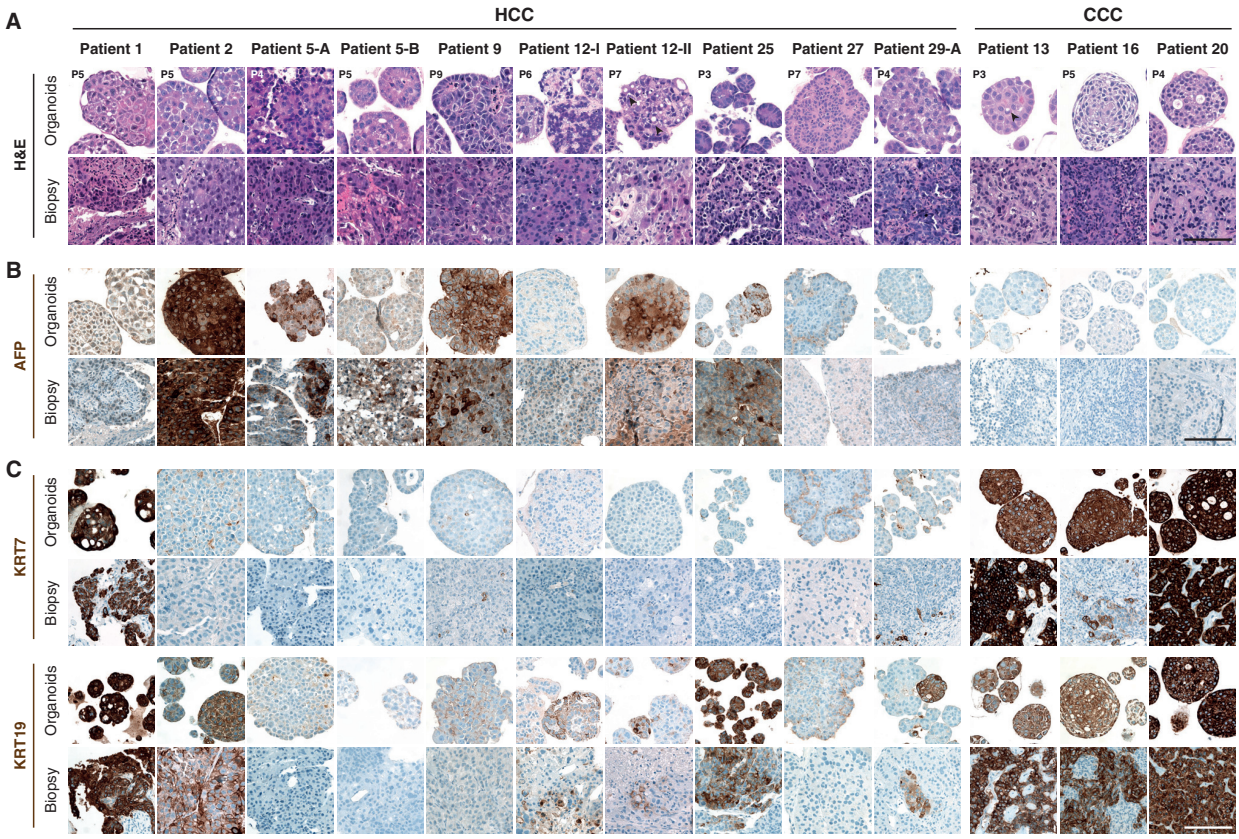

Figure 3. Histopathological Characteristics of HCC and CCC Organoids and Their Primary Tumors

(A) Histological sections of HCC and CCC organoids and their original tumors stained with H&E. The originating tumors display primarily a solid-trabecular architectural pattern with poor differentiation (Edmondson grades III and IV), features that are maintained in the corresponding HCC organoids. Arrowheads indicate pseudoglandular structures in HCC organoids and intracytoplasmic lumen in CCC organoids.

(B) AFP expression detected by immunohistochemistry on organoids and original biopsies.

(C) Expression of biliary markers KRT7 and KRT19 detected by immunohistochemistry on organoids and original biopsies. Organoids were imaged at the indicated passage numbers.

Scale bars: 100 μm.

hotspot p.Arg342* in patient 9, and p.Val157Phe in patient 12-II), *ARID1A* (c.5125-2A > T in patients 5-A and 5-B), *CTNNB1* (hotspot p.Ser45Ala and p.Arg528Cys in patients 5-A and 5-B), *TSC1* (p.Gln767* in patient 2), and *LRP1B* (p.Cys2903Arg in patient 9), were found in the organoids at both early and late passages (Figures 5B, S3, and S7B). Of all the non-synonymous mutations in bona fide cancer genes, only two were lost in the corresponding HCC organoid (*BRD7* p.Phe340Ile in patient 9; *ARHGAP35* p.Glu1273Ala in patient 12-I). However, these mutations were subclonal in the originating HCC biopsies (Figures S3D and S4A), have not been previously reported in HCC, and are predicted to be passenger mutations (Table S4). Overall, we identified a median of 19 (range 8–29) and 14 (range 5–24) novel somatic and non-synonymous somatic mutations in the HCC organoids that were not present in the originating biopsies, representing a median of 15% and 12% of the mutations present

Figure 2. Clinical, Histopathological, and Molecular Features of HCC Biopsies Used for Organoid Generation

(A) Color-coded table of patient characteristics of all biopsies (n = 38) used for organoid generation. Edmondson grade (Edmondson and Steiner, 1954) and the growth pattern were determined in each biopsy on H&E-stained sections by two experienced hepato-pathologists (M.S.M. and L.M.T.). Clinical data were extracted from the electronic patient information system of the hospital. Of note, only the Edmondson grade III was a significant determinant of successful organoid generation (p = 0.01, Fisher's exact test, two-sided). For the Edmondson grade, calculations were performed per biopsy, whereas all other parameters were calculated per patient. ALD, alcoholic liver disease; AFP, alpha-fetoprotein; BCLC, Barcelona Clinic Liver Cancer; HBV, hepatitis B virus; HCV, hepatitis C virus; MVI, macrovascular invasion; NAFLD, nonalcoholic fatty liver disease.

(B and C) Unsupervised hierarchical clustering analysis.

(B) Biopsy (organoid) cohort (this study) combined with all HCCs from TCGA cohort.

(C) Biopsy (organoid) cohort (this study) combined with high-grade (Edmondson grades III and IV) HCCs from TCGA cohort.

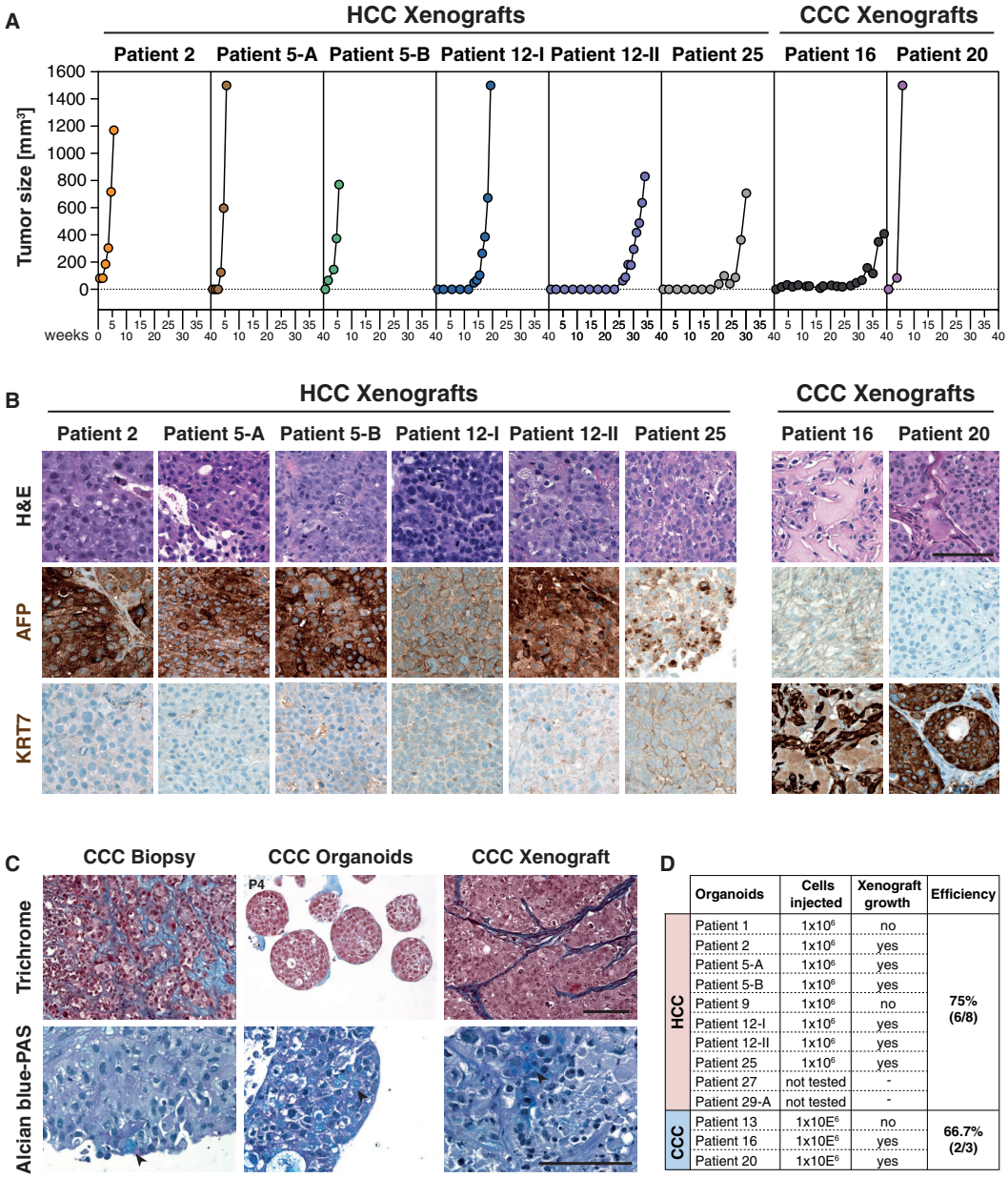

Figure 4. Histological Analysis of Xenografts Derived from HCC and CCC Organoids

(A) Growth curves of the xenograft tumors.

(B) Histological sections of xenograft tumors derived from HCC and CCC organoids stained with H&E. The HCC marker AFP and the biliary marker KRT7 were detected by immunohistochemistry. Scale bar: 100 μm.

(C) Trichrome and Alcian blue-PAS staining on biopsy, derivative organoids, and xenograft of patient 20. Collagen-rich areas representing the desmoplastic stroma reaction are colored in blue in Trichrome-stained sections. Mucin production appears light blue in sections stained with Alcian blue-PAS (arrowheads). Organoids were imaged at the indicated passage numbers. Scale bars: 100 μm.

(D) Statistics of the xenograft experiments.

in the HCC organoids, respectively. Most of these novel mutations did not occur in bona fide cancer genes. Indeed, in four of the seven tumor organoid lines, no additional non-synonymous mutations in cancer genes were identified. In patient 5-A, an *ASXL1* mutation was found in both early- and late-passage HCC organoids, a *PDGFRA* mutation was found only in the early passage, and an *AXIN2* mutation only in the late passage, but not in the originating HCC biopsies (Figures 5B and

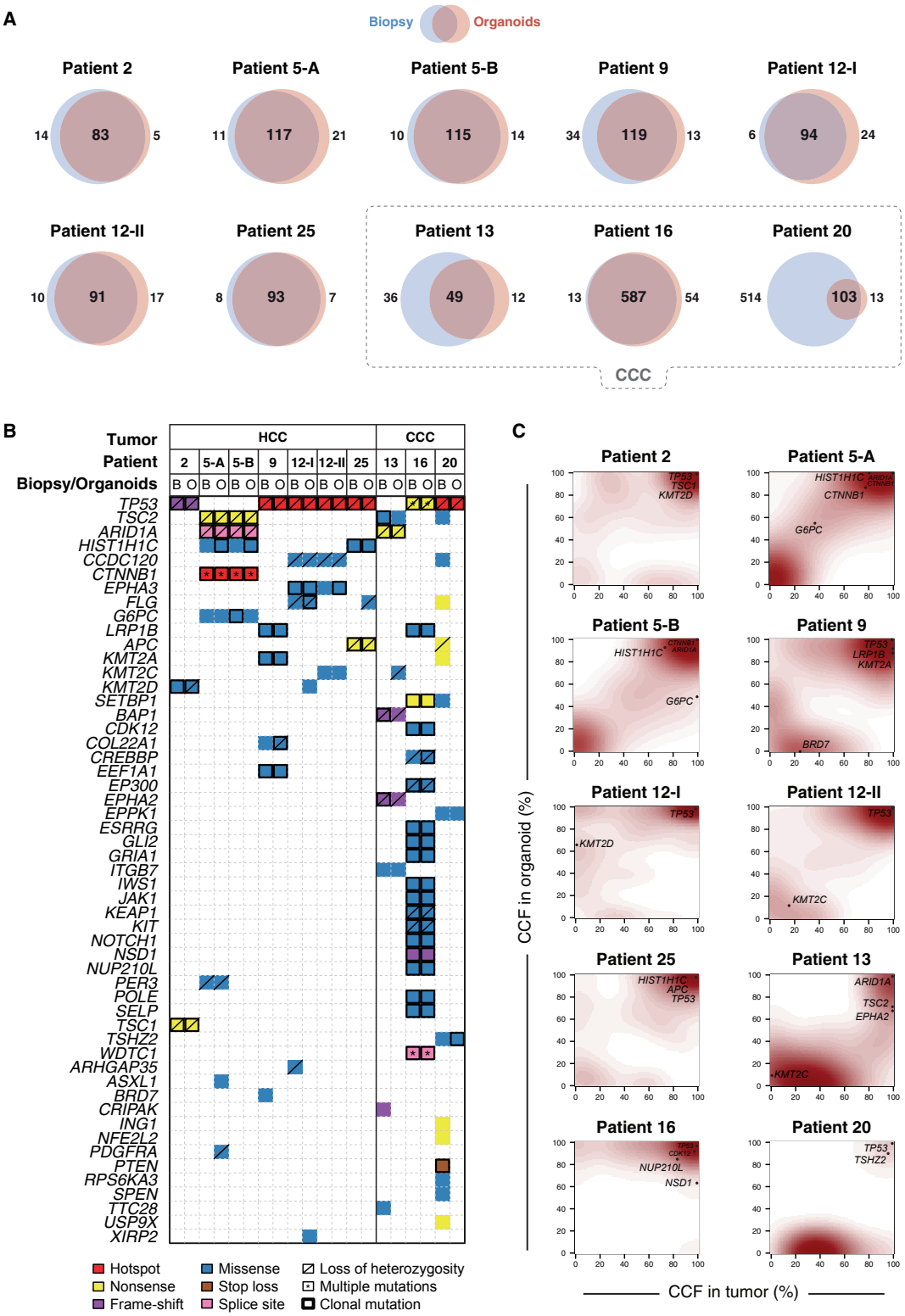

(legend on next page)

S7B). However, 23%–46% of the organoid-specific mutations were present in both early- and late-passage organoids originating from patient 2, patient 5-A, and patient 5-B (Table S3), strongly suggesting that a substantial proportion of the HCC organoid-specific mutations were likely present in the originating tumors at low frequencies, rather than being genuinely novel.

A detailed analysis of the cancer cell fraction (CCF) of the somatic mutations (i.e., the proportion of cancer cells harboring a given genetic alteration) between the organoid cultures and their matched originating tumor indicated that both harbored subclonal mutations (Figures 5C and S3–S6). For example, we observed similar extents of intratumor heterogeneity between the biopsies and organoids of patient 5 (Figures 5C and S3–S6). This has been previously observed in colorectal cancer organoids (van de Wetering et al., 2015) and is likely to be a genuine advantage of organoid cultures compared with cancer cell lines.

Copy number analysis showed that most amplifications were preserved in HCC organoids, and the overall patterns of copy number alterations were similar between the biopsies and the derivative HCC organoids at early and late passage (Figures S7C and S7D). For instance, the amplifications of chr1q21.3 (encompassing *MCL1*, *SETDB1*, *ARNT*, and *MLLT11*) in patient 5 (A and B), 8q24.13-24.23 (*MYC* and *NDRG1*) in patient 2, and 11q13.2-13.4 (*CCND1*, *FGF19*, *FGF4*, and *FGF3*) in patient 12-II were all found in their corresponding organoids. However, the heterogeneity observed at mutational level was also present at the copy number alteration (CNA) level. In fact, an amplification on 18q12.2 restricted to the HCC biopsy of patient 9, but not seen in the respective HCC organoids and two amplifications on 19q12 (*CCNE1*) and 19q13.2 (*MAP3K10* and *AKT2*), was found only in the derivative HCC organoids.

We next investigated whether the biological and chemical processes that shape the mutational landscape were maintained in the organoid cultures. The analysis of the mutational signatures demonstrated that the mutational landscape of the HCC biopsies and the organoids was largely driven by mutational processes associated with signatures 1 (associated with aging), 3 (homologous recombination DNA repair deficiency), 6 (mismatch repair deficiency), and 16 (previously found in liver cancer with unknown etiology) (Alexandrov et al., 2013) (Figure S8). The mutational signatures were remarkably consistent between the organoids and the originating HCC biopsies. These results suggest that the mutational processes that drive tumor development were maintained in the organoids. Of note, the same patterns of mutational signatures were also maintained in late-passage organoids (Figure S8).

Taken together, these results demonstrate that the HCC organoids derived from tumor biopsies largely maintain the genetic alterations and mutational signatures observed in their originating HCCs. Importantly, mutations and amplifications affecting bona fide cancer genes found in the biopsies were preserved in the organoids. Furthermore, in line with previously published reports (Lee et al., 2018; van de Wetering et al., 2015), each HCC organoid line retained a remarkable intratumoral mutational heterogeneity.

Generation of Organoids from Intrahepatic CCCs

In our consecutive series of patients with suspected primary liver cancer who had a diagnostic needle biopsy (Table S1) there were four cases of intrahepatic CCCs and one case of a rare variant of CCC, a lymphoepithelioma-like cholangiocarcinoma. All five cases were poorly differentiated CCCs. In three cases we successfully established CCC-derived tumor organoids. Morphologically, CCC organoids resembled HCC organoids and formed compact spheroids (Figures 1C and 3A), whereas the corresponding non-tumor liver organoids formed single-cell layered epithelial cysts as expected (Figures 1C and S1A). CCC organoids displayed similar histological properties such as trabecular and/or solid growth with cytoplasmic eosinophilia and highly atypical cells like the poorly differentiated adenocarcinomas from which they were derived (Figure 3A). Furthermore, some cells within CCC organoids and their originating biopsies formed intracytoplasmic lumens and produced Mucin, two characteristic features of adenocarcinomas (Figures 3A and 4C). As expected, AFP expression was not detected in CCC tumor biopsies and organoids (Figure 3B). All CCC organoid lines expressed typical biliary markers such as KRT7 and KRT19 consistent with the expression pattern in the originating tumor biopsies (Figure 3C).

The genetic analysis revealed hyper-mutator phenotypes in patient 16 (with the lymphoepithelioma-like cholangiocarcinoma) and in patient 20 (Figure 5). Both tumors had >500 somatic mutations. In patient 16, most of the mutations were maintained in the organoids, whereas in patient 20, most were lost during the derivation of organoids (Figure 5A). Interestingly, the vast majority of somatic mutations in patient 16 were present in >80% of the tumor cells, whereas in patient 20, most of them were found only in subclonal cell populations (Figures S5 and S6; Table S4). It is likely that most of the subclones in the originating tumor were lost during the early steps of organoid culture. Patient 13 had 85 non-synonymous somatic mutations in the tumor. 36 were not preserved in the organoids. Most of them were subclonal and were not in bona fide cancer genes. The presumed cancer driver mutations were preserved (Figure 5).

Figure 5. Repertoire of Genetic Alterations Found in the HCC and CCC Organoids and Their Originating Tumors

(A) Venn diagrams illustrate the number of somatic non-synonymous mutations present in each HCC biopsy and their derivative HCC organoids. The dashed line denotes CCC-derived tumors and corresponding organoids.

(B) Repertoire of somatic non-synonymous mutations affecting cancer genes (Fujimoto et al., 2016; Kandoth et al., 2013; Lawrence et al., 2014; Cancer Genome Atlas Research Network, 2017). The effects of the mutations are color-coded according to the legend, with hotspots (Chang et al., 2016; Gao et al., 2017) colored in red. Multiple non-synonymous mutations in the same gene are indicated by an asterisk. Loss of heterozygosity of the wild-type allele of a mutated gene is represented by a diagonal bar, and mutations found to be clonal by ABSOLUTE (Carter et al., 2012) are indicated by a black box.

(C) Contour plots illustrate the distribution of the cancer cell fractions (CCFs) of somatic mutations in the tumors and their corresponding organoids, with the increasing shades of red indicating higher number of somatic mutations at a given CCF.

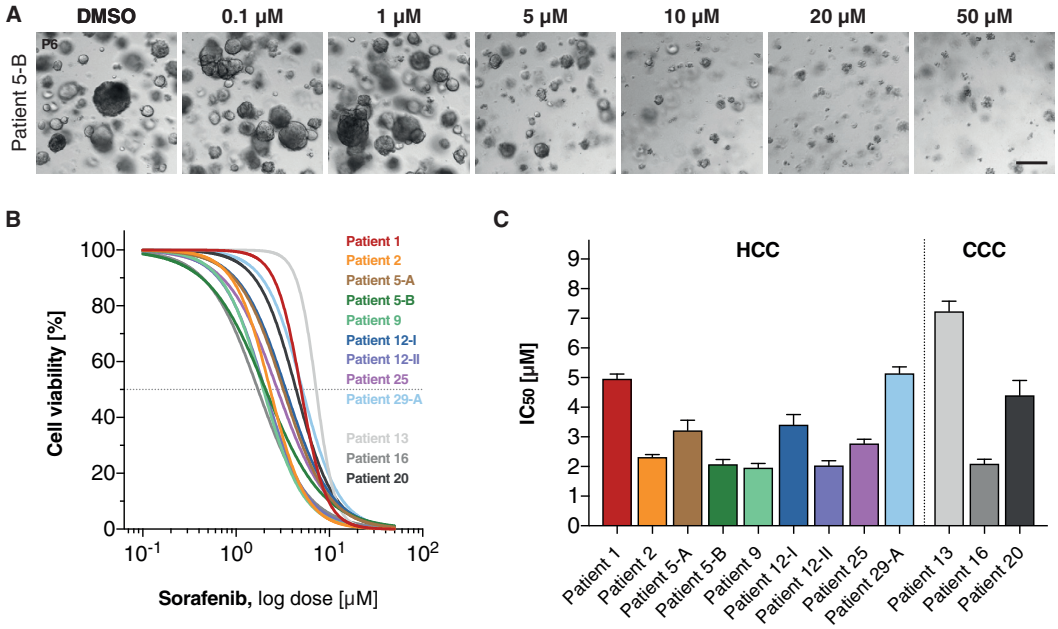

Figure 6. Differential Drug Responses in Patient-Derived HCC and CCC Organoids under Sorafenib Treatment

HCC and CCC organoids were exposed to sorafenib at the indicated concentration for 6 days. DMSO-treated tumor organoids were used as control.

(A) Representative bright-field images of sorafenib-treated HCC organoids (patient 5-B). Scale bar: 200 µm.

(B) Sorafenib reduces cell viability of HCC and CCC organoids in a dose-dependent manner. The dashed line represents the IC_{50}. Data are presented as the percentage of control DMSO-treated tumor organoids and are the mean of at least two independent experiments performed in duplicate.

(C) Differential IC_{50} (in µM) of HCC and CCC organoids shown as mean ± SEM. Patient numbers correspond to Table 1.

We could successfully transplant the CCC organoids from patients 16 and 20 into immunodeficient mice. No xenografts could be established from patient 13 despite repeated transplantation attempts (Figure 4D). Surprisingly, histologic analysis of the xenograft tissue revealed tumor areas with a desmoplastic stroma reaction, a typical CCC feature that was also present in the originating tumors, but not in the organoids due to the lack of stromal cells (Figure 4C). This demonstrates that the capability to induce a desmoplastic reaction and thus to reproduce the tumor microenvironment *in vivo* is intrinsically programmed in CCC cells. Finally, Mucin-producing cells were also detected in the xenograft tumors from CCC organoids (Figure 4C).

HCC and CCC Organoids Display Variable Sensitivity to Sorafenib

In order to assess whether HCC-derived organoids would be a suitable system for preclinical drug development, we treated HCC organoid cultures with different concentrations of sorafenib and monitored cell viability with CellTiter-Glo. The concentration range was based on pharmacokinetic data from patients treated with sorafenib (Nexavar) (Abou-Alfa et al., 2006). In our *in vitro* assay, sorafenib reduced HCC organoid growth in a dose-dependent manner (Figure 6A) with half-maximal inhibitory concentration (IC_{50}) values that varied by 2.5-fold from 2.0 to 5.0 µM (Figures 6B and 6C). Direct comparison of *in vitro* sorafenib activity with the clinical response was not feasible because none of the patients from whom we generated organoid cultures were treated with sorafenib. The validation of the organoid models as test systems for sorafenib response *in vivo* will require the recruitment of many more patients and the generation of a sizable number of additional HCC organoids derived from patients treated with sorafenib.

We also tested the efficacy of sorafenib on the three CCC organoid lines. Notably, a CCC organoid derived from a rare subtype of CCC (lymphoepithelioma-like CCC, patient 16) responded to sorafenib treatment *in vitro* with IC_{50} values comparable with sorafenib-sensitive HCC organoids (Figures 6B and 6C). Sorafenib is not an established treatment for CCCs, but it has recently been explored in a multicenter prospective study that showed a modest effect on disease control rate (Luo et al., 2017).

Taken together, our results demonstrate that organoids derived from biopsies of primary liver cancers can be used to test tumor-specific sensitivities to growth-inhibitory substances.

DISCUSSION

In vitro studies of HCC biology have so far been restricted to a limited number of hepatoma and HCC cell lines. Most of them have been established decades ago, and it is unclear how well they represent the tumor biology of HCCs. HCC organoids overcome many of the limitations of these cell lines. They can be directly linked to a patient and to spatiotemporal information such as a specific tumor nodule or a metastasis, or a specific

time during the evolution of the cancer in a patient. Importantly, we found that the organoids are polyclonal and thereby preserve an important feature of the originating tumor that is linked to cancer evolution, immune evasion, and resistance to oncostatic and targeted therapies. Patient-derived tumor organoids have recently been described for prostate (Gao et al., 2014), pancreatic (Boj et al., 2015), colorectal (van de Wetering et al., 2015), breast (Sachs et al., 2018), and bladder cancer (Lee et al., 2018). Broutier et al. (2017) reported the establishment of organoid cultures derived from resections of primary liver cancers. In our study, we report the establishment of organoids from HCC needle biopsies, overcoming a major limitation of approaches that use surgically resected HCC specimens. Indeed, surgical resection is a treatment option for the minority of HCC patients with early tumor stages and/or a non-cirrhotic liver. These patients usually do not receive systemic therapies. In contrast, biopsies can also be obtained from patients with intermediate and advanced tumor stages who frequently receive systemic therapies. The use of biopsies therefore allows for establishment of an organoid biobank that reflects the entire spectrum of HCCs. Furthermore, such a biobank can be enriched to include clinical data such as response to treatments, resistance development, and survival.

The use of tumor biopsies also allowed a comparison of tumor and organoids. Of note, several biopsies from the same location in a tumor could be obtained using an ultrasound-guided coaxial biopsy technique. The resulting set of biopsies is mutually representative and can be used for multidimensional analysis. We found a striking similarity between originating tumors and organoids in routine histopathology and immunostaining analysis. Moreover, the individual tumor features were also maintained after transplantations into immunodeficient mice. We conclude that these morphological features are inherently programmed in the tumor cells and are not subject to the tumor environment (Figure 3). Furthermore, the expression of well-established HCC biomarkers, as well as the mutational landscape, is preserved in HCC organoids (Figure 5). When compared with the previous study by Broutier et al. (2017) that used resected specimens, our tissue collection procedure allowed for collection of non-tumor liver biopsies at a site distant from the tumor nodule(s) to generate non-tumor liver organoids for all patients and to perform patient-specific normalization of our genomic and transcriptomic data.

In our series of tumor biopsies we derived HCC organoids with a success rate of ~26% (per number of biopsies) and 33% (per number of patients). This is lower compared with the reported success rates for pancreatic cancer (75%–83%) (Boj et al., 2015) and colorectal cancers (90%) (van de Wetering et al., 2015), possibly because the cell of origin of HCCs, the hepatocytes, lack features of epithelial stem cells that favor their propagation in the organoid culture system.

However, our success rate is in line with a recent study by Pauli et al. (2017) reporting an average success rate of ~38% across different tumor types. In their report, the authors used small-needle biopsies as tumor tissue source in some of their cases and conclude that the major limitation to establish tumor organoids was the insufficient amount of fresh tissue. Indeed, given the limited amount of starting material (needle biopsies), we could not set up a systematic screening of different culture systems to improve the derivation efficiency. Broutier et al. (2017) tried to optimize the culture conditions for the generation of liver cancer organoids by removing some of the growth factors contained in the original media recipe in order to reduce the outgrowth of normal liver organoids. However, the changes they performed did not result in organoid generation from all of their tumor specimen. Based on informed guesses, we tried to optimize culture conditions in a small number of cases where we had more than one biopsy as a starting material. For example, we removed compounds with potential negative effects on HCC proliferation such as Forskolin, *N*-acetyl-L-cysteine, nicotinamide, and HGF from the medium, and added FGF19, a factor with potential growth-promoting effects for HCCs. However, these limited efforts did not result in the establishment of additional HCC organoid lines. Nevertheless, we anticipate that additional efforts in refining the media recipes (Fujii et al., 2016), and possibly also the use of tailored 3D matrices (Gjorevski et al., 2016), to specifically accommodate the growth of HCC- and CCC-derived organoids, respectively, will improve the success rate. This would be a prerequisite for using HCC organoids as patient-specific *in vitro* models of drug sensitivity with the aim to inform treatment decisions on an individualized basis. Of note, the time required to expand the organoid cultures for drug testing is presently 4–12 weeks. Urgent treatment decisions will therefore not rely on *in vitro* drug testing of individual patient-derived organoids, even if the success rate should be much higher in the future. More realistically, systematic drug testing in a large enough number of HCC organoids will allow to predict patient responses to different treatments based on matching molecular characteristics of tumor biopsies and organoids (Drost and Clevers, 2018).

One other potential reason for the limited success rate could be that HCC organoids can be generated only from a restricted subset of HCCs. We therefore compared clinical, histopathological, and molecular features of HCCs that could be propagated as organoids with HCCs that could not. No significant correlations were found with a comprehensive set of clinical data (Figure 2A). Indeed, HCC organoids could be derived from patients with all major underlying liver diseases and different clinical stages of HCC, demonstrating the potential of the organoid technique for building up larger biobanks representing the entire clinical spectrum of liver cancer. On the other side, there was a significant correlation with one of the histopathological features, the Edmondson grade of the tumors. HCC organoids could only be generated from poorly differentiated tumors. It is conceivable that the generation of HCC organoids requires a cell proliferation rate threshold that is not reached in highly differentiated, slow-growing Edmondson grade I and II tumors. This is supported by our finding that the proliferation marker KI-67 and cell-cycle pathway genes were upregulated in tumor biopsies with successful organoid derivations compared with those where organoids could not be generated (Figures S2A and S2B; Table S5). These data are in line with those from Broutier et al. (2017) showing that only moderately to poorly differentiated HCCs with a KI-67 index >5% were able to generate organoids. Of note, other histopathological features in our HCC cohort such as the percentage of viable tumor cells in the biopsy, the amount

of stroma or immune cell infiltration, the growth pattern of the tumor, or the degree of tumor necrosis were not correlated with success or failure of organoid derivation (Table S1).

Finally, to investigate whether HCC organoids can only be derived from a specific molecular subtype of HCC, we compared transcriptome data of all of our tumor biopsies with a reference set of poorly differentiated HCCs from the TCGA database (Cancer Genome Atlas Research Network, 2017). We found no enrichment of our samples in distinct subclasses of HCCs (Figure 2C). We conclude that the organoid technique described in this manuscript allows the generation of a heterogeneous tumor organoid biobank that is a representative sample of the entire clinical, histopathological, and molecular spectrum of poorly differentiated HCCs.

The analysis of the relative frequency of non-synonymous somatic mutations in the tumor biopsies and the HCC organoids revealed the expected preservation of highly prevalent putative driver mutations. However, it also revealed that mutations present in only a subset of tumor cells, i.e., subclone-specific mutations, were also preserved, often with surprisingly similar relative frequencies between tumor biopsies and HCC organoids (Figures 5C and S3–S6; Table S4). This is somewhat unexpected, because it does not support a model where tumor organoids are derived from a single cancer stem cell. There is compelling evidence that intestinal organoids can be derived from single LGR5-positive stem cells (Clevers, 2016). For liver-derived organoids, this is less clear (Huch et al., 2015). It remains to be investigated whether the stem cell model is applicable for HCC tumor organoids. In any case, the coexistence of different cancer cell subclones with different sensitivities to targeted therapies is an important factor linked to therapy failure (Fisher et al., 2013). Therefore, we believe that organoid models will play a major role in the development of novel drug candidates able to target different genetic subclones within tumors to impede the selection of resistant cells present at low frequencies at therapy onset. Furthermore, the knowledge of the patient-specific genetic background will allow the unique opportunity to correlate response to specific drugs with putative driver mutations, a prerequisite for future efforts of personalized management of targeted therapies.

EXPERIMENTAL PROCEDURES

Human Tissues and Biopsy Procedure

Human tissues were obtained from patients undergoing diagnostic liver biopsy at the University Hospital Basel. Written informed consent was obtained from all patients. The study was approved by the ethics committee of the northwestern part of Switzerland (Protocol Number EKNZ 2014-099). Ultrasound (US)-guided needle biopsies were obtained from tumor lesion(s) with a coaxial liver biopsy technique that allows taking several biopsy samples through a single biopsy needle tract. After local anesthesia, the introducer needle was advanced 2–3 cm into the liver parenchyma. In case of a focal lesion, the needle was positioned precisely at the tumor border. The trocar of the introducer needle was removed, and up to five cylindrical biopsies of ~1 mm diameter and 10–30 mm in length were obtained with an automatic spring-loaded biopsy needle (BioPince). The introducer needle was kept in place during the entire procedure to ensure that all specimens came from the same area of the tumor. One cylinder was fixed in formalin and paraffin-embedded for diagnosis and staging. Additional cylinders were immediately snap-frozen in liquid nitrogen for later use in DNA and RNA extraction or embedded in O.C.T. (Tissue-Tek) and frozen using standard procedures. For organoid generation, biopsy pieces were placed in advanced DMEM/F-12 (GIBCO). For control tissue, all patients who underwent US-guided HCC biopsy also got a biopsy of the liver parenchyma at a site distant from the tumor. The needle tract was filled with absorbable gelatin sponge before removal of the introducer needle.

Organoid Culture

Tumor biopsy fragments designated for organoid generation typically measured ~1 mm × 5–10 mm corresponding to a volume of ~3.9–7.9 mm^3. They were transported to the laboratory on ice and further processed for organoid generation within 20 min after collection. For tumor organoid generation, biopsies underwent a limited digestion to small-cell clusters. We avoided complete digestion into single cells because it has been reported that preservation of cell-cell contacts enhances derivation efficiency (Kondo et al., 2011). Tumor tissue was minced and shortly (maximum [max.] 2–4 min) digested with 2.5 mg/mL collagenase IV (Sigma), 0.1 mg/mL DNase (Sigma) at 37°C. The yield of the procedure varied because of differences in the size of the tumor biopsy available for the generation of organoids and the variable content of viable tumor cells in the biopsies. Cell clusters were then seeded into reduced growth factor BME2 (Basement Membrane Extract, Type 2; Amsbio). After polymerization of BME2, expansion medium (Huch et al., 2015) was added to the cells. The composition is advanced DMEM/F-12 (GIBCO) supplemented with 1:50 B-27 (GIBCO), 1:100 N-2 (GIBCO), 10 mM nicotinamide (Sigma), 1.25 mM *N*-acetyl-L-cysteine (Sigma), 10 nM [Leu^{15}]-gastrin (Sigma), 10 μM forskolin (Tocris), 5 μM A83-01 (Tocris), 50 ng/mL EGF (PeproTech), 100 ng/mL FGF10 (PeproTech), 25 ng/ml HGF (PeproTech), 10% RSpo1-conditioned medium, (homemade), and 30% Wnt3a-conditioned medium (homemade). In the few cases for which enough biopsy material was available, we tried an adapted version of the culture medium in comparison with the normal one. The adapted medium lacked some of the original components reported to have a negative effect on HCC cell proliferation (forskolin, *N*-acetyl-L-cysteine, nicotinamide, HGF) and contained FGF19 because of the frequent amplification of the *FGF19* gene detected in HCCs and its positive effect on proliferation of HCC cells. However, these attempts did not result in the establishment of additional HCC organoid lines. Organoid cultures from non-tumor liver biopsies were generated as previously described (Huch et al., 2015). Tumor organoids were passaged after dissociation with 0.25% Trypsin-EDTA (GIBCO). Non-tumor liver organoids were passaged by mechanical dissociation through a fire-polished Pasteur-pipette or incubation in 0.25% Trypsin-EDTA (GIBCO) for 2 min. Cryovials were prepared at regular intervals by dissociating organoids and resuspending in Recovery Cell Culture Freezing Medium (GIBCO) prior to freezing.

We could prepare frozen stocks of early (≤P4) passages from all the samples that yielded tumor organoids. All organoid lines could be kept in long-term cultures with regular splitting for at least 1 year. All organoid cultures were regularly tested for *Mycoplasma* contamination with the MycoAlert Mycoplasma Detection Kit (Lonza) according to the manufacturer's instructions.

Organoid Xenotransplantation

All experiments involving organoid transplantations into mice were performed in strict accordance with Swiss law and were approved by the ethics committee of the northwestern part of Switzerland (Protocol Number EKNZ 2014-099) and the Animal Care Committee of the Canton Basel-Stadt, Switzerland. Tumor organoids, corresponding to 1 × 10^6 cells, were released from BME2 by incubating in Cell Recovery Solution (Corning), resuspended in ~100 μL 50:50 (v/v) BME2:expansion medium, and injected subcutaneously into immunodeficient non-obese diabetic (NOD) severe combined immunodeficiency (SCID) gamma (NSG) mice (The Jackson Laboratory) at young age (6–8 weeks). Paired non-tumor liver organoids were used as negative control.

Histology and Immunohistochemistry

Liver biopsies from tumoral and non-tumor tissue, as well as tumor organoid xenografts, were fixed in 4% phosphate-buffered formalin and embedded in paraffin using standard procedures. Additional biopsies were also embedded in O.C.T. (Tissue-Tek) and frozen using standard procedures. Tumor organoids were released from BME2 by incubating in Cell Recovery Solution (Corning)

following the manufacturer's instructions. Organoids were then fixed in freshly prepared 4% formalin solution in PBS for 30 min at room temperature following dehydration and paraffin embedding. Sections were subjected to H&E, Masson's trichrome, Alcian blue-periodic acid-Schiff (PAS), as well as immunohistochemical staining, using standard procedures. Histopathological evaluation was assessed by two board-certified pathologists (M.S.M. and L.M.T.). Tumors were classified based on architecture and cytological features, and graded according to the Edmondson grading system (Edmondson and Steiner, 1954).

For immunohistochemistry, the following primary antibodies were used for automated staining on a Benchmark XT device (Ventana Medical Systems): AFP (Ventana catalog number [Cat. No.] 760-2603), GS (Ventana Cat. No. 760-4898), GPC3 (Ventana Cat. No. 790-4564), HSP70 (Biocare Medical CM407A), Keratin 7 (Ventana Cat. No. 790-4462), Keratin 19 (Ventana Cat. No. 760-4281), and KI-67 (Ventana Cat. No. 760-4286).

Drug Treatment

Sorafenib tosylate (Cat. No. S-8502) was purchased from LC Laboratories, dissolved in DMSO at 10 mM aliquots, and stored at −20°C. Tumor organoids were plated at a density of 5×10^3 cells in 15 μL BME2 droplets in order to form organoids. At day 6, sorafenib was added to the medium, and cell viability was measured after 6 days using CellTiter-Glo 3D reagent (Promega). Luminescence was measured on a Synergy H1 Multi-Mode Reader (BioTek Instruments). Results were normalized to vehicle (=100% DMSO). Curve fitting was performed using Prism (GraphPad) software and the nonlinear regression equation. All experiments were performed at least two times in duplicate. Results are shown as mean ± SEM.

DNA and RNA Extraction

Genomic DNA from tumor organoids was extracted using the DNeasy Blood & Tissue kit (Qiagen) following the manufacturer's instructions. Genomic DNA and total RNA from biopsies were extracted using the ZR-Duet DNA and RNA MiniPrep Plus kit (Zymo Research) following the manufacturer's instructions. Prior to extraction, biopsies were crushed in liquid nitrogen to facilitate lysis. Extracted DNA was quantified using the Qubit Fluorometer (Invitrogen).

Whole-Exome Sequencing

DNA extracted from eight HCC biopsy-derived organoid lines (patients 1, 2, 5-A, 5-B, 9, 12-I, 12-II, and 25), three CCC biopsy-derived organoid lines (patients 13, 16, and 20), the corresponding original biopsies, and the control paired non-tumor biopsies were sequenced using whole-exome sequencing. The eight HCC biopsies were derived from six patients and for three of the biopsies, early- and late-passage organoids were profiled (Table S2). The tumor biopsy sample corresponding to patient 1 had to be excluded from further analyses because of low tumor cell content in the biopsy. Whole-exome capture was performed using the SureSelectXT Clinical Research Exome (Agilent) platform according to the manufacturer's guidelines. Sequencing was performed on an Illumina HiSeq 2500 at the Genomics Facility Basel according to the manufacturer's guidelines. Paired-end 101-bp reads were generated.

Whole-Exome Sequencing Analysis

Sequence reads were aligned to the reference human genome GRCh37 using Burrows-Wheeler Aligner (BWA, v0.7.12) (Li and Durbin, 2009). Local realignment, duplicate removal and base quality adjustment were performed using the Genome Analysis Toolkit (GATK, v3.6) (McKenna et al., 2010) and Picard (http://broadinstitute.github.io/picard/). Somatic single nucleotide variants (SNVs) and small insertions and deletions (indels) were detected using MuTect (v1.1.4) (Landau et al., 2013) and Strelka (v1.0.15) (Saunders et al., 2012), respectively. We filtered out SNVs and indels outside of the target regions: those with variant allelic fraction (VAF) of <1% and/or those supported by <3 reads. We excluded variants for which the tumor VAF was <5 times that of the paired non-tumor VAF, as well as those found at >5% global minor allele frequency of dbSNP (build 137). We further excluded variants identified in at least two of a panel of 123 non-tumor samples, including the 4 non-tumor samples included in the current study, captured and sequenced using the same protocols using the artifact detection mode of MuTect2 implemented in GATK. All indels were manually inspected using the Integrative Genomics Viewer (Thorvaldsdóttir et al., 2013). To account for the presence of somatic mutations that may be present below the limit of sensitivity of somatic mutation callers, we used GATK Unified Genotyper to interrogate the positions of all unique mutations in all samples from a given patient to define the presence of additional mutations.

Allele-specific CNAs were identified using FACETS (v0.5.5) (Shen and Seshan, 2016) as previously described (Piscuoglio et al., 2016), which performs a joint segmentation of the total and allelic copy ratio and infers allele-specific copy number states. Somatic mutations associated with the loss of the wild-type allele (i.e., loss of heterozygosity [LOH]) were identified as those where the lesser (minor) copy number state at the locus was 0. All mutations on chromosome X in male patients were considered to be associated with LOH. All gene amplifications and homozygous deletions were visually inspected using plots of raw $\log_2$ and allelic copy ratios. Copy number states were collapsed to the gene level based on the median values to coding gene resolution based on all coding genes retrieved from the Ensembl (release GRCh37.p13).

The CCF of each mutation on the autosomes was inferred using the number of reads supporting the reference and the alternate alleles, and the segmented $\log_2$ ratio from WES as input for ABSOLUTE (v1.0.6) (Carter et al., 2012). Solutions from ABSOLUTE were manually reviewed as recommended (Carter et al., 2012; Landau et al., 2013). A mutation was classified as clonal if its clonal probability, as defined by ABSOLUTE, was >50%, or if the upper bound of the 95% confidence interval of its CCF crosses 1. Mutations that did not meet the above criteria were considered subclonal.

Cancer genes were annotated according to the cancer gene lists described by Kandoth et al. (2013) (127 significantly mutated genes), Lawrence et al. (2014) (Cancer5000-S gene set), Fujimoto et al. (2016), or the TCGA (Cancer Genome Atlas Research Network, 2017). Mutations affecting hotspot residues (Chang et al., 2016; Gao et al., 2017) were annotated. Pathogenicity of missense mutations was predicted using CHASM (liver cancer predictor, viral or non-viral as appropriate) (Carter et al., 2009) and FATHMM (cancer predictor) (Shihab et al., 2013).

Decomposition of the mutational signature was performed using deconstructSigs (Rosenthal et al., 2016), based on the set of 30 mutational signatures ("signature.cosmic," based on the signatures at https://cancer.sanger.ac.uk/cosmic/signatures; Alexandrov et al., 2013; Nik-Zainal et al., 2016).

RNA-Seq

RNA extracted from all HCC biopsies (n = 38; Table S1) and the paired non-tumor biopsies were sequenced using RNA-seq. Tumor samples corresponding to patients 1, 7-B (C959), 15-B, and 29-A had to be excluded from further analyses because of low tumor cell content in the biopsy. 200 ng total RNA was used for RNA-seq library prep with the TruSeq Stranded Total RNA Library Prep Kit with Ribo-Zero Gold (Illumina) according to manufacturer's specifications. SR126 sequencing was performed on an Illumina HiSeq 2500 using v4 SBS chemistry at the Genomics Facility Basel according to the manufacturer's guidelines. Primary data analysis was performed with the Illumina RTA version 1.18.66.3.

RNA Sequencing Analysis

Sequence reads were aligned to the human reference genome GRCh37 by STAR (Dobin et al., 2013) using the two-pass approach. Transcript quantification was performed using RSEM (Li and Dewey, 2011). For unsupervised cluster analysis, we retrieved the TCGA Liver dataset RNA-seq data ("V2_MapSpliceRSEM") from the Genomics Data Commons Data Portal (Cancer Genome Atlas Research Network, 2017). We performed gene-level upper quartile normalization of the combined dataset to the fixed threshold 1,000 as described in the TCGA study (Cancer Genome Atlas Research Network, 2017). Genes whose expression was quantified to zero by RSEM (Li and Dewey, 2011) in >75% of the samples were removed. RSEM values were subsequently $\log_2$-transformed, adding 0.5 to RSEM values prior to transformation. To identify genes with variable expression for clustering, genes with standard deviation < 2 were excluded. Batch correction using the edgeR package (Nikolayeva and Robinson, 2014) was performed to correct for systematic biases between the datasets. Cluster analysis was performed using hierarchical

clustering using the Ward method and with a 1-Pearson correlation distance (Cancer Genome Atlas Research Network, 2017).

For the TCGA HCC cohort (Cancer Genome Atlas Research Network, 2017), images of diagnostic H&E slides were retrieved from the cbioportal (http://www.cbioportal.org; accessed December 2017) (Gao et al., 2013) and reviewed by two expert hepato-pathologists (M.S.M. and L.M.T.) according to the Edmondson grading system (Edmondson and Steiner, 1954) for comparison purposes. Differential expression analysis between biopsies that did or did not yield organoids was performed using the edgeR package (Nikolayeva and Robinson, 2014). Specifically, genes with <1 count per million in more than five HCC biopsies were removed. Normalization was performed using the "TMM" (weighted trimmed mean) method, and differential expression was assessed using the quasi-likelihood F-test.

Statistical Analysis

p values were calculated with Fisher's exact test or Mann-Whitney test using Prism (GraphPad) software, as specified in the Results section and in the figure legends.

Data and Software Availability

Sequence data have been deposited at the European Genome-phenome Archive (EGA), which is hosted by the EBI and the CRG, under accession number EGAS00001003115.

SUPPLEMENTAL INFORMATION

Supplemental Information includes eight figures and five tables and can be found with this article online at https://doi.org/10.1016/j.celrep.2018.07.001.

ACKNOWLEDGMENTS

We thank all the patients who participated in this study, Hans Clevers for providing the Wnt3a cell line and Calvin Kuo for providing the RSpo1-Fc cell line, Petra Hirschmann for performing histopathological staining, Christian Beisel (Genomics Facility Basel) for performing whole-exome and RNA-seq, and Xueya Wang and Sylvia Ketterer for excellent technical assistance. This work was funded by European Research Council Synergy grant 609883 (MERiC) and by SystemsX.ch grant MERiC. L.M.T. and S.P. had support from Oncosuisse (KFS-3995-08-2016) and S.P. from the Swiss National Science Foundation (Ambizione PZ00P3_168165).

AUTHOR CONTRIBUTIONS

M.H.H., S.N., and I.F. conceived the study and designed experiments; M.H.H. and T. Boldanova recruited patients, performed biopsies, and collected and curated clinical annotation data; S.N., T. Blumer, and D.C. performed the experiments; M.S.M. and L.M.T. performed the histopathological analysis; S.P. and C.K.Y.N. processed, computed, and analyzed the genomics data; F.R. and G.S. provided essential reagents and protocols for establishment of organoid cultures; all authors were involved in data analysis and interpretation of the results; M.H.H. coordinated the study; S.N., I.F., S.W., S.P., C.K.Y.N., and M.H.H. wrote the manuscript.

DECLARATION OF INTERESTS

The authors declare no competing interests.

Received: March 13, 2018
Revised: May 24, 2018
Accepted: June 29, 2018
Published: July 31, 2018

REFERENCES

Abou-Alfa, G.K., Schwartz, L., Ricci, S., Amadori, D., Santoro, A., Figer, A., De Greve, J., Douillard, J.Y., Lathia, C., Schwartz, B., et al. (2006). Phase II study of sorafenib in patients with advanced hepatocellular carcinoma. J. Clin. Oncol. *24*, 4293–4300.

Alexandrov, L.B., Nik-Zainal, S., Wedge, D.C., Aparicio, S.A., Behjati, S., Biankin, A.V., Bignell, G.R., Bolli, N., Borg, A., Børresen-Dale, A.L., et al.; Australian Pancreatic Cancer Genome Initiative; ICGC Breast Cancer Consortium; ICGC MMML-Seq Consortium; ICGC PedBrain (2013). Signatures of mutational processes in human cancer. Nature *500*, 415–421.

Boj, S.F., Hwang, C.I., Baker, L.A., Chio, I.I., Engle, D.D., Corbo, V., Jager, M., Ponz-Sarvise, M., Tiriac, H., Spector, M.S., et al. (2015). Organoid models of human and mouse ductal pancreatic cancer. Cell *160*, 324–338.

Broutier, L., Mastrogiovanni, G., Verstegen, M.M., Francies, H.E., Gavarró, L.M., Bradshaw, C.R., Allen, G.E., Arnes-Benito, R., Sidorova, O., Gaspersz, M.P., et al. (2017). Human primary liver cancer-derived organoid cultures for disease modeling and drug screening. Nat. Med. *23*, 1424–1435.

Bruix, J., Qin, S., Merle, P., Granito, A., Huang, Y.-H., Bodoky, G., Pracht, M., Yokosuka, O., Rosmorduc, O., Breder, V., et al.; RESORCE Investigators (2017). Regorafenib for patients with hepatocellular carcinoma who progressed on sorafenib treatment (RESORCE): a randomised, double-blind, placebo-controlled, phase 3 trial. Lancet *389*, 56–66.

Carter, H., Chen, S., Isik, L., Tyekucheva, S., Velculescu, V.E., Kinzler, K.W., Vogelstein, B., and Karchin, R. (2009). Cancer-specific high-throughput annotation of somatic mutations: computational prediction of driver missense mutations. Cancer Res. *69*, 6660–6667.

Carter, S.L., Cibulskis, K., Helman, E., McKenna, A., Shen, H., Zack, T., Laird, P.W., Onofrio, R.C., Winckler, W., Weir, B.A., et al. (2012). Absolute quantification of somatic DNA alterations in human cancer. Nat. Biotechnol. *30*, 413–421.

Chang, M.T., Asthana, S., Gao, S.P., Lee, B.H., Chapman, J.S., Kandoth, C., Gao, J., Socci, N.D., Solit, D.B., Olshen, A.B., et al. (2016). Identifying recurrent mutations in cancer reveals widespread lineage diversity and mutational specificity. Nat. Biotechnol. *34*, 155–163.

Chen, K.W., Ou, T.M., Hsu, C.W., Horng, C.T., Lee, C.C., Tsai, Y.Y., Tsai, C.C., Liou, Y.S., Yang, C.C., Hsueh, C.W., and Kuo, W.H. (2015). Current systemic treatment of hepatocellular carcinoma: a review of the literature. World J. Hepatol. *7*, 1412–1420.

Clevers, H. (2016). Modeling development and disease with organoids. Cell *165*, 1586–1597.

Di Tommaso, L., Destro, A., Seok, J.Y., Balladore, E., Terracciano, L., Sangiovanni, A., Iavarone, M., Colombo, M., Jang, J.J., Yu, E., et al. (2009). The application of markers (HSP70 GPC3 and GS) in liver biopsies is useful for detection of hepatocellular carcinoma. J. Hepatol. *50*, 746–754.

Dobin, A., Davis, C.A., Schlesinger, F., Drenkow, J., Zaleski, C., Jha, S., Batut, P., Chaisson, M., and Gingeras, T.R. (2013). STAR: ultrafast universal RNA-seq aligner. Bioinformatics *29*, 15–21.

Drost, J., and Clevers, H. (2018). Organoids in cancer research. Nat. Rev. Cancer *18*, 407–418.

Edmondson, H.A., and Steiner, P.E. (1954). Primary carcinoma of the liver: a study of 100 cases among 48,900 necropsies. Cancer *7*, 462–503.

El-Khoueiry, A.B., Sangro, B., Yau, T., Crocenzi, T.S., Kudo, M., Hsu, C., Kim, T.-Y., Choo, S.-P., Trojan, J., Welling, T.H., et al. (2017). Nivolumab in patients with advanced hepatocellular carcinoma (CheckMate 040): an open-label, non-comparative, phase 1/2 dose escalation and expansion trial. Lancet *389*, 2492–2502.

Fisher, R., Pusztai, L., and Swanton, C. (2013). Cancer heterogeneity: implications for targeted therapeutics. Br. J. Cancer *108*, 479–485.

Fujii, M., Shimokawa, M., Date, S., Takano, A., Matano, M., Nanki, K., Ohta, Y., Toshimitsu, K., Nakazato, Y., Kawasaki, K., et al. (2016). A colorectal tumor organoid library demonstrates progressive loss of niche factor requirements during tumorigenesis. Cell Stem Cell *18*, 827–838.

Fujimoto, A., Furuta, M., Totoki, Y., Tsunoda, T., Kato, M., Shiraishi, Y., Tanaka, H., Taniguchi, H., Kawakami, Y., Ueno, M., et al. (2016). Whole-genome mutational landscape and characterization of noncoding and structural mutations in liver cancer. Nat. Genet. *48*, 500–509.

Gao, J., Aksoy, B.A., Dogrusoz, U., Dresdner, G., Gross, B., Sumer, S.O., Sun, Y., Jacobsen, A., Sinha, R., Larsson, E., et al. (2013). Integrative analysis of complex cancer genomics and clinical profiles using the cBioPortal. Sci. Signal. *6*, pl1.

Gao, D., Vela, I., Sboner, A., Iaquinta, P.J., Karthaus, W.R., Gopalan, A., Dowling, C., Wanjala, J.N., Undvall, E.A., Arora, V.K., et al. (2014). Organoid cultures derived from patients with advanced prostate cancer. Cell *159*, 176–187.

Gao, J., Chang, M.T., Johnsen, H.C., Gao, S.P., Sylvester, B.E., Sumer, S.O., Zhang, H., Solit, D.B., Taylor, B.S., Schultz, N., and Sander, C. (2017). 3D clusters of somatic mutations in cancer reveal numerous rare mutations as functional targets. Genome Med. *9*, 4.

Gjorevski, N., Sachs, N., Manfrin, A., Giger, S., Bragina, M.E., Ordóñez-Morán, P., Clevers, H., and Lutolf, M.P. (2016). Designer matrices for intestinal stem cell and organoid culture. Nature *539*, 560–564.

Huch, M., Gehart, H., van Boxtel, R., Hamer, K., Blokzijl, F., Verstegen, M.M., Ellis, E., van Wenum, M., Fuchs, S.A., de Ligt, J., et al. (2015). Long-term culture of genome-stable bipotent stem cells from adult human liver. Cell *160*, 299–312.

Kandoth, C., McLellan, M.D., Vandin, F., Ye, K., Niu, B., Lu, C., Xie, M., Zhang, Q., McMichael, J.F., Wyczalkowski, M.A., et al. (2013). Mutational landscape and significance across 12 major cancer types. Nature *502*, 333–339.

Kondo, J., Endo, H., Okuyama, H., Ishikawa, O., Iishi, H., Tsujii, M., Ohue, M., and Inoue, M. (2011). Retaining cell-cell contact enables preparation and culture of spheroids composed of pure primary cancer cells from colorectal cancer. Proc. Natl. Acad. Sci. USA *108*, 6235–6240.

Landau, D.A., Carter, S.L., Stojanov, P., McKenna, A., Stevenson, K., Lawrence, M.S., Sougnez, C., Stewart, C., Sivachenko, A., Wang, L., et al. (2013). Evolution and impact of subclonal mutations in chronic lymphocytic leukemia. Cell *152*, 714–726.

Lawrence, M.S., Stojanov, P., Mermel, C.H., Robinson, J.T., Garraway, L.A., Golub, T.R., Meyerson, M., Gabriel, S.B., Lander, E.S., and Getz, G. (2014). Discovery and saturation analysis of cancer genes across 21 tumour types. Nature *505*, 495–501.

Lee, S.H., Hu, W., Matulay, J.T., Silva, M.V., Owczarek, T.B., Kim, K., Chua, C.W., Barlow, L.J., Kandoth, C., Williams, A.B., et al. (2018). Tumor evolution and drug response in patient-derived organoid models of bladder cancer. Cell *173*, 515–528.e17.

Li, B., and Dewey, C.N. (2011). RSEM: accurate transcript quantification from RNA-Seq data with or without a reference genome. BMC Bioinformatics *12*, 323.

Li, H., and Durbin, R. (2009). Fast and accurate short read alignment with Burrows-Wheeler transform. Bioinformatics *25*, 1754–1760.

Llovet, J.M., and Hernandez-Gea, V. (2014). Hepatocellular carcinoma: reasons for phase III failure and novel perspectives on trial design. Clin. Cancer Res. *20*, 2072–2079.

Llovet, J.M., Brú, C., and Bruix, J. (1999). Prognosis of hepatocellular carcinoma: the BCLC staging classification. Semin. Liver Dis. *19*, 329–338.

Llovet, J.M., Ricci, S., Mazzaferro, V., Hilgard, P., Gane, E., Blanc, J.F., de Oliveira, A.C., Santoro, A., Raoul, J.L., Forner, A., et al.; SHARP Investigators Study Group (2008). Sorafenib in advanced hepatocellular carcinoma. N. Engl. J. Med. *359*, 378–390.

Luo, X., Jia, W., Huang, Z., Li, X., Xing, B., Jiang, X., Li, J., Si, A., Yang, T., Gao, C., et al. (2017). Effectiveness and safety of sorafenib in the treatment of unresectable and advanced intrahepatic cholangiocarcinoma: a pilot study. Oncotarget *8*, 17246–17257.

Marquardt, J.U., Andersen, J.B., and Thorgeirsson, S.S. (2015). Functional and genetic deconstruction of the cellular origin in liver cancer. Nat. Rev. Cancer *15*, 653–667.

McKenna, A., Hanna, M., Banks, E., Sivachenko, A., Cibulskis, K., Kernytsky, A., Garimella, K., Altshuler, D., Gabriel, S., Daly, M., and DePristo, M.A. (2010). The Genome Analysis Toolkit: a MapReduce framework for analyzing next-generation DNA sequencing data. Genome Res. *20*, 1297–1303.

Nik-Zainal, S., Davies, H., Staaf, J., Ramakrishna, M., Glodzik, D., Zou, X., Martincorena, I., Alexandrov, L.B., Martin, S., Wedge, D.C., et al. (2016). Landscape of somatic mutations in 560 breast cancer whole-genome sequences. Nature *534*, 47–54.

Nikolayeva, O., and Robinson, M.D. (2014). edgeR for differential RNA-seq and ChIP-seq analysis: an application to stem cell biology. Methods Mol. Biol. *1150*, 45–79.

Pauli, C., Hopkins, B.D., Prandi, D., Shaw, R., Fedrizzi, T., Sboner, A., Sailer, V., Augello, M., Puca, L., Rosati, R., et al. (2017). Personalized *in vitro* and *in vivo* cancer models to guide precision medicine. Cancer Discov. *7*, 462–477.

Piscuoglio, S., Ng, C.K., Murray, M.P., Guerini-Rocco, E., Martelotto, L.G., Geyer, F.C., Bidard, F.C., Berman, S., Fusco, N., Sakr, R.A., et al. (2016). The genomic landscape of male breast cancers. Clin. Cancer Res. *22*, 4045–4056.

Rosenthal, R., McGranahan, N., Herrero, J., Taylor, B.S., and Swanton, C. (2016). DeconstructSigs: delineating mutational processes in single tumors distinguishes DNA repair deficiencies and patterns of carcinoma evolution. Genome Biol. *17*, 31.

Sachs, N., de Ligt, J., Kopper, O., Gogola, E., Bounova, G., Weeber, F., Balgobind, A.V., Wind, K., Gracanin, A., Begthel, H., et al. (2018). A living biobank of breast cancer organoids captures disease heterogeneity. Cell *172*, 373–386.e10.

Saunders, C.T., Wong, W.S., Swamy, S., Becq, J., Murray, L.J., and Cheetham, R.K. (2012). Strelka: accurate somatic small-variant calling from sequenced tumor-normal sample pairs. Bioinformatics *28*, 1811–1817.

Shen, R., and Seshan, V.E. (2016). FACETS: allele-specific copy number and clonal heterogeneity analysis tool for high-throughput DNA sequencing. Nucleic Acids Res. *44*, e131.

Shihab, H.A., Gough, J., Cooper, D.N., Stenson, P.D., Barker, G.L., Edwards, K.J., Day, I.N., and Gaunt, T.R. (2013). Predicting the functional, molecular, and phenotypic consequences of amino acid substitutions using hidden Markov models. Hum. Mutat. *34*, 57–65.

Cancer Genome Atlas Research Network (2017). Comprehensive and integrative genomic characterization of hepatocellular carcinoma. Cell *169*, 1327–1341.e23.

Thorvaldsdóttir, H., Robinson, J.T., and Mesirov, J.P. (2013). Integrative Genomics Viewer (IGV): high-performance genomics data visualization and exploration. Brief. Bioinform. *14*, 178–192.

van de Wetering, M., Francies, H.E., Francis, J.M., Bounova, G., Iorio, F., Pronk, A., van Houdt, W., van Gorp, J., Taylor-Weiner, A., Kester, L., et al. (2015). Prospective derivation of a living organoid biobank of colorectal cancer patients. Cell *161*, 933–945.

Cell Reports, Volume *24*

Supplemental Information

Organoid Models of Human Liver Cancers Derived from Tumor Needle Biopsies

Sandro Nuciforo, Isabel Fofana, Matthias S. Matter, Tanja Blumer, Diego Calabrese, Tujana Boldanova, Salvatore Piscuoglio, Stefan Wieland, Femke Ringnalda, Gerald Schwank, Luigi M. Terracciano, Charlotte K.Y. Ng, and Markus H. Heim

SUPPLEMENTAL INFORMATION

Figure S1

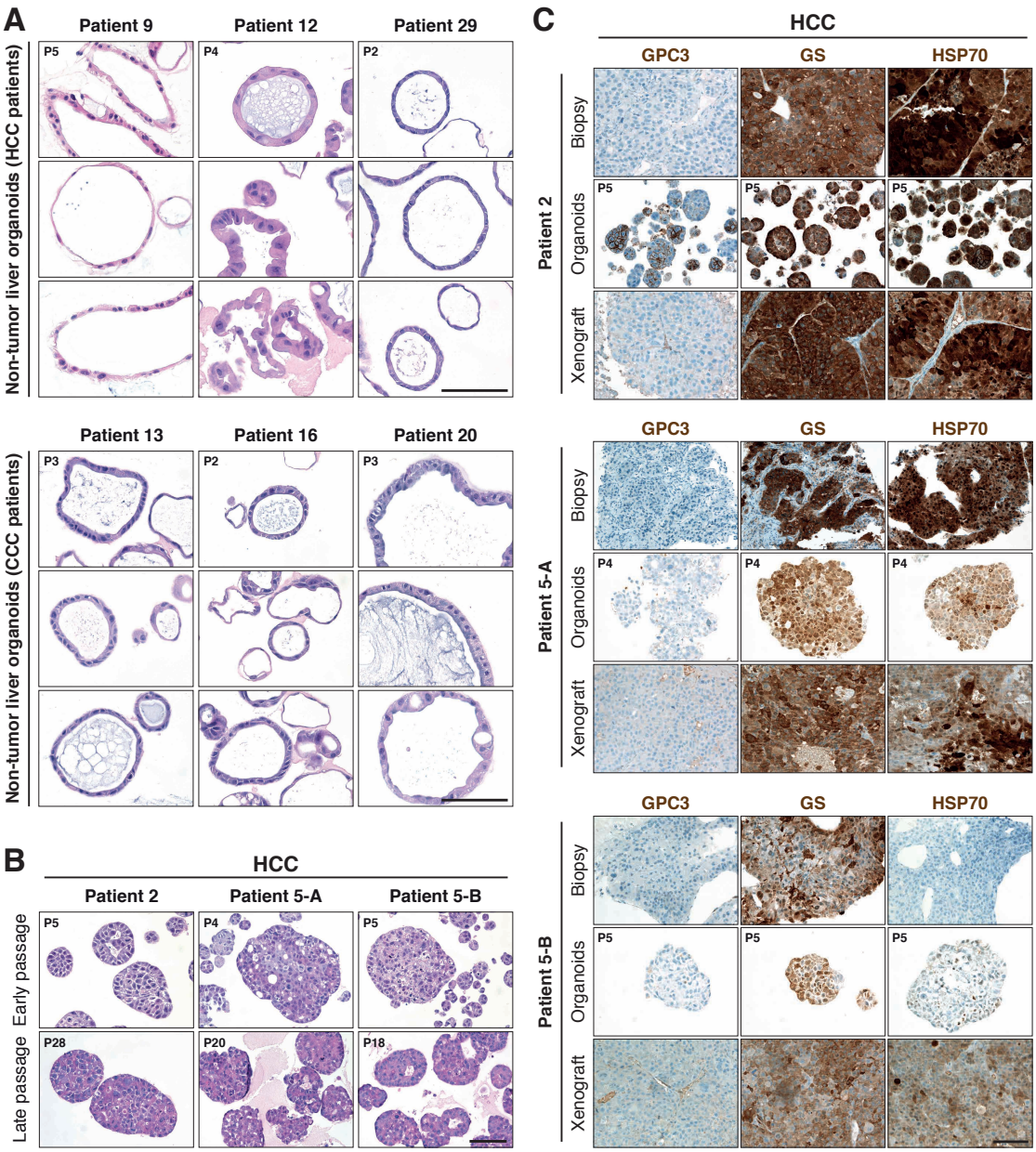

Figure S1. Histological Analysis of Tumor and Non-tumor Derived Organoids from HCC and CCC Patients. **Related to Figure 1, Figure 3 and Figure 4.** (**A**) Representative Hematoxylin and Eosin images of paired non-tumor liver organoids derived from HCC and CCC patients. Scale bars: 100 μm. (**B**) Representative Hematoxylin and Eosin images of HCC organoids at early and late passage (range P4-P28), showing no morphological differences after long-term culture. For Patient 2, HCC organoid culture time between early and late passage corresponds to 52 weeks, for Patient 5-A 29 weeks and Patient 5-B 26 weeks. Scale bar: 100 μm. (**C**) Histological sections of three representative HCC biopsies, their derivative organoids and organoid-derived xenografts stained for Glypican 3 (GCP3), Glutamine Synthetase (GS) and Heat Shock Protein 70 (HSP70) by immunohistochemistry. Organoids were imaged at the indicated passage numbers. Scale bar: 100 μm.

Figure S2

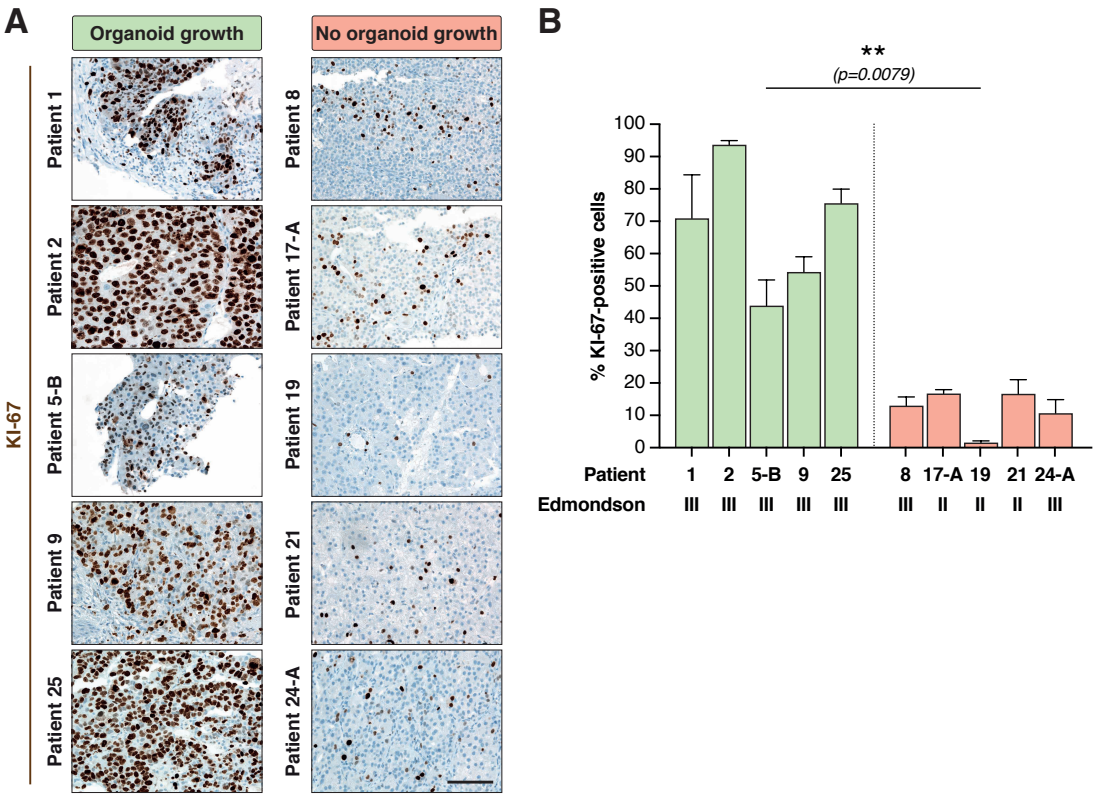

Figure S2. KI-67 Analysis on HCC Tumor Biopsies Used for Organoid Generation. Related to Figure 2. (**A**) Representative tissue sections of ten randomly chosen HCC biopsies stained for the proliferation marker KI-67 by immunohistochemistry. Tumors that did not result in organoid growth have only few KI-67-positive nuclei. Scale bar: 100 µm. (**B**) Quantification of KI-67-positive nuclei for the ten HCC biopsies (p=0.0079, two-tailed t-test). Shown is the mean ± SEM of at least three images for each tissue section and patient. Approximately 1'000 cells were counted per patient.

Figure S3

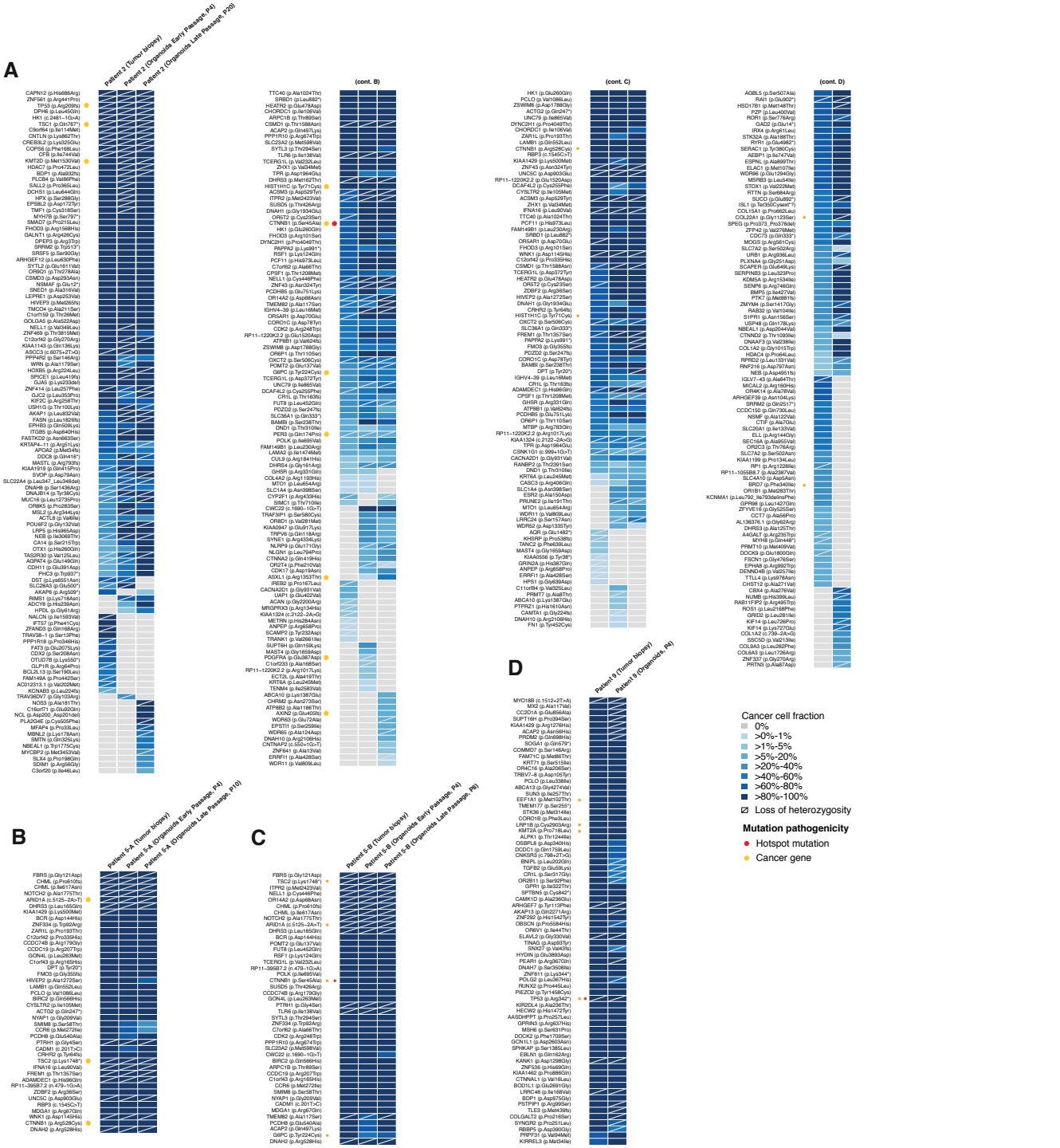
A
Patient 2 (Tumor biopsy)
Patient 2 (Organoids Early Passage, P4)
Patient 2 (Organoids Late Passage, P20)
(cont. B)
(cont. C)
(cont. D)
B
Patient 5-A (Tumor biopsy)
Patient 5-A (Organoids Early Passage, P4)
Patient 5-A (Organoids Late Passage, P10)
C
Patient 5-B (Tumor biopsy)
Patient 5-B (Organoids Early Passage, P4)
Patient 5-B (Organoids Late Passage, P8)
D
Patient 9 (Tumor biopsy)
Patient 9 (Organoids, P4)
Cancer cell fraction
0%
>0%-1%
>1%-5%
>5%-20%
>20%-40%
>40%-60%
>60%-80%
>80%-100%
Loss of heterozygosity
Mutation pathogenicity
Hotspot mutation
Cancer gene

Figure S3. Repertoire of Somatic Mutations in Tumor Biopsies and Derivative Organoids of Patients 2, 5-A, 5-B and 9. Related to Figure 5. Heatmaps indicate the cancer cell fraction of somatic non-synonymous autosomal mutations as determined by ABSOLUTE (Carter et al., 2012) (blue, see color key) or their absence (grey) in each sequenced HCC tumor biopsy/ HCC organoids (**A**-**D**). Mutations affecting cancer genes (Fujimoto et al., 2016; Kandoth et al., 2013; Lawrence et al., 2014) or hotspot residues (Chang et al., 2016; Gao et al., 2017) are indicated by yellow and red dots, respectively.

Figure S4

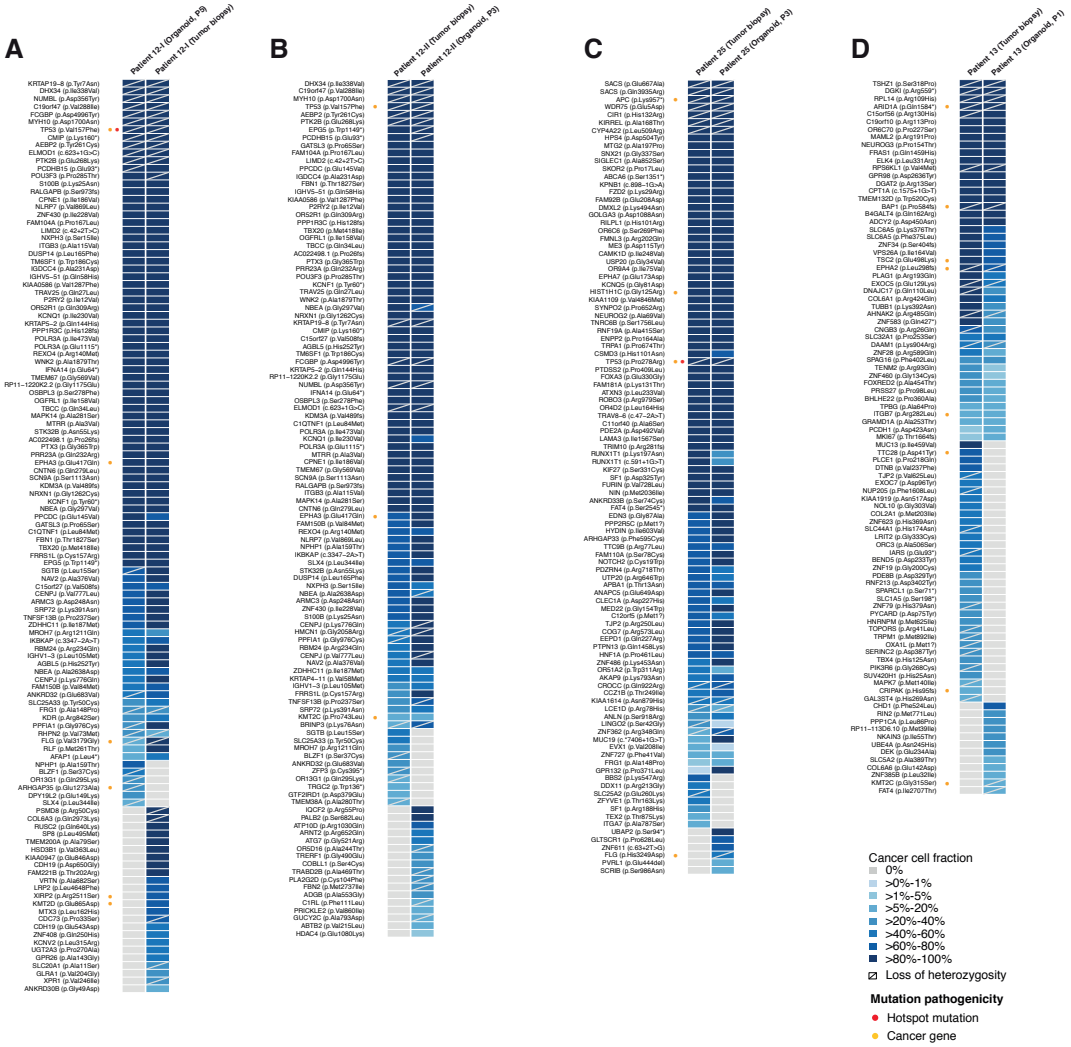
A
Patient 12-I (Organoid, P9)
Patient 12-I (Tumor biopsy)
B
Patient 12-II (Tumor biopsy)
Patient 12-II (Organoid, P3)
C
Patient 25 (Tumor biopsy)
Patient 25 (Organoid, P3)
D
Patient 13 (Tumor biopsy)
Patient 13 (Organoid, P1)
Cancer cell fraction
0%
>0%-1%
>1%-5%
>5%-20%
>20%-40%
>40%-60%
>60%-80%
>80%-100%
Loss of heterozygosity
Mutation pathogenicity
Hotspot mutation
Cancer gene

Figure S4. Repertoire of Somatic Mutations in Tumor Biopsies and Derivative Organoids in Patients 12-I, 12-II, 25 and 13. Related to Figure 5. Heatmaps indicate the cancer cell fraction of somatic non-synonymous autosomal mutations as determined by ABSOLUTE (Carter et al., 2012) (blue, see color key) or their absence (grey) in each sequenced HCC tumor biopsy/ HCC organoids (**A**-**D**). Mutations affecting cancer genes (Fujimoto et al., 2016; Kandoth et al., 2013; Lawrence et al., 2014) or hotspot residues (Chang et al., 2016; Gao et al., 2017) are indicated by yellow and red dots, respectively.

Figure S5

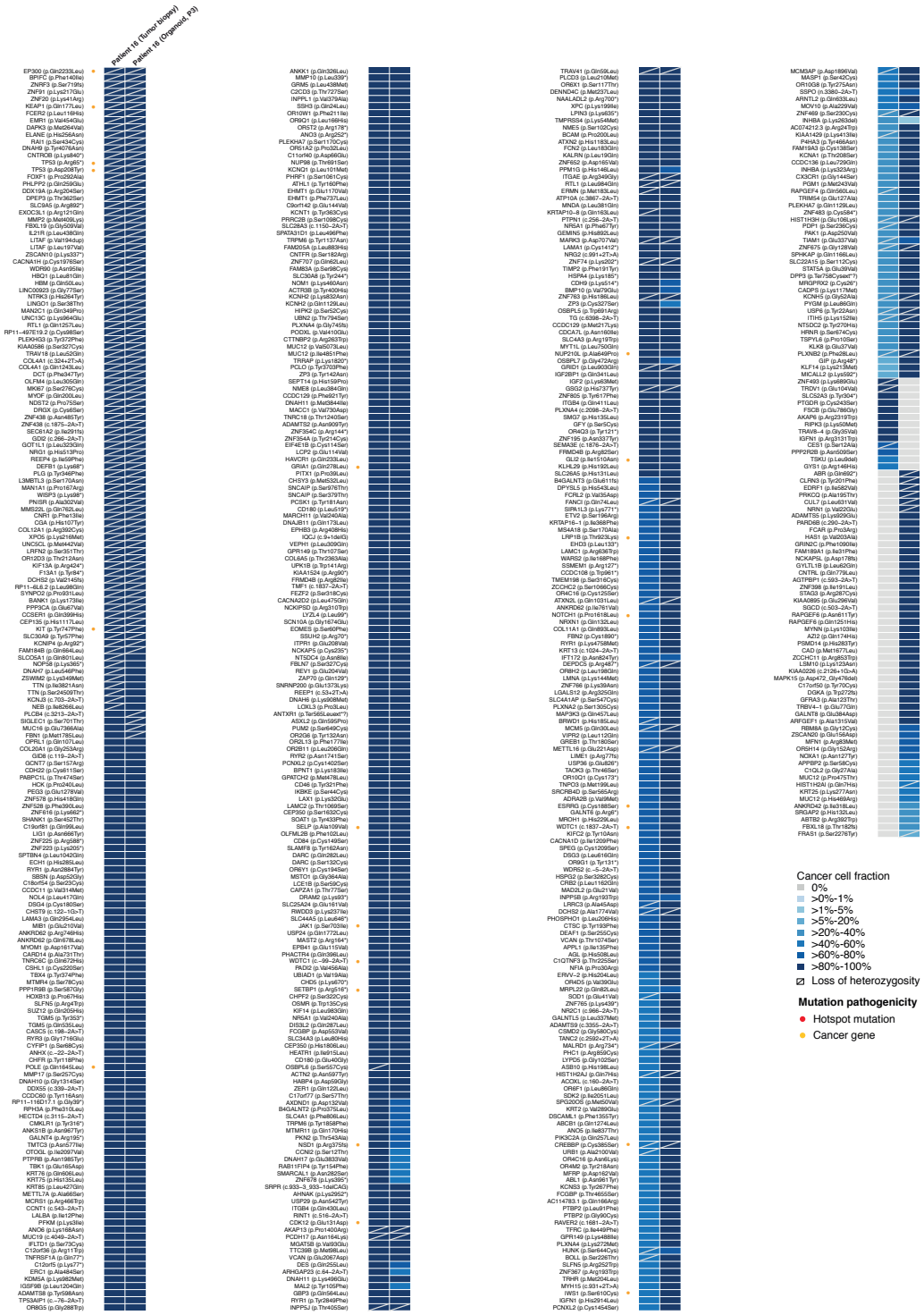
Patient 15 (Tumor biopsy)
Patient 16 (Organoid, P3)
Cancer cell fraction
0%
>0%-1%
>1%-5%
>5%-20%
>20%-40%
>40%-60%
>60%-80%
>80%-100%
Loss of heterozygosity
Mutation pathogenicity
Hotspot mutation
Cancer gene

Figure S5. Repertoire of Somatic Mutations in Tumor Biopsies and Derivative Organoids in Patient 16. Related to Figure 5. Heatmaps indicate the cancer cell fraction of somatic non-synonymous autosomal mutations as determined by ABSOLUTE (Carter et al., 2012) (blue, see color key) or their absence (grey) in each sequenced HCC tumor biopsy/ HCC organoids. Mutations affecting cancer genes (Fujimoto et al., 2016; Kandoth et al., 2013; Lawrence et al., 2014) or hotspot residues (Chang et al., 2016; Gao et al., 2017) are indicated by yellow and red dots, respectively.

Figure S6


Patient 20 (Tumor biopsy)
Patient 20 (Organoid, P5)
Cancer cell fraction
0%
>0%-1%
>1%-5%
>5%-20%
>20%-40%
>40%-60%
>60%-80%
>80%-100%
Loss of heterozygosity
Mutation pathogenicity
Hotspot mutation
Cancer gene

Figure S6. Repertoire of Somatic Mutations in Tumor Biopsies and Derivative Organoids in Patient 20. Related to Figure 5. Heatmaps indicate the cancer cell fraction of somatic non-synonymous autosomal mutations as determined by ABSOLUTE (Carter et al., 2012) (blue, see color key) or their absence (grey) in each sequenced HCC tumor biopsy/ HCC organoids. Mutations affecting cancer genes (Fujimoto et al., 2016; Kandoth et al., 2013; Lawrence et al., 2014) or hotspot residues (Chang et al., 2016; Gao et al., 2017) are indicated by yellow and red dots, respectively.

Figure S7

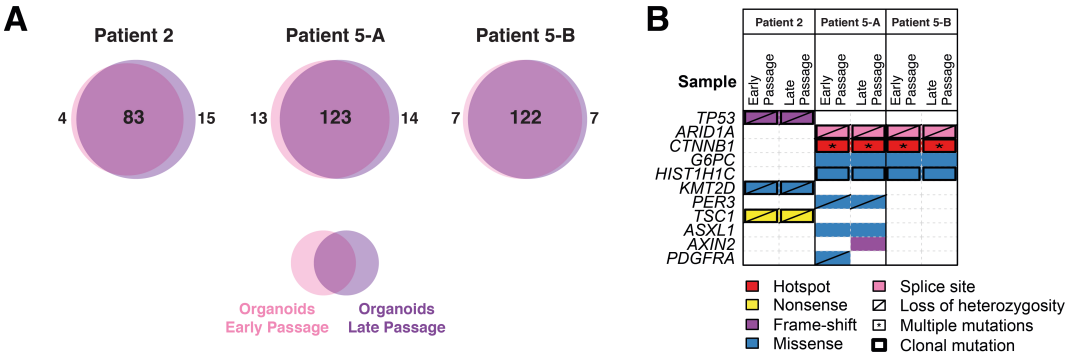
A
Patient 2
Patient 5-A
Patient 5-B
4
83
15
13
123
14
7
122
7
Organoids
Early Passage
Organoids
Late Passage
B
Patient 2
Patient 5-A
Patient 5-B
Sample
Early Passage
Late Passage
TP53
ARID1A
CTNNB1
G6PC
HIST1H1C
KMT2D
PER3
TSC1
ASXL1
AXIN2
PDGFRA
Hotspot
Nonsense
Frame-shift
Missense
Splice site
Loss of heterozygosity
Multiple mutations
Clonal mutation

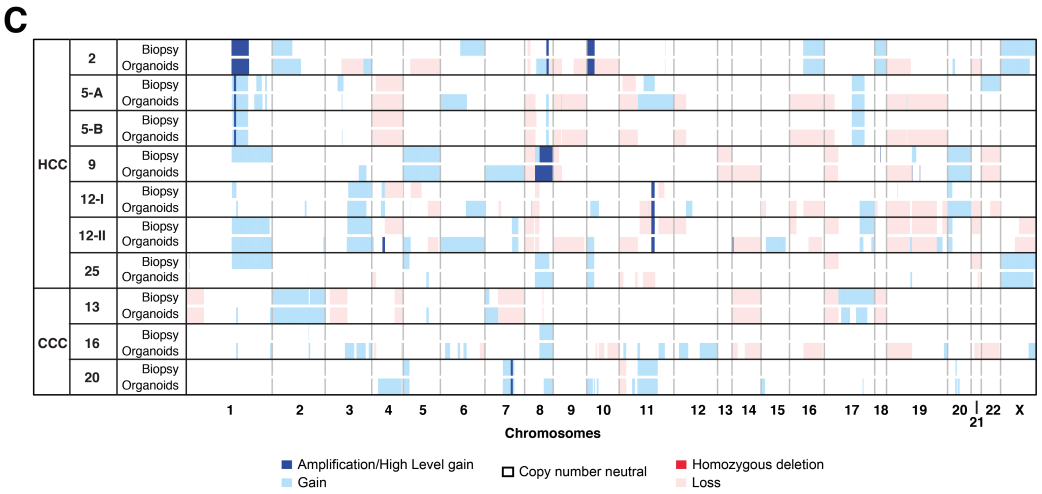
C
HCC
CCC
2
5-A
5-B
9
12-I
12-II
25
13
16
20
Biopsy
Organoids
1 2 3 4 5 6 7 8 9 10 11 12 13 14 15 16 17 18 19 20 21 22 X
Chromosomes
Amplification/High Level gain
Gain
Copy number neutral
Homozygous deletion
Loss

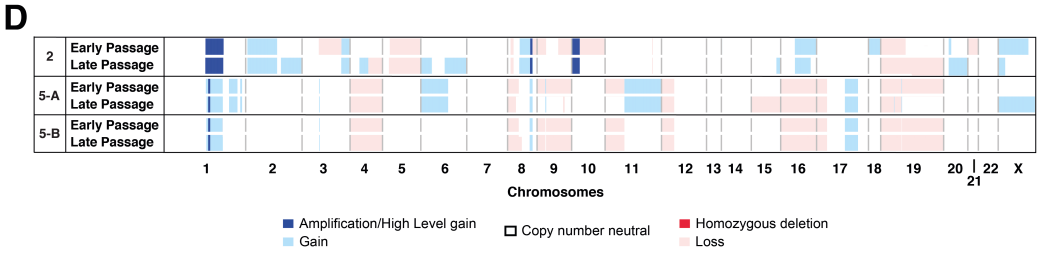
D
2
5-A
5-B
Early Passage
Late Passage
1 2 3 4 5 6 7 8 9 10 11 12 13 14 15 16 17 18 19 20 21 22 X
Chromosomes
Amplification/High Level gain
Gain
Copy number neutral
Homozygous deletion
Loss

Figure S7. Analysis of Long-term Genetic Stability in HCC and CCC Organoids. Related to Figure 5. (**A**) Venn diagrams illustrate the number of somatic non-synonymous mutations present in three representative HCC organoid lines at early and late passage. For whole exome sequencing analysis of the HCC organoids derived from Patient 2, culture time between early and late passage was 32 weeks, corresponding to 16 passages. For the HCC organoid lines 5-A and 5-B culture time was 8 weeks corresponding to 6 and 4 passages, respectively. (**B**) Repertoire of somatic non-synonymous mutations affecting cancer genes (Fujimoto et al., 2016; Kandoth et al., 2013; Lawrence et al., 2014) at early and late passage. The effects of the mutations are color-coded according to the legend, with hotspots (Chang et al., 2016; Gao et al., 2017) colored in red. The presence of multiple non-synonymous mutations in the same gene is represented by an asterisk. The presence of loss of heterozygosity of the wild-type allele of a mutated gene is represented by a diagonal bar, and mutations found to be clonal by ABSOLUTE (Carter et al., 2012) are indicated by a black box. (**C**) Heatmap of copy number alterations in HCC biopsies and derivative organoids (Patients 2, 5-A, 5-B, 9, 12-I, 12-II and 25) and CCC biopsies and derivative organoids (Patients 13, 16 and 20). Samples are presented in rows and chromosomal positions on the x-axis (columns). Dark blue: amplification, light blue: copy number gain; white: neutral; light red: copy number loss; dark red: homozygous deletion. (**D**) Heatmap illustrating the copy number alterations between early and late passage organoids.

Figure S8

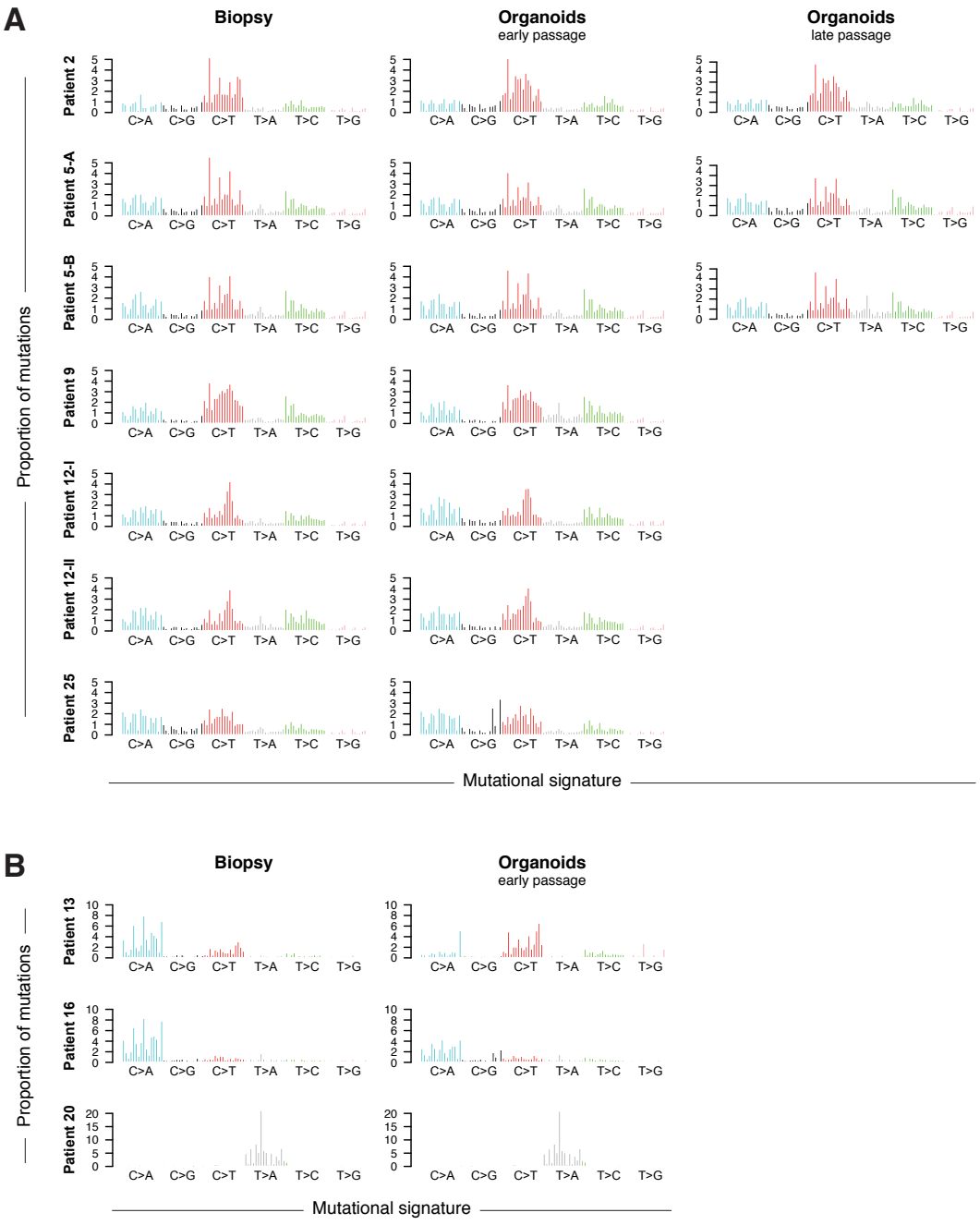
A
Biopsy
Organoids
early passage
Organoids
late passage
Patient 2
Patient 5-A
Patient 5-B
Patient 9
Patient 12-I
Patient 12-II
Patient 25
C>A C>G C>T T>A T>C T>G
Proportion of mutations
Mutational signature
B
Biopsy
Organoids
early passage
Patient 13
Patient 16
Patient 20
C>A C>G C>T T>A T>C T>G
Proportion of mutations
Mutational signature

Figure S8. Mutational Signatures in Tumor Biopsies and Derivative Organoids. Related to Figure 5. (**A**) Barplots illustrate the mutational signatures of the HCC biopsies and the corresponding organoids at early and late passage (late passage only for Patients 2, 5-A and 5-B). In each panel, the colored barplot illustrates each mutational signature according to the 96 substitution classification (Alexandrov et al., 2013) defined by the substitution classes (C>A, C>G, C>T, T>A, T>C and T>G bins) and the 5' and 3' sequence context, normalized using the observed trinucleotide frequency in the human exome to that in the human genome. The bars are ordered first by mutation class (C>A/G>T, C>G/G>C, C>T/G>A, T>A/A>T, T>C/A>G, T>G/A>C), then by the 5' flanking base (A, C, G, T) and then by the 3' flanking base (A, C, G, T). (**B**) Mutational signature for CCC biopsies and corresponding organoids.

7. DISCUSSION

7.1. Liver-derived organoid cultures

In 2016, an estimate of 45 million people worldwide suffered from chronic liver disease owing to different underlying factors including viral hepatitis, alcohol abuse, non-alcoholic fatty liver disease and other risk factors leading to the development of cirrhosis[182]. Failure in the management of CLD can be attributed to the lack of sufficient organs for liver transplantations. Cell therapies might offer an alternative to liver transplantation, however, current models based on iPSCs raise uncertainty regarding their genetic stability in culture since the reprogramming procedure of adult differentiated cells into iPSCs can induce genetic and epigenetic alterations[183]. The recently-developed liver organoid system based on the expansion of aSCs could provide a new alternative to iPSCs-based cell therapies[127]. Importantly, the reprogramming step is not required for organoids because the starting cell, the adult stem cell, has the intrinsic capability to proliferate and generate differentiated cells of its own lineage, provided that the essential niche factors are present in the culture medium. This convenient advantage is reflected in the high genetic stability of organoids in culture and therefore, they could represent a valuable alternative to iPSCs for regenerative medicine purposes.

The present thesis demonstrates the feasibility of generating organoid cultures from small needle biopsies of patients undergoing diagnostic liver biopsy procedure (Figure 10). Patients referred to our outpatient clinic present with the whole spectrum of liver disease and, accordingly, the organoid biobank generated in our lab encompasses most of these etiologies. Differently than for tissue material obtained from surgical resection, liver needle biopsies can be performed in almost every patient with liver disease, even in those with compromised liver function that are usually not amenable for surgery. In addition, it allows the establishment of large biobanks. Such biobanks can be used to identify inter-individual features that impact on therapy response and therefore help to stratify patients in different treatment groups. In addition, liver biopsies can be obtained during the course of treatment to generate a longitudinal set of *in vitro* cultures that reflects the cellular and molecular changes in response to therapy.

Our biobank currently encompasses more than 100 organoid cultures derived from patients with different liver disease backgrounds, namely, HBV, HCV, AIH, ALD, cirrhosis, DILI, fibrosis, Morbus Wilson, NAFLD, PBC. A large proportion of our cultures was derived from the non-tumor tissue of liver cancer patients that, as previously outlined, suffer from the same underlying chronic liver diseases as those patients without liver cancer.
Organoids could be established in 100% of the cases, even from biopsy fragments as small as 5 mm in length by ~1 mm in diameter. After 3–4 weeks, the quantity of expanded organoids was sufficient to allow downstream histological and molecular analysis as well as cryopreservation for biobanking purposes.

Liver organoids are composed of bipotent progenitors[127] and their differentiation into the hepatocyte fate resulted in a strong upregulation of transcripts encoding major hepatocyte markers (Figure 11). Glycogen synthesis and Albumin secretion, two hallmarks of mature hepatocytes, were also detected upon differentiation. However, when compared to primary human hepatocytes and primary liver tissue (biopsy), the expression levels of the three assessed markers were significantly lower. HepG2 cells — a widely used tumor-derived cell line with several hepatocyte features — also displayed higher levels of these markers, however, due to the fact that these are cancer cells, the difference in transcript levels may be explained by a general dysregulation of gene expression or their polyclonality as compared to non-tumoral cells. Nevertheless, the main reason may be related to the fact that the differentiation protocol is not optimal, and the cells do not reach the same maturation level as in the *in vivo* situation. Indeed, when comparing the expression levels of two major cholangiocyte markers, EpCAM and KRT19, we did not observe a reduction following differentiation, despite the fact that the protocol is designed to inhibit cholangiocyte- and promote hepatocyte maturation. The fact that these markers are already present in undifferentiated organoids could be explained by the cellular origin within the liver. Indeed, the original report found that the organoid-initiating cell is residing in the cholangiocyte-harboring ductal compartment of the liver that forms the biliary tree[127]. The cells residing there are EpCAM- and KRT19-positive, two markers that are absent in mature hepatocytes. As previously reported, only EpCAM-positive cells were able to grow as organoids *in vitro*[127]. This excludes the possibility that mature hepatocytes could serve as the cell of origin in liver organoids. However, it does not exclude the fact that liver organoids may arise from adult stem- or progenitor cells

residing within the ducts in close proximity to mature cholangiocytes. Alternatively, organoids may arise from dedifferentiated hepatocytes or cholangiocytes. Indeed, the single cell-layered epithelium of liver organoids shares similarities with bile ducts *in vivo* (Figure 1). Hepatocytes in contrast, do not form cysts or ducts implying that liver organoids arise from cells that have the ability to do so.

One of the main concepts of liver regeneration is based on the presence of bipotent progenitors in the *Canal of Hering*, a structure at the junction between cholangiocytes and hepatocytes (Figure 1). If organoids originated from such cells, it would explain their cystic or tubular growth. In some reports, the bipotent progenitors residing in the *Canal of Hering* are referred to as oval cells[10]. These cells are characterized by their ability to differentiate into hepatocytes as well as cholangiocytes, similarly to hepatoblasts during liver development. This could explain the expression of both, cholangiocyte- (EpCAM, KRT19, SOX9) and hepatocyte (HNF4a) markers in liver organoids[127]. Oval cells are thought to be dormant adult stem cells only appearing upon liver injury. The factors released during hepatocyte damage function as activators of oval cell proliferation and differentiation[10]. *In vitro*, this would be achieved through the numerous growth factors provided with the culture medium. Moreover, a recent study convincingly demonstrated the ability of ductal cells to proliferate and convert into hepatocytes to repopulate the liver upon massive hepatocyte loss[24]. The question whether all ductal cells or only the oval cell subpopulation is driving this regenerative response remains to be answered. Nevertheless, the study confirms the intrinsic ability of ductal cells to transdifferentiate into hepatocytes under specific circumstances. Therefore, an improved differentiation protocol may also lead to such a conversion *in vitro*. To achieve this, we need to deepen our understanding of the signals regulating the maturation of newly-formed hepatocytes *in vivo*, independently from their origin. Indeed, transplantation of differentiated liver organoids into recipient mice, suggested that full hepatocyte maturation may only be reached after *in vivo* engraftment[127].

Despite the drawbacks of the current differentiation protocol, the goal to generate fully mature hepatocytes from undifferentiated organoids is probably not that far away. Indeed, examination of the ultrastructural features of liver organoids revealed structures exclusively found in mature hepatocytes, namely bile canaliculi (Figure 12). Bile canaliculi are small tubes that collect the bile produced by hepatocytes (Fig-

ure 1). The bile canalicular membrane represents the apical side of the hepatocyte and contains specific transporters that export bile acids into the canaliculi. This function is crucial for hepatocyte homeostasis, because bile acids are natural detergents and therefore toxic if they accumulate in the cell. Therefore, given that differentiated organoids produce bile acids[127], the bile canaliculi-like structures revealed by TEM may actually be functional. In addition, the fact that these structures were also found in undifferentiated organoids (Figure 12), suggests that the cell of origin is indeed distinct from mature ductal cells/cholangiocytes that, in contrast to hepatocytes, don't form bile canaliculi *in vivo*. Again, this speaks in favor of oval cells as the source of organoid-initiating cells because, as previously outlined, they share characteristics of both hepatocytes and cholangiocytes and this may include the formation of early/immature canalicular-like structures.

One recognized factor that influences cellular behavior *in vitro* is the matrix in which cells are suspended for three-dimensional growth. Matrigel® and BME2® are two widely-used extracellular matrix (ECM) hydrogels derived from Engelbreth-Holm-Swarm mouse sarcoma, a tumor rich in laminin and, to a minor extent, collagen IV, heparin sulfate proteoglycans, and fibronectin. The use of laminin-rich matrices enables the growth of organoids irrespective of their tissue origin. This is due to one common feature of all epithelial organoid systems that have been developed so far: the cells from which they are derived are sitting on a basement membrane, whose main constituents are in fact laminin and collagen IV. For the liver, the only cells in contact with a basement membrane are ductal cells, whereas hepatocytes are primarily embedded within collagen III, IV, V and fibronectin, while laminin is completely absent[184]. Therefore, the fact that Matrigel and BME2 are mainly composed of laminin and lack sufficiently high concentrations of collagen III, IV and V, may explain why liver organoids fail to completely mature into hepatocytes under these conditions *in vitro*. Recent efforts to optimize the culture and differentiation of organoids include the generation of matrices directly from liver tissue instead of using murine tumors[185], or the *de novo* synthesis of artificial hydrogels complemented with short peptides required for ECM signaling[186]. Importantly, these approaches also allow to define the stiffness of the matrix, an additional factor that regulates (stem) cell fate *in vivo* and *in vitro*[187,188].

In conclusion, the development of the liver organoid system allows for the first time to systematically culture and expand liver-derived progenitor cells from human tissue specimens. Contrary to PHHs, liver organoids can grow indefinitely and produce large cell numbers within short time frames. Provided that an improved differentiation protocol will allow the conversion of progenitors into fully mature hepatocytes, such cultures may represent a precious source for cell therapies and overcome the limited number of donors for liver transplantation.

7.2. Liver cancer-derived organoid cultures

Liver cancer, with HCC accounting for ~80% of the cases, is a global health problem that causes 830'000 deaths every year. The incidence continuously increased during the last years and is predicted to continue mostly due to an increase of liver pathologies related to obesity. A small proportion of HCC is diagnosed at early stages, for which curative treatments exist, however, most of the tumors are detected at later stages, for which the therapeutic management of the disease is ineffective.

A major drawback in HCC research has been the lack of appropriate models that reflect the biology and heterogeneity of HCCs observed in patients. This is mainly due to two reasons: first, the current human *in vitro* models in HCC research, cancer cell lines, were all derived decades ago and it is not clear how well they represent the primary tumors. Moreover, despite their broad utility, cell lines suffer from significant shortcomings such as the lack of a three-dimensional structure that preserves the cellular interactions of the primary tumor as well as the different cellular components. Second, in the specific case of HCCs, the material used to generate cell lines is predominantly derived from surgically resected specimens. But as previously outlined, surgical resection is not broadly applicable to HCC patients, especially at later disease stages, and the models generated with tissue obtained thereof fails to represent the whole spectrum of HCCs. Furthermore, current drug discovery programs aim at developing new therapies for patients with advanced HCC and therefore, the models used in basic- and pre-clinical research should ideally reflect the targeted patient spectrum to effectively translate into the clinic.

The organoid system, initially developed for the culture of intestinal stem cells, offers new opportunities to develop personalized cancer models from a much larger spectrum of patients and individual tumors, than it was so far possible with conventional cancer cell lines. Organoids retain several features of the primary tumors, can be

successfully derived from different tumor nodules within the same patient and, importantly, they can robustly model treatment response in patients[148]. It was therefore obvious to apply the organoid derivation protocol to HCC and combine it with the use of needle biopsy-derived tissue specimens, to cover all disease stages and overcome the limitations of current models.

We collected a series of tumor biopsies from patients with suspected HCC and processed the tissue for organoid generation. Additional biopsies from the same tumor site were collected and immediately snap-frozen for later use in omics analyses, or formalin-fixed for histological evaluation.
The examination of the histological properties of our HCC organoids revealed a remarkable similarity with their originating tumors in terms of growth patterns and differentiation grades. In addition, the expression of common HCC tumor markers was equally preserved, and their expression followed the same pattern that was observed in the primary tumors. Our biopsy cohort also included tumor tissue derived from CCCs that could also be propagated as organoids *in vitro*. Despite the different cell of origin, the culture medium used for all organoids, allowed the growth of CCC cells without altering their morphological features, indicating that the ability to reproduce the tissue architecture is an intrinsic property of the tumor cells. We further confirmed this with the generation of xenografts from transplanted tumor organoids. Indeed, the same histological features were maintained in the xenografts despite the different microenvironment that, in comparison to *in vitro* organoids, also contained other cell types and growth factors. The transplantation experiments also allowed the generation of xenografts from CCC organoids and the resulting tumors displayed various degrees of desmoplastic stroma, i.e. the accumulation of ECM around tumor cells typical for adenocarcinomas.

The molecular landscape of the originating tumors was very well preserved in the corresponding organoids, complementing the high histological similarity. The number of non-synonymous somatic mutations between biopsy and organoids concorded to ~90% across the different patients. Moreover, when specifically looking at mutations in cancer genes, nearly all identified oncogenes and tumor suppressors were preserved in the organoids. However, some mutations were lost during organoid derivation and new mutations, absent in the originating biopsy, were detected in the organoids. The loss can be explained by the fact that some mutations were subclonal and

presumably not present in the whole biopsy since we only used a fragment of the entire biopsy. Mutations exclusively found in the organoids can derive from *in vitro* culturing and the increased mutation rate of tumor cells (tumor evolution). Importantly, only seven mutations throughout all the HCC cultures, either lost or newly acquired in organoids, affected cancer genes. These mutations were all subclonal and could therefore explain the discordance with the primary tumors.

The analysis of somatic mutations in CCC biopsies and organoids revealed hypermutator phenotype in two patients, with more than 500 somatic mutations per tumor. For one of the patients most of the mutations were preserved in the corresponding organoids, whereas for the other patient, 83% of the mutations detected in the biopsy were lost in the organoids. This again can be attributed to the fact that the mutations that were not preserved in the organoids were only present in subclonal cell populations within the originating tumor biopsy. However, in most of the cases, analysis of the cancer cell fraction (CCF) in the originating HCC and CCC biopsies, revealed the presence of subclonal mutations that were maintained at similar frequencies in the organoids. This underlines the advantage of organoids compared to typically clonal cancer cell lines.

The different etiologies of HCC and CCC were all reflected in our organoid biobank, indicating that the underlying disease does not dictate the efficiency of generating organoid cultures. However, the overall efficiency to generate organoids from HCC biopsies was ~26% and ~33% per number of biopsies or patients, respectively. This seems low compared to other tumor organoid models such as colorectal cancer[136,144], pancreatic cancer[128], and breast cancer[137], with efficiencies above 75%. The lower efficiency could be explained by the fact that, as previously outlined, the cell of origin of HCCs, the hepatocytes, do not form organoids with the actual organoid culture system (identical to the one used for HCC organoids). Indeed, colorectal-, pancreatic- and breast cancers, all derive from epithelial (stem) cells that can be propagated as organoids *in vitro*[125]. Within the liver, only cholangiocyte-/ductal-like cells can form organoids and therefore, the culture conditions used to derive tumor organoids from liver cancers may be suboptimal for HCCs.

Alternatively, the low success rate could imply that only a subclass of HCCs can be propagated *in vitro*. To investigate possible factors determining success or failure to generate organoids, we collected clinical- and histopathological data for all tumors used to generate organoids. There was no correlation with clinical parameters such

as the disease background, the presence or absence of cirrhosis, the severity of liver disease, the level of serum AFP, the metastatic status, and the tumor stage, again indicating the broad diversity of our tumor organoids. However, when looking at the histopathological features, one parameter in our analysis was clearly noticeable: the differentiation grade of the tumor. All tumors that successfully generated organoids *in vitro*, were derived from poorly differentiated (grades III and IV) HCCs according to the staging system by Edmondson and Steiner[89]. This finding may be explained by a progressive loss of the cells' requirements for specific environmental cues with increasing differentiation grade. Indeed, low-grade HCCs (grades I and II) retain nearly all features of normal hepatocytes and can be difficult to diagnose. One of these features is the low proliferative activity of hepatocytes *in vivo* and *in vitro* under homeostatic conditions. Accordingly, low-grade HCCs are predominantly slow-growing *in vivo*[189] and may explain why they do not proliferate *in vitro* once they are processed for organoid generation. Indeed, when analyzing the expression of the proliferation marker KI-67, we only found <20% proliferating cells in those biopsies who did not generate organoids. In contrast, all biopsies that could be successfully propagated as tumor organoids harbored >50% proliferating cells. However, there is no sharp separation between grade II and III tumors, as we also found high-grade HCCs with only few proliferating cells. It seems therefore, that a certain proliferative threshold represents the dominant feature dictating the success to generate organoids, independently from their (micro-)environmental requirements. These findings however, does not imply that our tumor organoids are biased for a specific molecular subclass. Indeed, hierarchical clustering analysis of all biopsies used in our study together with a recently-published set of poorly differentiated HCCs from the TCGA cohort[90], did not identify an enrichment for a defined subclass. We therefore conclude that our high-grade HCC organoids generated from tumor biopsies are a genuine representation of all classes of poorly differentiated HCCs.

As outlined before, we anticipate that the organoid system will improve future drug development because of the higher physiological relevance compared to cancer cell lines and the ability to derive cultures from virtually all patient groups while preserving their respective tumor features. We tested the effect of sorafenib on our cohort of HCC organoids using the clinically-relevant dose range applied in patients[159] and found different sensitivities across the different lines. It was not possible to conclude whether the response in organoids could be classified as sensitive or resistant to so-

rafenib using dose-response curves only. Most of the patients from whom we derived organoids were treated with other modalities. Because of side effects, treatment on the two sole sorafenib-treated patients from our cohort had to be discontinued before treatment efficacy could be determined. The clinical relevance of drug testing in tumor organoids has been recently confirmed in direct comparisons with patients suffering from various gastrointestinal tumors[148]. For such direct comparisons we will need additional tumor organoids from patients undergoing sorafenib treatment. Importantly, the generation of tumor organoids from patients resistant to sorafenib treatment could also allow to study the intrinsic resistance mechanisms in tumor cells.

Increasing the efficiency to generate organoids from tumor biopsies will reduce the time needed to expand the biobank to a size that allows meaningful correlations with clinical outcomes in patients. It's still not excluded that some of the HCCs might benefit from an adapted version of the culture protocol. This could include a refined recipe of the growth factor-enriched medium as well as novel matrices that may facilitate the growth of well differentiated HCCs with higher requirements to their microenvironment. Other improvements may come from the culture of tumor organoids under hypoxic conditions, an approach previously shown to expand the spectrum of CRCs that could be propagated *in vitro*[144].

Finally, the importance of the tumor microenvironment is well recognized[69]. Tumor organoids are purely composed of cancer cells and therefore, not completely representative of the whole cancer ecosystem. Recently, culture systems that aimed to co-culture tumor cells with endothelial cells[190], fibroblasts[145], or immune cells[146] provided first insights into the interactions and/or dependencies of cancer cells and their cellular neighbors in the tumor microenvironment.

7.3. Concluding remarks

An important advantage of the organoid system is that long-term cultivation and biobanking of living cells becomes for the first time possible in a substantial percentage of patients. The latest progress in organoid derivation from small biopsy tissue promises a big boost to personalized treatment approaches. However, using HCC organoids for informed decision-making before treatment onset in the corresponding patient, may not be feasible. First, the time to derive and establish a new patient-

derived HCC organoid line ranges from 4–12 weeks. Only then, cells will be sufficiently expanded to allow their characterization together with a predictive drug testing *in vitro*. However, patients with advanced HCCs progress rapidly and treatment needs to be started immediately. Second, personalized treatment implies the generation of organoids for every patient, a premise that requires greater efficiencies in establishing organoids from HCCs.

In our opinion, tumor organoids will rather demonstrate their utility to predict treatment response based on the molecular features of the tumors in a non-individualized manner. Large pan-cancer molecular analyses revealed that driver gene mutations can affect 12 different signaling pathways and lead to the alteration of three core cellular processes: cell fate, cell survival, and genome maintenance[91]. Therefore, it would be sufficient to generate a tumor organoid biobank encompassing all altered pathways and then link *in vitro* drug response to specific molecular alterations, e.g. mutations or copy number alterations, that are present in the respective tumor (organoids). Following this approach, we could reduce the number of models needed to cover the molecular spectrum to ~50–100 organoid lines. To serve as a true reference set, tumor organoids will require a comprehensive characterization by various omics approaches, also including proteomics/phosphoproteomics. Indeed, most signaling pathways rely on phosphorylation cascades across multiple protein-protein interactions, obviously not captured by exome- or transcriptome-based sequencing methods. Importantly, small molecule inhibitors such as sorafenib act by preventing kinases to forward a signal along the pathway. We hypothesize that sorafenib resistance may in part result from treatment-induced or pre-existing activation of bypass signaling pathways that are (only) detectable with phosphoproteomic analysis. These follow-up experiments are currently ongoing and will complement the existing molecular profile, as well as provide a dataset to investigate the effects of kinase modulators on tumor organoids with different backgrounds and molecular alterations.

In conclusion, we developed a novel *in vitro* tool for the study of liver cancers and provide evidence for their physiological relevance and future clinical utility. The biobank can be continuously expanded, clinical and molecular data annotated, and drug response profiles correlated with individual tumor features, offering a helpful resource for further research in liver cancer.

8. REFERENCES

1. Koolman, J. & Roehm, K.H. *Color Atlas of Biochemistry*, (Thieme, 2012).

2. Trefts, E., Gannon, M. & Wasserman, D.H. The liver. *Curr Biol* **27**, R1147-R1151 (2017).

3. Bianconi, E.*, et al.* An estimation of the number of cells in the human body. *Ann Hum Biol* **40**, 463-471 (2013).

4. Si-Tayeb, K., Lemaigre, F.P. & Duncan, S.A. Organogenesis and development of the liver. *Dev Cell* **18**, 175-189 (2010).

5. Jungermann, K. & Kietzmann, T. Zonation of parenchymal and nonparenchymal metabolism in liver. *Annu Rev Nutr* **16**, 179-203 (1996).

6. Zorn, A.M. & Wells, J.M. Vertebrate endoderm development and organ formation. *Annu Rev Cell Dev Biol* **25**, 221-251 (2009).

7. Zaret, K.S. Regulatory phases of early liver development: paradigms of organogenesis. *Nat Rev Genet* **3**, 499-512 (2002).

8. Gordillo, M., Evans, T. & Gouon-Evans, V. Orchestrating liver development. *Development* **142**, 2094-2108 (2015).

9. Lemaigre, F.P. Mechanisms of liver development: concepts for understanding liver disorders and design of novel therapies. *Gastroenterology* **137**, 62-79 (2009).

10. Stanger, B.Z. Cellular homeostasis and repair in the mammalian liver. *Annu Rev Physiol* **77**, 179-200 (2015).

11. Michalopoulos, G.K. Liver regeneration after partial hepatectomy: critical analysis of mechanistic dilemmas. *Am J Pathol* **176**, 2-13 (2010).

12. Gehart, H. & Clevers, H. Repairing organs: lessons from intestine and liver. *Trends Genet* **31**, 344-351 (2015).

13. Barker, N.*, et al.* Identification of stem cells in small intestine and colon by marker gene Lgr5. *Nature* **449**, 1003-1007 (2007).

14. Yanger, K.*, et al.* Adult hepatocytes are generated by self-duplication rather than stem cell differentiation. *Cell Stem Cell* **15**, 340-349 (2014).

15. Planas-Paz, L.*, et al.* The RSPO-LGR4/5-ZNRF3/RNF43 module controls liver zonation and size. *Nat Cell Biol* **18**, 467-479 (2016).

16. He, L.*, et al.* Enhancing the precision of genetic lineage tracing using dual recombinases. *Nat Med* **23**, 1488-1498 (2017).

17. Popper, H., Kent, G. & Stein, R. Ductular cell reaction in the liver in hepatic injury. *Journal of the Mount Sinai Hospital, New York* **24**, 551-556 (1957).

18. Furuyama, K.*, et al.* Continuous cell supply from a Sox9-expressing progenitor zone in adult liver, exocrine pancreas and intestine. *Nat Genet* **43**, 34-41 (2011).

19. Tarlow, B.D., Finegold, M.J. & Grompe, M. Clonal tracing of Sox9+ liver progenitors in mouse oval cell injury. *Hepatology* **60**, 278-289 (2014).

20. Stueck, A.E. & Wanless, I.R. Hepatocyte buds derived from progenitor cells repopulate regions of parenchymal extinction in human cirrhosis. *Hepatology* **61**, 1696-1707 (2015).

21. Tarlow, B.D.*, et al.* Bipotential adult liver progenitors are derived from chronically injured mature hepatocytes. *Cell Stem Cell* **15**, 605-618 (2014).

22. Lu, W.Y.*, et al.* Hepatic progenitor cells of biliary origin with liver repopulation capacity. *Nat Cell Biol* **17**, 971-983 (2015).

23. Font-Burgada, J.*, et al.* Hybrid Periportal Hepatocytes Regenerate the Injured Liver without Giving Rise to Cancer. *Cell* **162**, 766-779 (2015).

24. Deng, X.*, et al.* Chronic Liver Injury Induces Conversion of Biliary Epithelial Cells into Hepatocytes. *Cell Stem Cell* **23**, 114-122 e113 (2018).

25. Wang, B., Zhao, L., Fish, M., Logan, C.Y. & Nusse, R. Self-renewing diploid Axin2(+) cells fuel homeostatic renewal of the liver. *Nature* **524**, 180-185 (2015).

26. Global Burden of Disease Cancer, C.*, et al.* Global, Regional, and National Cancer Incidence, Mortality, Years of Life Lost, Years Lived With Disability, and Disability-Adjusted Life-Years for 29 Cancer Groups, 1990 to 2016: A Systematic Analysis for the Global Burden of Disease Study. *JAMA Oncol* (2018).

27. Valery, P.C.*, et al.* Projections of primary liver cancer to 2030 in 30 countries worldwide. *Hepatology* (2017).

28. El-Serag, H.B. Hepatocellular carcinoma. *N Engl J Med* **365**, 1118-1127 (2011).

29. Llovet, J.M., Villanueva, A., Lachenmayer, A. & Finn, R.S. Advances in targeted therapies for hepatocellular carcinoma in the genomic era. *Nat Rev Clin Oncol* **12**, 408-424 (2015).

30. European Association For The Study Of The, L., European Organisation For, R. & Treatment Of, C. EASL-EORTC clinical practice guidelines: management of hepatocellular carcinoma. *J Hepatol* **56**, 908-943 (2012).

31. El-Serag, H.B. & Rudolph, K.L. Hepatocellular carcinoma: epidemiology and molecular carcinogenesis. *Gastroenterology* **132**, 2557-2576 (2007).

32. Yang, J.D.*, et al.* Cirrhosis is present in most patients with hepatitis B and hepatocellular carcinoma. *Clin Gastroenterol Hepatol* **9**, 64-70 (2011).

33. Llovet, J.M.*, et al.* Hepatocellular carcinoma. *Nat Rev Dis Primers* **2**, 16018 (2016).

34. Baffy, G., Brunt, E.M. & Caldwell, S.H. Hepatocellular carcinoma in non-alcoholic fatty liver disease: an emerging menace. *J Hepatol* **56**, 1384-1391 (2012).

35. Schweitzer, A., Horn, J., Mikolajczyk, R.T., Krause, G. & Ott, J.J. Estimations of worldwide prevalence of chronic hepatitis B virus infection: a systematic review of data published between 1965 and 2013. *The Lancet* **386**, 1546-1555 (2015).

36. Nelson, N.P., Easterbrook, P.J. & McMahon, B.J. Epidemiology of Hepatitis B Virus Infection and Impact of Vaccination on Disease. *Clin Liver Dis* **20**, 607-628 (2016).

37. Liang, T.J. Hepatitis B: the virus and disease. *Hepatology* **49**, S13-21 (2009).

38. Rehermann, B. & Nascimbeni, M. Immunology of hepatitis B virus and hepatitis C virus infection. *Nat Rev Immunol* **5**, 215-229 (2005).

39. Bouchard, M.J. & Schneider, R.J. The enigmatic X gene of hepatitis B virus. *J Virol* **78**, 12725-12734 (2004).

40. Tu, T., Budzinska, M.A., Shackel, N.A. & Urban, S. HBV DNA Integration: Molecular Mechanisms and Clinical Implications. *Viruses* **9**(2017).

41. Chisari, F.V., Isogawa, M. & Wieland, S.F. Pathogenesis of hepatitis B virus infection. *Pathol Biol (Paris)* **58**, 258-266 (2010).

42. Koshy, R., Maupas, P., Muller, R. & Hofschneider, P.H. Detection of Hepatitis-B Virus-Specific DNA in the Genomes of Human Hepatocellular-Carcinoma and Liver-Cirrhosis Tissues. *Journal of General Virology* **57**, 95-102 (1981).

43. Chakraborty, P.R., Ruiz-Opazo, N., Shouval, D. & Shafritz, D.A. Identification of integrated hepatitis B virus DNA and expression of viral RNA in an HBsAg-producing human hepatocellular carcinoma cell line. *Nature* **286**, 531-533 (1980).

44. Edman, J.C., Gray, P., Valenzuela, P., Rall, L.B. & Rutter, W.J. Integration of hepatitis B virus sequences and their expression in a human hepatoma cell. *Nature* **286**, 535-538 (1980).

45. Brechot, C., Pourcel, C., Louise, A., Rain, B. & Tiollais, P. Presence of integrated hepatitis B virus DNA sequences in cellular DNA of human hepatocellular carcinoma. *Nature* **286**, 533-535 (1980).

46. Sung, W.K.*, et al.* Genome-wide survey of recurrent HBV integration in hepatocellular carcinoma. *Nat Genet* **44**, 765-769 (2012).

47. Tu, T., Budzinska, M.A., Shackel, N.A. & Jilbert, A.R. Conceptual models for the initiation of hepatitis B virus-associated hepatocellular carcinoma. *Liver Int* **35**, 1786-1800 (2015).

48. Bhatia, S.N., Underhill, G.H., Zaret, K.S. & Fox, I.J. Cell and tissue engineering for liver disease. *Sci Transl Med* **6**, 245sr242 (2014).

49. Arzumanyan, A., Reis, H.M. & Feitelson, M.A. Pathogenic mechanisms in HBV- and HCV-associated hepatocellular carcinoma. *Nat Rev Cancer* **13**, 123-135 (2013).

50. Farazi, P.A. & DePinho, R.A. Hepatocellular carcinoma pathogenesis: from genes to environment. *Nat Rev Cancer* **6**, 674-687 (2006).

51. Kish, T., Aziz, A. & Sorio, M. Hepatitis C in a New Era: A Review of Current Therapies. *P T* **42**, 316-329 (2017).

52. Bartenschlager, R., Lohmann, V. & Penin, F. The molecular and structural basis of advanced antiviral therapy for hepatitis C virus infection. *Nat Rev Microbiol* **11**, 482-496 (2013).

53. Heim, M.H. 25 years of interferon-based treatment of chronic hepatitis C: an epoch coming to an end. *Nat Rev Immunol* **13**, 535-542 (2013).

54. Osna, N.A., Donohue, T.M., Jr. & Kharbanda, K.K. Alcoholic Liver Disease: Pathogenesis and Current Management. *Alcohol Res* **38**, 147-161 (2017).

55. Becker, U.*, et al.* Prediction of risk of liver disease by alcohol intake, sex, and age: a prospective population study. *Hepatology* **23**, 1025-1029 (1996).

56. French, S.W. The Pathophysiology of Alcoholic Liver Disease ∗. in *Liver Pathophysiology* 141-157 (2017).

57. Xu, W. & Yu, J. Obesity and Hepatocellular Carcinoma. in *Liver Pathophysiology* 267-277 (2017).

58. Suthar, A.B. & Harries, A.D. A public health approach to hepatitis C control in low- and middle-income countries. *PLoS Med* **12**, e1001795 (2015).

59. Mittal, S.*, et al.* Temporal trends of nonalcoholic fatty liver disease-related hepatocellular carcinoma in the veteran affairs population. *Clin Gastroenterol Hepatol* **13**, 594-601 e591 (2015).

60. Yasui, K.*, et al.* Characteristics of patients with nonalcoholic steatohepatitis who develop hepatocellular carcinoma. *Clin Gastroenterol Hepatol* **9**, 428-433; quiz e450 (2011).

61. Torres, D.M. & Harrison, S.A. Nonalcoholic steatohepatitis and noncirrhotic hepatocellular carcinoma: fertile soil. *Semin Liver Dis* **32**, 30-38 (2012).

62. Trail, F., Mahanti, N. & Linz, J. Molecular biology of aflatoxin biosynthesis. *Microbiology* **141 (Pt 4)**, 755-765 (1995).

63. Hamid, A.S., Tesfamariam, I.G., Zhang, Y. & Zhang, Z.G. Aflatoxin B1-induced hepatocellular carcinoma in developing countries: Geographical distribution, mechanism of action and prevention. *Oncol Lett* **5**, 1087-1092 (2013).

64. Liu, Y. & Wu, F. Global burden of aflatoxin-induced hepatocellular carcinoma: a risk assessment. *Environ Health Perspect* **118**, 818-824 (2010).

65. Kew, M.C. Hepatic iron overload and hepatocellular carcinoma. *Liver Cancer* **3**, 31-40 (2014).

66. Villanueva, A., Newell, P. & Hoshida, Y. Inherited hepatocellular carcinoma. *Best Pract Res Clin Gastroenterol* **24**, 725-734 (2010).

67. Ala, A., Walker, A.P., Ashkan, K., Dooley, J.S. & Schilsky, M.L. Wilson's disease. *The Lancet* **369**, 397-408 (2007).

68. Xu, R. & Hajdu, C.H. Wilson disease and hepatocellular carcinoma. *Gastroenterol Hepatol (N Y)* **4**, 438-439 (2008).

69. Hanahan, D. & Weinberg, R.A. Hallmarks of cancer: the next generation. *Cell* **144**, 646-674 (2011).

70. Forner, A., Reig, M. & Bruix, J. Hepatocellular carcinoma. *The Lancet* **391**, 1301-1314 (2018).

71. Morgan, R.L.*, et al.* Eradication of Hepatitis C Virus Infection and the Development of Hepatocellular Carcinoma A Meta-analysis of Observational Studies. *Annals of Internal Medicine* **158**, 329-+ (2013).

72. Li, W.Q.*, et al.* Index-based dietary patterns and risk of incident hepatocellular carcinoma and mortality from chronic liver disease in a prospective study. *Hepatology* **60**, 588-597 (2014).

73. European Association for the Study of the Liver. Electronic address, e.e.e. & European Association for the Study of the, L. EASL Clinical Practice Guidelines: Management of hepatocellular carcinoma. *J Hepatol* **69**, 182-236 (2018).

74. Heimbach, J.K.*, et al.* AASLD guidelines for the treatment of hepatocellular carcinoma. *Hepatology* **67**, 358-380 (2018).

75. Yang, Z.F. & Poon, R.T. Vascular changes in hepatocellular carcinoma. *Anat Rec (Hoboken)* **291**, 721-734 (2008).

76. Di Tommaso, L.*, et al.* The application of markers (HSP70 GPC3 and GS) in liver biopsies is useful for detection of hepatocellular carcinoma. *J Hepatol* **50**, 746-754 (2009).

77. Llovet, J.M., Brú, C. & Bruix, J. Prognosis of Hepatocellular Carcinoma: The BCLC Staging Classification. *Semin Liver Dis* **19**, 329-338 (1999).

78. Llovet, J.M., Montal, R., Sia, D. & Finn, R.S. Molecular therapies and precision medicine for hepatocellular carcinoma. *Nat Rev Clin Oncol* (2018).

79. Wilhelm, S.M.*, et al.* BAY 43-9006 exhibits broad spectrum oral antitumor activity and targets the RAF/MEK/ERK pathway and receptor tyrosine kinases involved in tumor progression and angiogenesis. *Cancer Res* **64**, 7099-7109 (2004).

80. Llovet, J.M.*, et al.* Sorafenib in advanced hepatocellular carcinoma. *N Engl J Med* **359**, 378-390 (2008).

81. Llovet, J.M. & Hernandez-Gea, V. Hepatocellular carcinoma: reasons for phase III failure and novel perspectives on trial design. *Clinical cancer research : an official journal of the American Association for Cancer Research* **20**, 2072-2079 (2014).

82. Kudo, M.*, et al.* Lenvatinib versus sorafenib in first-line treatment of patients with unresectable hepatocellular carcinoma: a randomised phase 3 non-inferiority trial. *The Lancet* **391**, 1163-1173 (2018).

83. Bruix, J.*, et al.* Regorafenib for patients with hepatocellular carcinoma who progressed on sorafenib treatment (RESORCE): a randomised, double-blind, placebo-controlled, phase 3 trial. *The Lancet* **389**, 56-66 (2017).

84. Abou-Alfa, G.K.*, et al.* Cabozantinib in Patients with Advanced and Progressing Hepatocellular Carcinoma. *N Engl J Med* **379**, 54-63 (2018).

85. Zhu, A.X.*, et al.* A randomized, double-blind, placebo-controlled phase III study of ramucirumab versus placebo as second-line treatment in patients with hepatocellular carcinoma and elevated baseline alpha-fetoprotein following first-line sorafenib (REACH-2). *Journal of Clinical Oncology* **34**, TPS4145-TPS4145 (2016).

86. El-Khoueiry, A.B.*, et al.* Nivolumab in patients with advanced hepatocellular carcinoma (CheckMate 040): an open-label, non-comparative, phase 1/2 dose escalation and expansion trial. *The Lancet* **389**, 2492-2502 (2017).

87. Iavarone, M.*, et al.* Diagnosis of hepatocellular carcinoma in cirrhosis by dynamic contrast imaging: the importance of tumor cell differentiation. *Hepatology* **52**, 1723-1730 (2010).

88. Schlageter, M., Terracciano, L.M., D'Angelo, S. & Sorrentino, P. Histopathology of hepatocellular carcinoma. *World J Gastroenterol* **20**, 15955-15964 (2014).

89. Edmondson, H.A. & Steiner, P.E. Primary carcinoma of the liver: a study of 100 cases among 48,900 necropsies. *Cancer* **7**, 462-503 (1954).

90. TCGA. Comprehensive and Integrative Genomic Characterization of Hepatocellular Carcinoma. *Cell* **169**, 1327-1341 e1323 (2017).

91. Vogelstein, B.*, et al.* Cancer genome landscapes. *Science* **339**, 1546-1558 (2013).

92. Nault, J.C.*, et al.* High frequency of telomerase reverse-transcriptase promoter somatic mutations in hepatocellular carcinoma and preneoplastic lesions. *Nat Commun* **4**, 2218 (2013).

93. Totoki, Y.*, et al.* Trans-ancestry mutational landscape of hepatocellular carcinoma genomes. *Nat Genet* **46**, 1267-1273 (2014).

94. Hoshida, Y.*, et al.* Integrative transcriptome analysis reveals common molecular subclasses of human hepatocellular carcinoma. *Cancer Res* **69**, 7385-7392 (2009).

95. Chiang, D.Y.*, et al.* Focal gains of VEGFA and molecular classification of hepatocellular carcinoma. *Cancer Res* **68**, 6779-6788 (2008).

96. Boyault, S.*, et al.* Transcriptome classification of HCC is related to gene alterations and to new therapeutic targets. *Hepatology* **45**, 42-52 (2007).

97. Lee, J.S., *et al.* Classification and prediction of survival in hepatocellular carcinoma by gene expression profiling. *Hepatology* **40**, 667-676 (2004).

98. Zucman-Rossi, J., Villanueva, A., Nault, J.C. & Llovet, J.M. Genetic Landscape and Biomarkers of Hepatocellular Carcinoma. *Gastroenterology* **149**, 1226-1239 e1224 (2015).

99. Makowska, Z., *et al.* Gene expression analysis of biopsy samples reveals critical limitations of transcriptome-based molecular classifications of hepatocellular carcinoma. *J Pathol Clin Res* **2**, 80-92 (2016).

100. Bakiri, L. & Wagner, E.F. Mouse models for liver cancer. *Mol Oncol* **7**, 206-223 (2013).

101. Li, Y., Tang, Z.Y. & Hou, J.X. Hepatocellular carcinoma: insight from animal models. *Nat Rev Gastroenterol Hepatol* **9**, 32-43 (2011).

102. Newell, P., Villanueva, A., Friedman, S.L., Koike, K. & Llovet, J.M. Experimental models of hepatocellular carcinoma. *J Hepatol* **48**, 858-879 (2008).

103. Byrne, A.T., *et al.* Interrogating open issues in cancer precision medicine with patient-derived xenografts. *Nat Rev Cancer* **17**, 254-268 (2017).

104. Gu, Q., *et al.* Genomic characterization of a large panel of patient-derived hepatocellular carcinoma xenograft tumor models for preclinical development. *Oncotarget* **6**, 20160-20176 (2015).

105. Xin, H., *et al.* Establishment and characterization of 7 novel hepatocellular carcinoma cell lines from patient-derived tumor xenografts. *PLoS One* **9**, e85308 (2014).

106. Yan, M., *et al.* Establishment of NOD/SCID mouse models of human hepatocellular carcinoma via subcutaneous transplantation of histologically intact tumor tissue. *Chin J Cancer Res* **25**, 289-298 (2013).

107. Huynh, H., Soo, K.C., Chow, P.K., Panasci, L. & Tran, E. Xenografts of human hepatocellular carcinoma: a useful model for testing drugs. *Clinical cancer research : an official journal of the American Association for Cancer Research* **12**, 4306-4314 (2006).

108. Armengol, C., *et al.* Orthotopic implantation of human hepatocellular carcinoma in mice: analysis of tumor progression and establishment of the BCLC-9 cell line. *Clinical cancer research : an official journal of the American Association for Cancer Research* **10**, 2150-2157 (2004).

109. Barretina, J., *et al.* The Cancer Cell Line Encyclopedia enables predictive modelling of anticancer drug sensitivity. *Nature* **483**, 603-607 (2012).

110. Nakabayashi, H., Taketa, K., Miyano, K., Yamane, T. & Sato, J. Growth of Human Hepatoma-Cell Lines with Differentiated Functions in Chemically Defined Medium. *Cancer Research* **42**, 3858-3863 (1982).

111. Aden, D.P., Fogel, A., Plotkin, S., Damjanov, I. & Knowles, B.B. Controlled synthesis of HBsAg in a differentiated human liver carcinoma-derived cell line. *Nature* **282**, 615-616 (1979).

112. Arellanes-Robledo, J., Hernández, C., Camacho, J. & Pérez-Carreón, J.I. In Vitro Models of HCC. in *Liver Pathophysiology* 563-579 (2017).

113. Qiu, Z.*, et al.* Hepatocellular carcinoma cell lines retain the genomic and transcriptomic landscapes of primary human cancers. *Sci Rep* **6**, 27411 (2016).

114. Lancaster, M.A. & Knoblich, J.A. Organogenesis in a dish: modeling development and disease using organoid technologies. *Science* **345**, 1247125 (2014).

115. Huch, M., Knoblich, J.A., Lutolf, M.P. & Martinez-Arias, A. The hope and the hype of organoid research. *Development* **144**, 938-941 (2017).

116. Clevers, H. Modeling Development and Disease with Organoids. *Cell* **165**, 1586-1597 (2016).

117. Sato, T.*, et al.* Single Lgr5 stem cells build crypt-villus structures in vitro without a mesenchymal niche. *Nature* **459**, 262-265 (2009).

118. de Lau, W.*, et al.* Lgr5 homologues associate with Wnt receptors and mediate R-spondin signalling. *Nature* **476**, 293-297 (2011).

119. Huch, M.*, et al.* In vitro expansion of single Lgr5+ liver stem cells induced by Wnt-driven regeneration. *Nature* **494**, 247-250 (2013).

120. Huch, M.*, et al.* Unlimited in vitro expansion of adult bi-potent pancreas progenitors through the Lgr5/R-spondin axis. *EMBO J* **32**, 2708-2721 (2013).

121. Barker, N.*, et al.* Lgr5(+ve) stem cells drive self-renewal in the stomach and build long-lived gastric units in vitro. *Cell Stem Cell* **6**, 25-36 (2010).

122. Chua, C.W.*, et al.* Single luminal epithelial progenitors can generate prostate organoids in culture. *Nat Cell Biol* **16**, 951-961, 951-954 (2014).

123. Karthaus, W.R.*, et al.* Identification of multipotent luminal progenitor cells in human prostate organoid cultures. *Cell* **159**, 163-175 (2014).

124. DeWard, A.D., Cramer, J. & Lagasse, E. Cellular heterogeneity in the mouse esophagus implicates the presence of a nonquiescent epithelial stem cell population. *Cell Rep* **9**, 701-711 (2014).

125. Fatehullah, A., Tan, S.H. & Barker, N. Organoids as an in vitro model of human development and disease. *Nat Cell Biol* **18**, 246-254 (2016).

126. Sato, T.*, et al.* Long-term expansion of epithelial organoids from human colon, adenoma, adenocarcinoma, and Barrett's epithelium. *Gastroenterology* **141**, 1762-1772 (2011).

127. Huch, M.*, et al.* Long-term culture of genome-stable bipotent stem cells from adult human liver. *Cell* **160**, 299-312 (2015).

128. Boj, S.F.*, et al.* Organoid models of human and mouse ductal pancreatic cancer. *Cell* **160**, 324-338 (2015).

129. Bartfeld, S.*, et al.* In vitro expansion of human gastric epithelial stem cells and their responses to bacterial infection. *Gastroenterology* **148**, 126-136 e126 (2015).

130. Schwank, G.*, et al.* Functional repair of CFTR by CRISPR/Cas9 in intestinal stem cell organoids of cystic fibrosis patients. *Cell Stem Cell* **13**, 653-658 (2013).

131. Date, S. & Sato, T. Mini-gut organoids: reconstitution of the stem cell niche. *Annu Rev Cell Dev Biol* **31**, 269-289 (2015).

132. Kretzschmar, K. & Clevers, H. Organoids: Modeling Development and the Stem Cell Niche in a Dish. *Dev Cell* **38**, 590-600 (2016).

133. Takasato, M.*, et al.* Kidney organoids from human iPS cells contain multiple lineages and model human nephrogenesis. *Nature* **526**, 564-568 (2015).

134. Lancaster, M.A.*, et al.* Cerebral organoids model human brain development and microcephaly. *Nature* **501**, 373-379 (2013).

135. Cancer Genome Atlas, N. Comprehensive molecular characterization of human colon and rectal cancer. *Nature* **487**, 330-337 (2012).

136. van de Wetering, M.*, et al.* Prospective derivation of a living organoid biobank of colorectal cancer patients. *Cell* **161**, 933-945 (2015).

137. Sachs, N.*, et al.* A Living Biobank of Breast Cancer Organoids Captures Disease Heterogeneity. *Cell* **172**, 373-386 e310 (2018).

138. Seidlitz, T.*, et al.* Human gastric cancer modelling using organoids. *Gut* (2018).

139. Gao, D.*, et al.* Organoid cultures derived from patients with advanced prostate cancer. *Cell* **159**, 176-187 (2014).

140. Lee, S.H.*, et al.* Tumor Evolution and Drug Response in Patient-Derived Organoid Models of Bladder Cancer. *Cell* **173**, 515-528 e517 (2018).

141. Broutier, L.*, et al.* Human primary liver cancer-derived organoid cultures for disease modeling and drug screening. *Nat Med* **23**, 1424-1435 (2017).

142. Nuciforo, S.*, et al.* Organoid Models of Human Liver Cancers Derived from Tumor Needle Biopsies. *Cell Reports* **24**, 1363-1376 (2018).

143. Drost, J. & Clevers, H. Organoids in cancer research. *Nat Rev Cancer* (2018).

144. Fujii, M.*, et al.* A Colorectal Tumor Organoid Library Demonstrates Progressive Loss of Niche Factor Requirements during Tumorigenesis. *Cell Stem Cell* **18**, 827-838 (2016).

145. Ohlund, D.*, et al.* Distinct populations of inflammatory fibroblasts and myofibroblasts in pancreatic cancer. *J Exp Med* **214**, 579-596 (2017).

146. Dijkstra, K.K.*, et al.* Generation of Tumor-Reactive T Cells by Co-culture of Peripheral Blood Lymphocytes and Tumor Organoids. *Cell* (2018).

147. Li, X.*, et al.* Oncogenic transformation of diverse gastrointestinal tissues in primary organoid culture. *Nat Med* **20**, 769-777 (2014).

148. Vlachogiannis, G.*, et al.* Patient-derived organoids model treatment response of metastatic gastrointestinal cancers. *Science* **359**, 920-926 (2018).

149. Sander, J.D. & Joung, J.K. CRISPR-Cas systems for editing, regulating and targeting genomes. *Nat Biotechnol* **32**, 347-355 (2014).

150. Drost, J.*, et al.* Sequential cancer mutations in cultured human intestinal stem cells. *Nature* **521**, 43-47 (2015).

151. Matano, M.*, et al.* Modeling colorectal cancer using CRISPR-Cas9-mediated engineering of human intestinal organoids. *Nat Med* **21**, 256-262 (2015).

152. Verissimo, C.S.*, et al.* Targeting mutant RAS in patient-derived colorectal cancer organoids by combinatorial drug screening. *Elife* **5**(2016).

153. Kondo, J.*, et al.* Retaining cell-cell contact enables preparation and culture of spheroids composed of pure primary cancer cells from colorectal cancer. *Proc Natl Acad Sci U S A* **108**, 6235-6240 (2011).

154. Liu, L.H., Xie, Y.L. & Lou, L.G. Cyclic AMP inhibition of proliferation of hepatocellular carcinoma cells is mediated by Akt. *Cancer Biology & Therapy* **4**, 1240-1247 (2005).

155. Kretzmann, N.A., Chiela, E., Matte, U., Marroni, N. & Marroni, C.A. N-acetylcysteine improves antitumoural response of Interferon alpha by NF-kB downregulation in liver cancer cells. *Comp Hepatol* **11**, 4 (2012).

156. Park, S.Y., Lee, K.B., Lee, M.J., Bae, S.C. & Jang, J.J. Nicotinamide inhibits the early stage of carcinogen-induced hepatocarcinogenesis in mice and suppresses human hepatocellular carcinoma cell growth. *J Cell Physiol* **227**, 899-908 (2012).

157. Shiota, G., Rhoads, D.B., Wang, T.C., Nakamura, T. & Schmidt, E.V. Hepatocyte growth factor inhibits growth of hepatocellular carcinoma cells. *Proc Natl Acad Sci U S A* **89**, 373-377 (1992).

158. Wu, X.*, et al.* FGF19-induced hepatocyte proliferation is mediated through FGFR4 activation. *J Biol Chem* **285**, 5165-5170 (2010).

159. Abou-Alfa, G.K.*, et al.* Phase II study of sorafenib in patients with advanced hepatocellular carcinoma. *J Clin Oncol* **24**, 4293-4300 (2006).

160. Li, H. & Durbin, R. Fast and accurate short read alignment with Burrows-Wheeler transform. *Bioinformatics* **25**, 1754-1760 (2009).

161. McKenna, A.*, et al.* The Genome Analysis Toolkit: a MapReduce framework for analyzing next-generation DNA sequencing data. *Genome Res* **20**, 1297-1303 (2010).

162. Landau, D.A.*, et al.* Evolution and impact of subclonal mutations in chronic lymphocytic leukemia. *Cell* **152**, 714-726 (2013).

163. Saunders, C.T.*, et al.* Strelka: accurate somatic small-variant calling from sequenced tumor-normal sample pairs. *Bioinformatics* **28**, 1811-1817 (2012).

164. Thorvaldsdottir, H., Robinson, J.T. & Mesirov, J.P. Integrative Genomics Viewer (IGV): high-performance genomics data visualization and exploration. *Brief Bioinform* **14**, 178-192 (2013).

165. Shen, R. & Seshan, V.E. FACETS: allele-specific copy number and clonal heterogeneity analysis tool for high-throughput DNA sequencing. *Nucleic acids research* **44**, e131 (2016).

166. Piscuoglio, S.*, et al.* The Genomic Landscape of Male Breast Cancers. *Clinical cancer research : an official journal of the American Association for Cancer Research* **22**, 4045-4056 (2016).

167. Carter, S.L.*, et al.* Absolute quantification of somatic DNA alterations in human cancer. *Nature biotechnology* **30**, 413-421 (2012).

168. Kandoth, C.*, et al.* Mutational landscape and significance across 12 major cancer types. *Nature* **502**, 333-339 (2013).

169. Lawrence, M.S.*, et al.* Discovery and saturation analysis of cancer genes across 21 tumour types. *Nature* **505**, 495-501 (2014).

170. Fujimoto, A.*, et al.* Whole-genome mutational landscape and characterization of noncoding and structural mutations in liver cancer. *Nat Genet* **48**, 500-509 (2016).

171. Chang, M.T.*, et al.* Identifying recurrent mutations in cancer reveals widespread lineage diversity and mutational specificity. *Nature biotechnology* **34**, 155-163 (2016).

172. Gao, J.*, et al.* 3D clusters of somatic mutations in cancer reveal numerous rare mutations as functional targets. *Genome Med* **9**, 4 (2017).

173. Carter, H.*, et al.* Cancer-specific high-throughput annotation of somatic mutations: computational prediction of driver missense mutations. *Cancer research* **69**, 6660-6667 (2009).

174. Shihab, H.A.*, et al.* Predicting the functional, molecular, and phenotypic consequences of amino acid substitutions using hidden Markov models. *Hum Mutat* **34**, 57-65 (2013).

175. Rosenthal, R., McGranahan, N., Herrero, J., Taylor, B.S. & Swanton, C. deconstructSigs: delineating mutational processes in single tumors distinguishes DNA repair deficiencies and patterns of carcinoma evolution. *Genome biology* **17**, 31 (2016).

176. Alexandrov, L.B.*, et al.* Signatures of mutational processes in human cancer. *Nature* **500**, 415-421 (2013).

177. Nik-Zainal, S.*, et al.* Landscape of somatic mutations in 560 breast cancer whole-genome sequences. *Nature* **534**, 47-54 (2016).

178. Dobin, A.*, et al.* STAR: ultrafast universal RNA-seq aligner. *Bioinformatics* **29**, 15-21 (2013).

179. Li, B. & Dewey, C.N. RSEM: accurate transcript quantification from RNA-Seq data with or without a reference genome. *BMC Bioinformatics* **12**, 323 (2011).

180. Nikolayeva, O. & Robinson, M.D. edgeR for differential RNA-seq and ChIP-seq analysis: an application to stem cell biology. *Methods Mol Biol* **1150**, 45-79 (2014).

181. Gao, J.*, et al.* Integrative analysis of complex cancer genomics and clinical profiles using the cBioPortal. *Sci Signal* **6**, pl1 (2013).

182. GHDX. http://ghdx.healthdata.org/gbd-results-tool?params=gbd-api-2016-permalink/2bc611800a2675324fa134b2688bb4cf.

183. Pera, M.F. The dark side of induced pluripotency. *Nature* **471**, 46 (2011).

184. Rojkind, M. & Ponce-Noyola, P. The Extracellular Matrix of the Liver. *Collagen and Related Research* **2**, 151-175 (1982).

185. Saheli, M.*, et al.* Three-dimensional liver-derived extracellular matrix hydrogel promotes liver organoids function. *J Cell Biochem* **119**, 4320-4333 (2018).

186. Gjorevski, N.*, et al.* Designer matrices for intestinal stem cell and organoid culture. *Nature* **539**, 560-564 (2016).

187. Guilak, F.*, et al.* Control of stem cell fate by physical interactions with the extracellular matrix. *Cell Stem Cell* **5**, 17-26 (2009).

188. Natarajan, V., Berglund, E.J., Chen, D.X. & Kidambi, S. Substrate stiffness regulates primary hepatocyte functions. *RSC Advances* **5**, 80956-80966 (2015).

189. Shingaki, N.*, et al.* Serological and histological indices of hepatocellular carcinoma and tumor volume doubling time. *Mol Clin Oncol* **1**, 977-981 (2013).

190. Shoval, H.*, et al.* Tumor cells and their crosstalk with endothelial cells in 3D spheroids. *Sci Rep* **7**, 10428 (2017).

9. APPENDIX

Supplementary tables of section 7.2.

Table S1

Patient	Biopsy ID	Sex	Age	Tumor	Liver Disease(s)	Cirrhosis	BCLC	Viable Tumor Cells	Immune Infiltrate	Necrosis	Stroma	Non-malignant Liver	Edmondson	Growth Pattern	AFP [IU/ml]	Liver Organoids	Tumor Organoids
1	C655	Male	55	HCC	HCV; ALD	no	C	10%	5%	80%	5%		III	trabecular-pseudoglandular	269	✓	✓
2	C798	Male	73	HCC	NAFLD	no	C	70%		5%	5%	20%	III	solid-trabecular	20'377	✓	✓
3-A	C937	Male	70	HCC	HBV	yes	B	95%	5%				II	solid-trabecular	701	✓	-
4-A	C942	Male	76	HCC	NAFLD	yes	C	70%					III	solid-trabecular	>100'000	✓	-
4-B	C944							30%					III	solid-pseudoglandular		✓	-
5-A	C948	Male	57	HCC	HCV; ALD	yes	C	80%	10%		10%		III	trabecular	12'054	✓	✓
5-B	C949							40%		30%	30%		III	trabecular		✓	✓
6	C951	Female	71	HCC	ALD	yes	C	80%	10%		10%		III	solid-trabecular	1'745	✓	-
7-A	C958	Male	53	HCC	HCV; ALD	yes	C	40%		10%	10%	40%	III	solid-trabecular	228	✓	-
7-B	C959							5%				95%	n.e.	n.e.		✓	-
8	C964	Male	71	HCC	ALD	yes	B	95%					III	solid-trabecular	2.6	✓	-
7-B	C965	Male	53	HCC	HCV; ALD	yes	C	50%	10%	40%			III	solid-trabecular	228	✓	-
9	C975	Male	59	HCC	HCV; ALD	yes	B	50%	30%		20%%		III	solid	250	✓	✓
3-B	C977	Male	70	HCC	HBV	yes	B	30%		20%		50%	III	solid	701	✓	-
10-I	D016	Male	83	HCC	none	no	A	85%		15%			III	trabecular-pseudoglandular	231	✓	-
10-II	D017							75%		25%			III	trabecular-pseudoglandular		✓	-
10-III	D018							85%		15%			II	trabecular-pseudoglandular		✓	-
11	D029	Female	73	HCC	ALD	yes	B	50%	40%			10%	II	solid-trabecular	7.9	✓	-
12-I	D045	Male	69	HCC	HCV	no	A	80%	10%	10%			III	solid-trabecular	7'852	✓	✓
12-II	D046							70%	10%	20%			III	solid-trabecular		✓	✓
13	*D091*	*Female*	*61*	*CCC*	*none*	*no*	*n.a.*	*n.a.*	*n.a.*	*n.a.*	*n.a.*	*n.a.*	*n.a.*	*n.a.*	*4.4*	✓	✓
14-I	D096	Male	75	HCC	ALD	no	A	40%		60%			IV	solid	2	✓	-
14-II	D097							30%	10%	60%			IV	solid		✓	-
14-III	D098							50%	20%	30%			IV	solid		✓	-
15-A	D135	Male	57	HCC	HCV	yes	C	80%	5%		15%		IV	solid-trabecular	11.4	✓	-
15-B	D136							5%	5%		10%	80%	IV	solid-trabecular		✓	-
16	*D141*	*Male*	*59*	*LELCC*	*HBV*	*yes*	*n.a.*	*n.a.*	*n.a.*	*n.a.*	*n.a.*	*n.a.*	*n.a.*	*n.a.*	*2.1*	✓	✓
17-A	D152	Male	73	HCC	HCV	yes	B	90%	5%		5%		II	solid	678	✓	-
17-B	D153							95%	5%				I/II	solid		✓	-
18	D156	Male	67	HCC	HBV	yes	A	95%	5%				II	trabecular	205	✓	-
19	D176	Male	79	HCC	none	no	C	95%					II	pseudoglandular	0.9	✓	-
20	*D178*	*Female*	*63*	*CCC*	*HCV*	*yes*	*n.a.*	*n.a.*	*n.a.*	*n.a.*	*n.a.*	*n.a.*	*n.a.*	*n.a.*	*3.1*	✓	✓
21	D268	Male	70	HCC	NAFLD	yes	B	95%					II	trabecular	10.2	✓	-
22-A	*D282*	*Female*	*83*	*CCC*	*NAFLD*	*no*	*n.a.*	*n.a.*	*n.a.*	*n.a.*	*n.a.*	*n.a.*	*n.a.*	*n.a.*	*201.9*	✓	-
22-B	*D283*							*n.a.*	*n.a.*	*n.a.*	*n.a.*	*n.a.*	*n.a.*	*n.a.*		✓	-
23-I	*D293*	*Female*	*74*	*CCC*	*none*	*no*	*n.a.*	*n.a.*	*n.a.*	*n.a.*	*n.a.*	*n.a.*	*n.a.*	*n.a.*	*11.8*	✓	-
23-II	*D296*							*n.a.*	*n.a.*	*n.a.*	*n.a.*	*n.a.*	*n.a.*	*n.a.*		✓	-
24-A	D301	Female	67	HCC	ALD	yes	C	90%	5%		5%		III	solid-pseudoglandular	>400'000	✓	-
24-B	D302							80%		20%			III	solid		✓	-
25	D324	Male	58	HCC	HCV	yes	D	70%	10%		20%		III	trabecular	104'710	✓	✓
26	D332	Male	72	HCC	ALD	no	A	90%	10%				II	solid-trabecular	3.1	✓	-
27	D359	Male	86	HCC	NAFLD	no	A	90%	10%				III	trabecular	5'917	✓	✓
28	D373	Female	79	HCC	HCV	no	C	65%					II	solid-trabecular	135	✓	-
29-A	D386	Male	80	HCC	ALD; NAFLD	no	A	20%	10%			70%	IV	solid	49.8	✓	✓
29-B	D388							70%	10%			20%	IV	solid-trabecular		✓	-

Table S1. Complete List of Patient Biopsies Used for the Generation of Liver Cancer Organoid Cultures. Samples were obtained between July 2015 and September 2017 and are ordered chronologically according to the date of the biopsy. If more than one tumor nodule was biopsied in a given patient, the different nodules are designated with letters (e.g. 5-A and 5-B). If more than one biopsy was taken from different locations of the same (large) nodule, the different locations are labeled with roman numbers (e.g. 12-I and 12-II). The five cholangiocellular carcinoma cases are shown in italic font. Sex, age, background liver disease, clinical staging according to the Barcelona Clinic Liver Cancer (BCLC) staging system and Alpha-Fetoprotein (AFP) serum concentrations were obtained from the clinical charts of the patients. The viable tumor cell content, Edmondson grade and the growth pattern were determined in each biopsy on Hematoxylin and Eosin stained sections by two experienced hepato-pathologists (M.S.M. and L.M.T.). All CCC tumors were poorly differentiated. ALD: Alcoholic Liver Disease; AFP: Alpha-Fetoprotein; BCLC: Barcelona Clinic Liver Cancer; CCC: Cholangiocellular Carcinoma; HBV: Hepatitis B Virus; HCC: Hepatocellular Carcinoma; HCV: Hepatitis C Virus; LELCC: Lymphoepithelioma-like Cholangiocarcinoma; NAFLD: Nonalcoholic Fatty Liver Disease; n.a.: not applicable; n.e.: not evaluable because of insufficient tumor cell content in the biopsy.

Table S2

Patient	Sample Type	Sample ID	Total Reads	Mean Target Coverage	% Target Bases 2X	% Target Bases 10X	% Target Bases 20X	% Target Bases 30X	% Target Bases 40X	% Target Bases 50X	% Target Bases 100X
Patient 2	HCC biopsy	C798	94'400'859	84.833832	0.986912	0.929052	0.846582	0.762986	0.679087	0.597782	0.299673
Patient 5-A	HCC biopsy	C948	182'374'059	158.418593	0.99129	0.973319	0.93111	0.882093	0.831304	0.780505	0.553611
Patient 5-B	HCC biopsy	C949	175'590'720	151.835666	0.991171	0.972848	0.932723	0.889122	0.844978	0.799712	0.570083
Patient 9	HCC biopsy	C975	106'802'239	96.985837	0.98905	0.946091	0.869019	0.788226	0.708543	0.633594	0.354944
Patient 12-I	HCC biopsy	D045	109'808'365	101.266678	0.990285	0.962181	0.902125	0.831947	0.758875	0.685875	0.384054
Patient 12-II	HCC biopsy	D046	106'176'163	93.784138	0.990509	0.96674	0.909361	0.839428	0.763436	0.685031	0.352563
Patient 13	CCC biopsy	D091	52'417'380	49.568261	0.98486	0.908378	0.774253	0.630126	0.497682	0.387621	0.105262
Patient 16	CCC biopsy	D141	51'804'174	48.658019	0.988706	0.934484	0.808445	0.660925	0.51506	0.389413	0.085029
Patient 20	CCC biopsy	D178	48'277'502	44.973331	0.986826	0.917074	0.770792	0.60697	0.458088	0.33793	0.072328
Patient 25	HCC biopsy	D324	169'053'773	145.133507	0.992001	0.982957	0.955138	0.916063	0.871091	0.822127	0.565329
Patient 2	Non-tumoral liver biopsy	C797	55'597'906	51.514998	0.987624	0.916564	0.780781	0.636293	0.505447	0.397432	0.118063
Patient 5-A/B	Non-tumoral liver biopsy	C562	55'247'613	50.936808	0.990132	0.959643	0.855046	0.716609	0.57204	0.436664	0.081186
Patient 9	Non-tumoral liver biopsy	C974	52'904'603	49.192584	0.985752	0.905382	0.765966	0.618861	0.486064	0.376917	0.104853
Patient 12-I/II	Non-tumoral liver biopsy	D043	47'954'416	44.604354	0.987038	0.912963	0.766297	0.604999	0.457908	0.339034	0.070557
Patient 13	Non-tumoral liver biopsy	D089	48'362'073	45.750593	0.988441	0.938396	0.808547	0.649892	0.493208	0.360386	0.063489
Patient 16	Non-tumoral liver biopsy	D140	58'733'948	54.028392	0.988459	0.929535	0.80807	0.673906	0.545263	0.433826	0.127464
Patient 20	Non-tumoral liver biopsy	D177	50'955'773	49.419051	0.979436	0.892369	0.764814	0.626612	0.498259	0.390868	0.107444
Patient 25	Non-tumoral liver biopsy	D323	100'073'292	88.711677	0.990714	0.964361	0.901141	0.82682	0.745931	0.663279	0.330326
Patient 2 early	Organoid	SN03	97'592'493	88.354733	0.989341	0.975786	0.932732	0.863128	0.7795	0.691544	0.322518
Patient 2 late	Organoid	SN04	91'169'165	82.477626	0.988877	0.971284	0.918346	0.838347	0.746465	0.652457	0.285949
Patient 5-A early	Organoid	SN05	99'157'797	88.881486	0.98934	0.97531	0.930665	0.860606	0.777803	0.690775	0.328442
Patient 5-A late	Organoid	SN06	101'447'853	93.594768	0.989411	0.976472	0.937101	0.873283	0.79587	0.713193	0.356365
Patient 5-B early	Organoid	SN07	98'038'120	89.963971	0.989228	0.974935	0.930919	0.861868	0.779373	0.693016	0.338199
Patient 5-B late	Organoid	SN08	91'421'651	85.565113	0.989111	0.973194	0.924945	0.850049	0.762593	0.672212	0.312226
Patient 9	Organoid	SN09	92'503'866	85.293773	0.989486	0.973246	0.922417	0.844441	0.755309	0.665404	0.308846
Patient 12-I	Organoid	SN11	48'607'137	44.986138	0.988373	0.933043	0.781295	0.61079	0.459165	0.336837	0.066151
Patient 12-II	Organoid	SN10	85'979'664	77.71085	0.989002	0.967542	0.904676	0.813179	0.712399	0.613627	0.261313
Patient 13	Organoid	SN12	46'906'182	43.317132	0.986808	0.927777	0.771911	0.599944	0.448793	0.326933	0.058203
Patient 16	Organoid	SN13	39'472'727	37.402368	0.98626	0.904481	0.712167	0.518329	0.362321	0.248342	0.036972
Patient 20	Organoid	SN14	64'941'346	57.49781	0.988992	0.959738	0.861499	0.73019	0.596509	0.473746	0.127552
Patient 25	Organoid	SN15	199'686'354	167.892064	0.991861	0.987713	0.979065	0.962377	0.936599	0.902926	0.679912

Table S2. Whole Exome Sequencing Statistics.

Table S3

Includes all somatic muations

Patient	Tumor biopsy	Total # mutations (in any sample)	# mutations in tumor biopsy (% of total number of mutations)	# of which in both organoids (% of mutations in biopsy)	# of which only in the early passage organoids (% of mutations in biopsy)	# of which only in the late passage organoids (% of mutations in biopsy)	# of which not in any organoid (% of mutations in biopsy)	# mutations not in tumor biopsy (% of total number of mutations)	# of novel mutations in both organoids (% of mutations not in biopsy)	# of novel mutations only in the early passage organoids (% of mutations not in biopsy)	# of novel mutations only in the late passage organoids (% of mutations not in biopsy)
Patient 2	C798	153	127 (83%)	106 (83%)	3 (2%)	1 (1%)	17 (13%)	26 (17%)	6 (23%)	2 (8%)	18 (69%)
Patient 5-A	C948	211	173 (82%)	146 (84%)	6 (3%)	3 (2%)	18 (10%)	38 (18%)	16 (42%)	9 (24%)	13 (34%)
Patient 5-B	C949	196	168 (86%)	153 (91%)	1 (1%)	1 (1%)	13 (8%)	28 (14%)	13 (46%)	13 (46%)	2 (7%)
Patient 9	C975	225	207 (92%)	NA	159 (77%)	NA	48 (23%)	18 (8%)	NA	18 (100%)	NA
Patient 12-I	D045	175	146 (83%)	NA	136 (93%)	NA	10 (7%)	29 (17%)	NA	29 (100%)	NA
Patient 12-II	D046	162	143 (88%)	NA	125 (87%)	NA	18 (13%)	19 (12%)	NA	19 (100%)	NA
Patient 13	D091	130	115 (88%)	NA	59 (51%)	NA	56 (49%)	15 (12%)	NA	15 (100%)	NA
Patient 16	D141	830	760 (92%)	NA	740 (97%)	NA	20 (3%)	70 (8%)	NA	70 (100%)	NA
Patient 20	D178	938	920 (98%)	NA	152 (17%)	NA	768 (83%)	18 (2%)	NA	18 (100%)	NA
Patient 25	D324	138	128 (93%)	NA	119 (93%)	NA	9 (7%)	10 (7%)	NA	10 (100%)	NA

Includes only non-synonymous somatic mutations

Patient	Tumor biopsy	Total # mutations (in any sample)	# mutations in tumor biopsy (% of total number of mutations)	# of which in both organoids (% of mutations in biopsy)	# of which only in the early passage organoids (% of mutations in biopsy)	# of which only in the late passage organoids (% of mutations in biopsy)	# of which not in any organoid (% of mutations in biopsy)	# mutations not in tumor biopsy (% of total number of mutations)	# of novel mutations in both organoids (% of mutations not in biopsy)	# of novel mutations only in the early passage organoids (% of mutations not in biopsy)	# of novel mutations only in the late passage organoids (% of mutations not in biopsy)
Patient 2	C798	116	97 (84%)	80 (82%)	2 (2%)	1 (1%)	14 (14%)	19 (16%)	3 (16%)	2 (11%)	14 (74%)
Patient 5-A	C948	161	128 (80%)	111 (87%)	4 (3%)	2 (2%)	11 (9%)	33 (20%)	12 (36%)	9 (27%)	12 (36%)
Patient 5-B	C949	139	125 (90%)	115 (92%)	0 (0%)	0 (0%)	10 (8%)	14 (10%)	7 (50%)	7 (50%)	7 (50%)
Patient 9	C975	166	153 (92%)	NA	119 (78%)	NA	34 (22%)	13 (8%)	NA	13 (100%)	NA
Patient 12-I	D045	124	100 (81%)	NA	94 (94%)	NA	6 (6%)	24 (19%)	NA	24 (100%)	NA
Patient 12-II	D046	118	101 (86%)	NA	91 (90%)	NA	10 (10%)	17 (14%)	NA	17 (100%)	NA
Patient 13	D091	97	85 (88%)	NA	49 (58%)	NA	36 (42%)	12 (12%)	NA	12 (100%)	NA
Patient 16	D141	654	600 (92%)	NA	587 (98%)	NA	13 (2%)	54 (8%)	NA	54 (100%)	NA
Patient 20	D178	630	617 (98%)	NA	103 (17%)	NA	514 (83%)	13 (2%)	NA	13 (100%)	NA
Patient 25	D324	108	101 (94%)	NA	93 (92%)	NA	8 (8%)	7 (6%)	NA	7 (100%)	NA

Includes only non-synonymous somatic mutations in Cancer Genes

Patient	Tumor biopsy	Total # mutations (in any sample)	# mutations in tumor biopsy (% of total number of mutations)	# of which in both organoids (% of mutations in biopsy)	# of which only in the early passage organoids (% of mutations in biopsy)	# of which only in the late passage organoids (% of mutations in biopsy)	# of which not in any organoid (% of mutations in biopsy)	# mutations not in tumor biopsy (% of total number of mutations)	# of novel mutations in both organoids (% of mutations not in biopsy)	# of novel mutations only in the early passage organoids (% of mutations not in biopsy)	# of novel mutations only in the late passage organoids (% of mutations not in biopsy)
Patient 2	C798	3	3 (100%)	3 (100%)	0 (0%)	0 (0%)	0 (0%)	0 (0%)	0 (NA)	0 (NA)	0 (NA)
Patient 5-A	C948	9	6 (67%)	6 (100%)	0 (0%)	0 (0%)	0 (0%)	3 (33%)	1 (33%)	1 (33%)	1 (33%)
Patient 5-B	C949	5	5 (100%)	5 (100%)	0 (0%)	0 (0%)	0 (0%)	0 (0%)	0 (NA)	0 (NA)	0 (NA)
Patient 9	C975	4	4 (100%)	NA	3 (75%)	NA	1 (25%)	0 (0%)	NA	0 (NA)	NA
Patient 12-I	D045	7	5 (71%)	NA	4 (80%)	NA	1 (20%)	2 (29%)	NA	2 (100%)	NA
Patient 12-II	D046	4	4 (100%)	NA	4 (100%)	NA	0 (0%)	0 (0%)	NA	0 (NA)	NA
Patient 13	D091	7	6 (86%)	NA	4 (67%)	NA	2 (33%)	1 (14%)	NA	1 (100%)	NA
Patient 16	D141	17	17 (100%)	NA	17 (100%)	NA	0 (0%)	0 (0%)	NA	0 (NA)	NA
Patient 20	D178	17	17 (100%)	NA	4 (24%)	NA	13 (76%)	0 (0%)	NA	0 (NA)	NA
Patient 25	D324	4	3 (75%)	NA	3 (100%)	NA	0 (0%)	1 (25%)	NA	1 (100%)	NA

Table S3. Somatic Mutation Counts in Tumor Biopsies and Derivative Organoids.

Table S4

SAMPLE	GENE	MUTATION	EFFECT	TUMOR VAF	NON-TUMOR VAF	TUMOR DEPTH	NON-TUMOR DEPTH	Cancer gene census	Kandoth	Lawrence	Fujimoto	Hotspot	Facets LOH Call	CHROM	POS	ALT	CCF	Absolute Clonal
Patient 2, Biopsy	C1orf159	p.Thr26Met	missense_variant	0.322	0	90	61	.	.	.	.	.	FALSE	1	1026359	A	1	Clonal
Patient 2, Biopsy	ACTL8	p.Val6Ile	missense_variant	0.0756303	0	119	88	.	.	.	.	.	FALSE	1	18149519	A	0.28	Subclonal
Patient 2, Biopsy	TMCO4	p.Ala211Ser	missense_variant	0.467	0	30	27	.	.	.	.	.	FALSE	1	20073075	A	1	Clonal
Patient 2, Biopsy	HIVEP3	p.Met265fs	frameshift_variant	0.40458	0	131	91	.	.	.	.	.	FALSE	1	42049671	C	1	Subclonal
Patient 2, Biopsy	LEPRE1	p.Asp253Val	missense_variant	0.313	0	224	147	.	.	.	.	.	FALSE	1	43224922	A	1	Clonal
Patient 2, Biopsy	KIF2C	p.Arg258Thr	missense_variant	0.231	0	13	24	.	.	.	.	.	FALSE	1	45221614	C	0.85	Clonal
Patient 2, Biopsy	ELTD1	p.Ile35Ile	synonymous_variant	0.57429	0	7	15	.	.	.	.	.	FALSE	1	79470822	A	1	Clonal
Patient 2, Biopsy	LRRC8C	p.Phe667Phe	synonymous_variant	0.217	0.019	60	53	.	.	.	.	.	FALSE	1	90180130	C	0.8	Clonal
Patient 2, Biopsy	GJA5	p.Lys233del	disruptive_inframe_deletion	0.0868545	0	426	82	.	.	.	.	.	FALSE	1	147230646	A	0.93	Clonal
Patient 2, Biopsy	OTUD7B	p.Lys550*	stop_gained	0.06	0	433	97	.	.	.	.	.	FALSE	1	149916640	A	0.64	Subclonal
Patient 2, Biopsy	CA14	p.Ser215Trp	missense_variant	0.016	0	250	138	.	.	.	.	.	FALSE	1	150235522	G	0.17	Subclonal
Patient 2, Biopsy	APOA2	p.Met34fs	frameshift_variant	0.0576923	0	624	188	.	.	.	.	.	FALSE	1	161193173	T	0.62	Subclonal
Patient 2, Biopsy	GJC2	p.Leu353Pro	missense_variant	0.192	0	26	22	.	.	.	.	.	FALSE	1	228346517	C	0.9	Clonal
Patient 2, Biopsy	OTX1	p.His260Gln	missense_variant	0.024	0	250	117	.	.	.	.	.	FALSE	2	63283166	G	0.14	Subclonal
Patient 2, Biopsy	PROM2	p.Leu119Leu	synonymous_variant	0.04	0	125	92	.	.	.	.	.	FALSE	2	95941738	T	0.19	Subclonal
Patient 2, Biopsy	CYP27C1	p.Pro243Pro	synonymous_variant	0.104	0	106	64	.	.	.	.	.	FALSE	2	127951434	G	0.49	Subclonal
Patient 2, Biopsy	NEB	p.Ile3069Thr	missense_variant	0.057	0	493	222	.	.	.	.	.	TRUE	2	152490376	G	0.21	Subclonal
Patient 2, Biopsy	FASTKD2	p.Asn663Ser	missense_variant	0.161	0	31	46	.	.	.	.	.	FALSE	2	207655385	G	0.76	Clonal
Patient 2, Biopsy	PIKFYVE	p.Asn383Asn	synonymous_variant	0.211	0	57	37	.	.	.	.	.	FALSE	2	209165759	T	0.99	Clonal
Patient 2, Biopsy	COL6A3	p.Ser2205er	synonymous_variant	0.19	0	205	126	.	.	.	.	.	FALSE	2	238303279	T	0.89	Clonal
Patient 2, Biopsy	SNED1	p.Ala316Val	missense_variant	0.62	0	179	92	.	.	.	.	.	FALSE	2	241976672	T	1	Clonal
Patient 2, Biopsy	ATG4B	p.Arg201Arg	synonymous_variant	0.626	0	195	108	.	.	.	.	.	FALSE	2	242606124	A	1	Clonal
Patient 2, Biopsy	KIAA1143	p.Gln136Lys	missense_variant	0.241	0	29	30	.	.	.	.	.	FALSE	3	44794892	T	1	Clonal
Patient 2, Biopsy	TMF1	p.Cys318Ser	missense_variant	0.647	0	17	24	.	.	.	.	.	FALSE	3	69096903	G	1	Clonal
Patient 2, Biopsy	PPP4R2	p.Ser146Arg	missense_variant	0.727	0	11	9	.	.	.	.	.	FALSE	3	73112842	A	1	Clonal
Patient 2, Biopsy	IFT57	p.Phe412Cys	missense_variant	0.259	0	54	20	.	.	.	.	.	FALSE	3	107941048	C	0.96	Clonal
Patient 2, Biopsy	SPICE1	p.Leu419fs	frameshift_variant	0.257143	0	35	61	.	.	.	.	.	FALSE	3	113184532	G	0.95	Clonal
Patient 2, Biopsy	ITGB5	p.Asp640His	missense_variant&splice_region_variant	0.208	0	24	31	.	.	.	.	.	FALSE	3	124487959	G	0.77	Clonal
Patient 2, Biopsy	MSL2	p.Arg344Lys	missense_variant	0.075	0	80	46	.	.	.	.	.	FALSE	3	135870692	T	0.28	Subclonal
Patient 2, Biopsy	PHC3	p.Trp937*	stop_gained	0.012987	0	77	25	.	.	.	.	.	FALSE	3	169802090	T	0.06	Subclonal
Patient 2, Biopsy	EPHB3	p.Gln509Lys	missense_variant	0.172	0	60	64	.	.	.	.	.	FALSE	3	184295491	A	0.78	Clonal
Patient 2, Biopsy	TMEM41A	p.Phe44Phe	synonymous_variant	0.333	0	18	22	.	.	.	.	.	FALSE	3	185214757	A	1	Clonal
Patient 2, Biopsy	ADH1A	p.Glu253Glu	synonymous_variant	0.0324074	0	216	102	.	.	.	.	.	TRUE	4	100203572	T	0.12	Subclonal
Patient 2, Biopsy	DNAJB14	p.Tyr38Cys	missense_variant	0.097	0	62	29	.	.	.	.	.	TRUE	4	100867616	C	0.36	Subclonal
Patient 2, Biopsy	FAM149A	p.Pro442Ser	missense_variant	0.146	0	96	59	.	.	.	.	.	TRUE	4	187077221	T	0.54	Subclonal
Patient 2, Biopsy	BDP1	p.Ala932fs	frameshift_variant	0.458333	0	48	56	.	.	.	.	.	FALSE	5	70805704	T	1	Clonal
Patient 2, Biopsy	SLC22A4	p.Leu347_Leu348del	disruptive_inframe_deletion	0.109375	0	64	72	.	.	.	.	.	FALSE	5	131667533	T	0.4	Subclonal
Patient 2, Biopsy	PPP1R18	p.Pro346His	missense_variant	0.137	0	153	121	.	.	.	.	.	TRUE	6	30652759	T	0.78	Clonal
Patient 2, Biopsy	CFB	p.Ile744Val	missense_variant	0.842	0	184	115	.	.	.	.	.	TRUE	6	31915584	G	1	Clonal
Patient 2, Biopsy	ZFAND3	p.Gln168Arg	missense_variant	0.159	0	44	18	.	.	.	.	.	TRUE	6	38084489	G	0.91	Clonal
Patient 2, Biopsy	DNAH8	p.Ser1436Arg	missense_variant	0.0666667	0	15	18	.	.	.	.	.	TRUE	6	38802396	G	0.38	Subclonal
Patient 2, Biopsy	GLP1R	p.Arg64Pro	missense_variant	0.102	0.00489	728	409	.	.	.	.	.	TRUE	6	39025263	C	0.58	Subclonal
Patient 2, Biopsy	DST	p.Lys6551Asn	missense_variant	0.107	0	168	40	.	.	.	.	.	TRUE	6	56366028	G	0.61	Subclonal
Patient 2, Biopsy	ASCC3	c.6075+2T>G	splice_donor_variant&intron_variant	0.219	0	32	9	.	.	.	.	.	TRUE	6	100964054	C	1	Clonal
Patient 2, Biopsy	KIAA1919	p.Gln415Pro	missense_variant	0.091	0	88	65	.	.	.	.	.	TRUE	6	111588009	C	0.52	Subclonal
Patient 2, Biopsy	AGPAT4	p.Glu149Gln	missense_variant	0.016	0	250	250	.	.	.	.	.	TRUE	6	161575246	G	0.09	Subclonal
Patient 2, Biopsy	POU6F2	p.Gly132Val	missense_variant	0.056	0	125	45	.	.	.	.	.	TRUE	7	39247103	T	0.26	Subclonal
Patient 2, Biopsy	COPS6	p.Phe168Leu	missense_variant	0.554	0	56	54	.	.	.	.	.	TRUE	7	99688542	A	1	Clonal
Patient 2, Biopsy	CREB3L2	p.Lys325Glu	missense_variant&splice_region_variant	0.903	0	62	26	TRUE	.	.	.	.	TRUE	7	137588706	C	1	Clonal
Patient 2, Biopsy	NUGGC	p.Thr176Thr	synonymous_variant	0.143	0	42	24	.	.	.	.	.	FALSE	8	27925214	T	0.81	Clonal
Patient 2, Biopsy	WRN	p.Ala1179Ser	missense_variant	0.24	0	25	28	TRUE	.	.	.	.	FALSE	8	31004955	T	1	Clonal
Patient 2, Biopsy	NSMAF	p.Glu12*	stop_gained	0.44	0	50	23	.	.	.	.	.	FALSE	8	59571872	A	1	Clonal
Patient 2, Biopsy	CSMD3	p.Asp293Asn	missense_variant	0.278	0	18	25	.	.	.	.	.	FALSE	8	114111025	T	1	Clonal
Patient 2, Biopsy	CNTLN	p.Lys862Thr	missense_variant	0.896	0	48	21	.	.	.	.	.	TRUE	9	17395037	C	1	Clonal
Patient 2, Biopsy	TRMT10B	p.Thr195Thr	synonymous_variant	0.831	0	89	71	.	.	.	.	.	TRUE	9	37769949	C	1	Clonal
Patient 2, Biopsy	C9orf64	p.Ile114Met	missense_variant	0.822	0	45	32	.	.	.	.	.	TRUE	9	86570551	C	1	Clonal
Patient 2, Biopsy	SLC28A3	p.Glu500*	stop_gained	0.063	0	144	109	.	.	.	.	.	TRUE	9	86900409	A	0.29	Subclonal
Patient 2, Biopsy	TSC1	p.Gln767*	stop_gained	0.841	0	270	173	TRUE	.	TRUE	.	.	TRUE	9	135778084	A	1	Clonal
Patient 2, Biopsy	INPP5E	p.Ser582Ser	synonymous_variant	0.038	0.006803	237	150	.	.	.	.	.	TRUE	9	139324785	A	0.18	Subclonal
Patient 2, Biopsy	PRKCQ	p.Asn462Asn	synonymous_variant	0.587	0	219	79	.	.	.	.	.	FALSE	10	6506334	A	1	Clonal
Patient 2, Biopsy	MASTL	p.Arg793fs	frameshift_variant	0.0602837	0	282	91	.	.	.	.	.	FALSE	10	27469986	G	0.58	Subclonal
Patient 2, Biopsy	HK1	c.2481-1G>A	splice_acceptor_variant&intron_variant	0.833	0	72	73	.	.	.	.	.	FALSE	10	71158350	A	1	Clonal
Patient 2, Biopsy	SFXN3	p.Val222Val	synonymous_variant	0.786	0	42	50	.	.	.	.	.	TRUE	10	102796893	T	1	Clonal
Patient 2, Biopsy	EPS8L2	p.Asp172Tyr	missense_variant	0.522	0	92	84	.	.	.	.	.	FALSE	11	720735	T	1	Clonal
Patient 2, Biopsy	HPX	p.Ser288Gly	missense_variant	0.441	0	59	60	.	.	.	.	.	FALSE	11	6453221	C	1	Clonal
Patient 2, Biopsy	DCHS1	p.Leu644Gln	missense_variant	0.617	0	222	168	.	.	.	.	.	FALSE	11	6655404	T	1	Clonal
Patient 2, Biopsy	NELL1	p.Val349Leu	missense_variant	0.333	0	30	23	.	.	.	.	.	FALSE	11	20949989	C	1	Clonal
Patient 2, Biopsy	KIAA1549L	p.Gly1602Gly	synonymous_variant	0.542	0	24	17	.	.	.	.	.	FALSE	11	33667501	A	1	Clonal
Patient 2, Biopsy	OR8K5	p.Pro283Ser	missense_variant	0.075	0	40	22	.	.	.	.	.	FALSE	11	55926947	A	0.28	Subclonal
Patient 2, Biopsy	OR9Q1	p.Thr278Ala	missense_variant	0.417	0	84	40	.	.	.	.	.	FALSE	11	57947748	G	1	Clonal
Patient 2, Biopsy	MS4A12	p.Pro255Pro	synonymous_variant	0.408	0	98	82	.	.	.	.	.	FALSE	11	60274558	A	1	Clonal
Patient 2, Biopsy	LRP5	p.His965Asp	missense_variant	0.049	0	678	407	.	.	.	.	.	FALSE	11	68183861	G	0.23	Subclonal
Patient 2, Biopsy	SYTL2	p.Glu161Val	missense_variant	0.378	0	37	28	.	.	.	.	.	FALSE	11	85411617	A	1	Clonal
Patient 2, Biopsy	FAT3	p.Glu2075Lys	missense_variant	0.159	0	44	30	.	.	.	.	.	FALSE	11	92532402	A	0.75	Clonal
Patient 2, Biopsy	ARHGEF12	p.Leu630Phe	missense_variant	0.45	0	211	76	TRUE	.	.	.	.	FALSE	11	120322267	T	1	Clonal
Patient 2, Biopsy	TAS2R30	p.Val125Leu	missense_variant	0.0357143	0	28	41	.	.	.	.	.	TRUE	12	11286471	G	0.13	Subclonal
Patient 2, Biopsy	HDAC7	p.Pro472Leu	missense_variant	0.701	0.013	97	76	.	.	.	.	.	FALSE	12	48188637	A	1	Clonal
Patient 2, Biopsy	KMT2D	p.Met1530Val	missense_variant	0.658	0	231	145	TRUE	TRUE	TRUE	.	.	FALSE	12	49439953	C	1	Clonal
Patient 2, Biopsy	C12orf42	p.Gly270Arg	missense_variant	0.185	0	92	30	.	.	.	.	.	FALSE	12	103896161	T	1	Clonal
Patient 2, Biopsy	SVOP	p.Asp79Asn	missense_variant	0.079	0	76	29	.	.	.	.	.	FALSE	12	109366201	T	0.45	Subclonal
Patient 2, Biopsy	ANKLE2	p.Gly46Gly	synonymous_variant	0.13	0	23	13	.	.	.	.	.	FALSE	12	133338247	T	0.74	Clonal
Patient 2, Biopsy	CDX2	p.Ser208Asn	missense_variant	0.147	0.013	143	75	TRUE	.	.	.	.	TRUE	13	28539071	T	0.69	Subclonal
Patient 2, Biopsy	PROSER1	p.Asn516Asn	synonymous_variant	0.2	0	60	27	.	.	.	.	.	TRUE	13	39587841	A	0.94	Clonal
Patient 2, Biopsy	KPNA3	p.Leu323Leu	synonymous_variant	0.405	0	74	36	.	.	.	.	.	TRUE	13	50283771	A	1	Clonal
Patient 2, Biopsy	NALCN	p.Ile1593Val	missense_variant	0.235	0	51	25	.	.	.	.	.	TRUE	13	101712298	C	1	Clonal
Patient 2, Biopsy	SALL2	p.Pro365Leu	missense_variant	0.531	0	192	95	.	.	.	.	.	FALSE	14	21992768	A	1	Clonal
Patient 2, Biopsy	TRAV38-1	p.Ser13Phe	missense_variant	0.148	0	54	13	.	.	.	.	.	FALSE	14	22739891	T	0.84	Clonal
Patient 2, Biopsy	AKAP6	p.Arg509*	stop_gained	0.122	0	74	34	.	.	.	.	.	FALSE	14	33015384	T	0.69	Subclonal
Patient 2, Biopsy	SRSF5	p.Ser90Gly	missense_variant	0.381	0	118	72	.	.	.	.	.	FALSE	14	70235585	G	1	Clonal
Patient 2, Biopsy	GOLGA5	p.Ala522Asp	missense_variant	0.458	0.012	118	86	TRUE	.	.	.	.	FALSE	14	93286126	A	1	Clonal
Patient 2, Biopsy	DPH6	p.Leu40Gln	missense_variant	0.875	0	32	22	.	.	.	.	.	FALSE	15	39530653	T	1	Clonal
Patient 2, Biopsy	SRRM2	p.Trp513*	stop_gained	0.326	0	139	84	.	.	.	.	.	FALSE	16	2812068	A	1	Clonal
Patient 2, Biopsy	C16orf89	p.Leu128Leu	synonymous_variant	0.298	0	84	46	.	.	.	.	.	FALSE	16	5112516	A	1	Clonal
Patient 2, Biopsy	ZNF843	p.Glu264Glu	synonymous_variant	0.0422535	0	71	26	.	.	.	.	.	FALSE	16	31447379	T	0.28	Subclonal
Patient 2, Biopsy	CDH11	p.Glu391Asp	missense_variant	0.011236	0	89	20	TRUE	.	.	.	.	FALSE	16	65016031	A	0.08	Subclonal
Patient 2, Biopsy	DPEP3	p.Arg31Trp	missense_variant	0.256	0	39	25	.	.	.	.	.	FALSE	16	68014352	A	1	Clonal
Patient 2, Biopsy	ZNF469	p.Thr3815Met	missense_variant	0.151	0	119	83	.	.	.	.	.	FALSE	16	88505322	T	1	Clonal
Patient 2, Biopsy	TP53	p.Arg209fs	frameshift_variant	0.819767	0	172	81	TRUE	TRUE	TRUE	TRUE	.	TRUE	17	7578221	T	1	Clonal
Patient 2, Biopsy	KCNAB3	p.Leu224fs	frameshift_variant	0.0201149	0	348	168	.	.	.	.	.	TRUE	17	7827765	C	0.11	Subclonal
Patient 2, Biopsy	RARA	p.Asp449Asp	synonymous_variant	0.225	0	41	40	TRUE	.	.	.	.	FALSE	17	38512388	T	1	Clonal
Patient 2, Biopsy	KRTAP4-11	p.Arg51Lys	missense_variant	0.122088	0	73	38	.	.	.	.	.	FALSE	17	39274416	T	0.7	Subclonal
Patient 2, Biopsy	HOXB5	p.Arg224Leu	missense_variant	0.17	0	153	74	.	.	.	.	.	FALSE	17	46669710	A	0.97	Clonal
Patient 2, Biopsy	AKAP1	p.Leu832Val	missense_variant	0.138	0	65	32	.	.	.	.	.	FALSE	17	55194282	G	0.79	Clonal
Patient 2, Biopsy	USH1G	p.Thr100Lys	missense_variant	0.142	0	338	165	.	.	.	.	.	FALSE	17	72916632	T	0.81	Subclonal
Patient 2, Biopsy	DOC8	p.Gln416*	stop_gained	0.105	0	172	100	.	.	.	.	.	FALSE	17	76887340	A	0.6	Subclonal
Patient 2, Biopsy	FASN	p.Leu1826fs	frameshift_variant	0.138889	0	288	142	.	.	.	.	.	FALSE	17	80041170	G	0.79	Subclonal
Patient 2, Biopsy	GALNT1	p.Arg426Cys	missense_variant	0.25	0	12	12	.	.	.	.	.	FALSE	18	33272261	T	1	Clonal
Patient 2, Biopsy	FHOD3	p.Leu261Leu	synonymous_variant	0.365	0	74	61	.	.	.	.	.	FALSE	18	34182699	T	1	Clonal
Patient 2, Biopsy	FHOD3	p.Arg1568His	missense_variant	0.553	0	258	94	.	.	.	.	.	FALSE	18	34349306	A	1	Clonal
Patient 2, Biopsy	SMAD7	p.Pro215Leu	missense_variant	0.633	0	60	49	.	.	.	.	.	FALSE	18	46474777	A	1	Clonal
Patient 2, Biopsy	DOT1L	p.Ile1251Ile	synonymous_variant	0.827	0.007519	151	134	.	.	.	.	.	TRUE	19	2226273	T	1	Clonal
Patient 2, Biopsy	ZNF414	p.Leu257Phe	missense_variant	0.244	0	41	32	.	.	.	.	.	TRUE	19	8576604	G	0.9	Clonal
Patient 2, Biopsy	ADAMTS10	p.Val904Val	synonymous_variant	0.516	0.011	124	94	.	.	.	.	.	TRUE	19	8650493	T	1	Clonal
Patient 2, Biopsy	MUC16	p.Leu12735Pro	missense_variant&splice_region_variant	0.087	0	46	48	.	.	.	.	.	TRUE	19	9015384	G	0.32	Subclonal
Patient 2, Biopsy	ZNF561	p.Arg441Pro	missense_variant	0.695	0	82	110	.	.	.	.	.	TRUE	19	9721015	G	1	Clonal
Patient 2, Biopsy	RAVER1	p.Ala477Ala	synonymous_variant	0.833	0	12	14	.	.	.	.	.	TRUE	19	10431817	A	1	Clonal
Patient 2, Biopsy	CAPN12	p.His686Arg	missense_variant	0.794	0	34	33	.	.	.	.	.	TRUE	19	39221764	C	1	Clonal
Patient 2, Biopsy	ERCC1	p.Gly133Gly	synonymous_variant	0.877	0	204	147	.	.	.	.	.	TRUE	19	45923608	A	1	Clonal
Patient 2, Biopsy	RTN2	p.Ser211Ser	synonymous_variant	0.073	0	206	153	.	.	.	.	.	TRUE	19	45997605	C	0.27	Subclonal
Patient 2, Biopsy	AC012313.1	p.Val202Met	missense_variant	0.133	0	45	31	.	.	.	.	.	TRUE	19	48908060	A	0.49	Subclonal
Patient 2, Biopsy	PLCB4	p.Val86Phe	missense_variant	0.578	0	45	30	.	.	.	.	.	FALSE	20	9319571	T	1	Clonal
Patient 2, Biopsy	MYH7B	p.Ser797*	stop_gained	0.381	0	194	90	.	.	.	.	.	FALSE	20	33580985	A	1	Clonal
Patient 2, Biopsy	BCL2L13	p.Ser190Leu	missense_variant	0.154	0	65	38	.	.	.	.	.	FALSE	22	18185121	T	0.57	Subclonal
Patient 2, Biopsy	PPP1R3F	p.Asn345Asn	synonymous_variant	0.936	0	47	23	.	.	.	.	.	TRUE	X	49137899	T		Did not evaluate
Patient 2, Biopsy	ARR3	p.Leu49Leu	splice_region_variant&synonymous_variant	0.156	0	32	16	.	.	.	.	.	TRUE	X	69495933	A		Did not evaluate
Patient 2, Biopsy	FGF13	p.Glu54Lys	missense_variant	0.881	0	59	15	.	.	.	.	.	TRUE	X	137939731	T		Did not evaluate
Patient 2, Biopsy	GABRE	p.Lys302Met	missense_variant	0.277	0	65	13	.	.	.	.	.	TRUE	X	151124212	A		Did not evaluate
Patient 2, Organoids early p.	C1orf159	p.Thr26Met	missense_variant	0.583	0	48	61	.	.	.	.	.	FALSE	1	1026359	A	1	Clonal
Patient 2, Organoids early p.	ACTL8	p.Val6Ile	missense_variant	0.104	0	78	70	.	.	.	.	.	FALSE	1	18149519	A	0.41	Subclonal
Patient 2, Organoids early p.	TMCO4	p.Ala211Ser	missense_variant	0.719	0	32	27	.	.	.	.	.	FALSE	1	20073075	A	1	Clonal
Patient 2, Organoids early p.	HIVEP3	p.Met265fs	frameshift_variant	0.40708	0	113	91	.	.	.	.	.	FALSE	1	42049671	C	1	Clonal
Patient 2, Organoids early p.	LEPRE1	p.Asp253Val	missense_variant	0.451	0	175	147	.	.	.	.	.	FALSE	1	43224922	A	1	Clonal
Patient 2, Organoids early p.	KIF2C	p.Arg258Thr	missense_variant	0.154	0	26	24	.	.	.	.	.	FALSE	1	45221614	C	0.62	Clonal
Patient 2, Organoids early p.	HPDL	p.Gly61Arg	missense_variant	0.00826446	0	121	112	.	.	.	.	.	FALSE	1	45793001	A	0.03	Subclonal
Patient 2, Organoids early p.	ELTD1	p.Ile35Ile	synonymous_variant	0.386	0	44	13	.	.	.	.	.	FALSE	1	79470822	A	1	Clonal
Patient 2, Organoids early p.	LRRC8C	p.Phe667Phe	synonymous_variant	0.361	0.019	158	53	.	.	.	.	.	FALSE	1	90180130	C	1	Clonal
Patient 2, Organoids early p.	GJA5	p.Lys233del	disruptive_inframe_deletion	0.0896739	0	368	82	.	.	.	.	.	FALSE	1	147230646	A	0.9	Clonal
Patient 2, Organoids early p.	CA14	p.Ser215Trp	missense_variant	0.065	0	277	112	.	.	.	.	.	FALSE	1	150235522	G	0.65	Subclonal
Patient 2, Organoids early p.	APOA2	p.Met34fs	frameshift_variant	0.0546218	0	476	188	.	.	.	.	.	FALSE	1	161193173	T	0.55	Subclonal
Patient 2, Organoids early p.	GJC2	p.Leu353Pro	missense_variant	0.111	0	36	22	.	.	.	.	.	TRUE	1	228346517	C	0.56	Subclonal
Patient 2, Organoids early p.	OTX1	p.His260Gln	missense_variant	0.065	0	186	86	.	.	.	.	.	FALSE	2	63283166	G	0.32	Subclonal
Patient 2, Organoids early p.	PROM2	p.Leu119Leu	synonymous_variant	0.208	0	96	68	.	.	.	.	.	FALSE	2	95941738	T	1	Clonal
Patient 2, Organoids early p.	CYP27C1	p.Pro243Pro	synonymous_variant	0.086	0	70	64	.	.	.	.	.	FALSE	2	127951434	G	0.43	Subclonal
Patient 2, Organoids early p.	NEB	p.Ile3069Thr	missense_variant	0.313	0	387	222	.	.	.	.	.	TRUE	2	152490376	G	0.94	Clonal
Patient 2, Organoids early p.	FASTKD2	p.Asn663Ser	missense_variant	0.399	0	138	46	.	.	.	.	.	FALSE	2	207655385	G	1	Clonal
Patient 2, Organoids early p.	PIKFYVE	p.Asn383Asn	synonymous_variant	0.262	0	130	37	.	.	.	.	.	FALSE	2	209165759	T	1	Clonal
Patient 2, Organoids early p.	COL6A3	p.Ser2205er	synonymous_variant	0.183	0	312	126	.	.	.	.	.	FALSE	2	238303279	T	0.91	Clonal
Patient 2, Organoids early p.	SNED1	p.Ala316Val	missense_variant	0.658	0	152	92	.	.	.	.	.	FALSE	2	241976672	T	1	Clonal
Patient 2, Organoids early p.	ATG4B	p.Arg201Arg	synonymous_variant	0.704	0	159	108	.	.	.	.	.	FALSE	2	242606124	A	1	Clonal
Patient 2, Organoids early p.	KIAA1143	p.Gln136Lys	missense_variant	0.245	0	53	30	.	.	.	.	.	TRUE	3	44794892	T	0.98	Clonal
Patient 2, Organoids early p.	TMF1	p.Cys318Ser	missense_variant	0.625	0	48	24	.	.	.	.	.	TRUE	3	69096903	G	1	Clonal

Patient 2, Organoids early p.	PPP4R2	p.Ser146Arg	missense_variant	0.1875	0	16	12						TRUE	3	73112842	A	0.56	Subclonal
Patient 2, Organoids early p.	SPICE1	p.Leu419fs	frameshift_variant	0.328358	0	67	61						TRUE	3	113184532	G	0.99	Clonal
Patient 2, Organoids early p.	ITGB5	p.Asp640Yis	missense_variant&splice_region_variant	0.462	0	13	31						TRUE	3	124487959	G	1	Clonal
Patient 2, Organoids early p.	MSL2	p.Arg344Lys	missense_variant	0.28	0	93	46						TRUE	3	135870692	T	0.84	Clonal
Patient 2, Organoids early p.	PHC3	p.Trp937*	stop_gained	0.099	0	141	19						FALSE	3	169820290	T	0.6	Subclonal
Patient 2, Organoids early p.	EPHB3	p.Gln509Lys	missense_variant	0.113924	0	79	67						FALSE	3	184295491	A	0.68	Clonal
Patient 2, Organoids early p.	TMEM41A	p.Phe44Phe	synonymous_variant	0.171	0	41	22						FALSE	3	185214757	A	1	Clonal
Patient 2, Organoids early p.	ADH1A	p.Glu253Glu	synonymous_variant	0.0281124	0	249	102						TRUE	4	100203572	T	0.08	Subclonal
Patient 2, Organoids early p.	DNAJB14	p.Tyr38Cys	missense_variant	0.4	0	70	29						TRUE	4	100867616	C	1	Clonal
Patient 2, Organoids early p.	BDP1	p.Ala932fs	frameshift_variant	0.580645	0	93	56						TRUE	5	70805704	T	1	Clonal
Patient 2, Organoids early p.	SLC22A4	p.Leu347_Leu348del	disruptive_inframe_deletion	0.25974	0	77	72						TRUE	5	131667533	T	0.78	Clonal
Patient 2, Organoids early p.	CFB	p.Ile744Val	missense_variant	0.824	0	125	115						TRUE	6	31915584	G	1	Clonal
Patient 2, Organoids early p.	DNAH8	p.Ser1436Arg	missense_variant	0.133	0	75	15						TRUE	6	38802396	G	0.67	Subclonal
Patient 2, Organoids early p.	DST	p.Lys6551Asn	missense_variant	0.125	0	283	40						TRUE	6	56366028	G	0.63	Subclonal
Patient 2, Organoids early p.	RIMS1	p.Lys718Asn	missense_variant	0.13	0	100	16						TRUE	6	72957743	T	0.65	Subclonal
Patient 2, Organoids early p.	ASCC3	c.6075+2T>G	splice_donor_variant&intron_variant	0.163	0	43	9						TRUE	6	100964054	C	0.81	Clonal
Patient 2, Organoids early p.	KIAA1919	p.Gln415Pro	missense_variant	0.185	0	130	65						TRUE	6	111588009	C	0.92	Clonal
Patient 2, Organoids early p.	AGPAT4	p.Glu149Gln	missense_variant	0.098	0	214	189						TRUE	6	161575246	G	0.49	Subclonal
Patient 2, Organoids early p.	POU6F2	p.Gly132Val	missense_variant	0.276	0	87	45						TRUE	7	39247103	T	1	Clonal
Patient 2, Organoids early p.	COPS8	p.Phe168Leu	missense_variant	0.583	0	48	54						TRUE	7	99688542	A	1	Clonal
Patient 2, Organoids early p.	CREB3L2	p.Lys325Glu	missense_variant&splice_region_variant	1	0	41	26	TRUE					TRUE	7	137588706	C	1	Clonal
Patient 2, Organoids early p.	MGAM	p.Ser1292Ser	synonymous_variant	0.0294118	0	34	49						TRUE	7	141759328	T	0.12	Subclonal
Patient 2, Organoids early p.	MGAM	p.Ser2188Ser	synonymous_variant	0.037	0	164	74						TRUE	7	141785689	T	0.15	Subclonal
Patient 2, Organoids early p.	NUGGC	p.Thr176Thr	synonymous_variant	0.343	0	35	24						TRUE	8	27925214	T	1	Clonal
Patient 2, Organoids early p.	WRN	p.Ala1179Ser	missense_variant	0.14	0	101	28	TRUE					TRUE	8	31004955	T	0.55	Subclonal
Patient 2, Organoids early p.	NSMAF	p.Glu12*	stop_gained	0.622	0	45	23						FALSE	8	59571872	A	1	Clonal
Patient 2, Organoids early p.	CSMD3	p.Asp293Asn	missense_variant	0.214	0	182	25						FALSE	8	114111025	T	1	Clonal
Patient 2, Organoids early p.	ADCY8	p.His239Asn	missense_variant	0.0070922	0	141	26						FALSE	8	132051865	T	0.07	Subclonal
Patient 2, Organoids early p.	CNTLN	p.Lys862Thr	missense_variant	1	0	44	21						TRUE	9	17395037	C	1	Clonal
Patient 2, Organoids early p.	TRMT10B	p.Thr195Thr	synonymous_variant	1	0	106	71						TRUE	9	37769949	C	1	Clonal
Patient 2, Organoids early p.	C9orf64	p.Ile114Met	missense_variant	0.975	0	40	32						TRUE	9	86570551	C	1	Clonal
Patient 2, Organoids early p.	SLC28A3	p.Glu500*	stop_gained	0.239	0	176	109						TRUE	9	86900409	A	0.95	Clonal
Patient 2, Organoids early p.	TSC1	p.Gln767*	stop_gained	1	0	193	173	TRUE		TRUE			TRUE	9	135778084	A	1	Clonal
Patient 2, Organoids early p.	PRKCQ	p.Asn462Asn	synonymous_variant	0.673	0	269	79						TRUE	10	6506334	A	1	Clonal
Patient 2, Organoids early p.	MASTL	p.Arg793fs	frameshift_variant	0.077951	0	449	91						FALSE	10	27469988	G	0.7	Subclonal
Patient 2, Organoids early p.	HK1	c.2481-1G>A	splice_acceptor_variant&intron_variant	1	0	54	73						TRUE	10	71158350	A	1	Clonal
Patient 2, Organoids early p.	SFXN3	p.Val222Val	synonymous_variant	1	0	31	50						TRUE	10	102796893	T	1	Clonal
Patient 2, Organoids early p.	EPS8L2	p.Asp172Tyr	missense_variant	0.697	0	66	84						TRUE	11	720735	T	1	Clonal
Patient 2, Organoids early p.	HPX	p.Ser288Gly	missense_variant	0.682	0	44	60						TRUE	11	6453221	C	1	Clonal
Patient 2, Organoids early p.	DCHS1	p.Leu644Gln	missense_variant	0.794	0	170	168						TRUE	11	6655404	T	1	Clonal
Patient 2, Organoids early p.	NELL1	p.Val349Leu	missense_variant	0.25	0	44	23						TRUE	11	20949989	C	1	Clonal
Patient 2, Organoids early p.	KIAA1549L	p.Gly1602Gly	synonymous_variant	0.69	0	29	17						TRUE	11	33667501	A	1	Clonal
Patient 2, Organoids early p.	OR8K5	p.Pro283Ser	missense_variant	0.219	0	96	18						FALSE	11	55926947	A	1	Clonal
Patient 2, Organoids early p.	OR9Q1	p.Thr278Ala	missense_variant	0.412	0	102	40						TRUE	11	57947748	G	1	Clonal
Patient 2, Organoids early p.	MS4A12	p.Pro255Pro	synonymous_variant	0.357	0	221	82						FALSE	11	60274558	A	1	Clonal
Patient 2, Organoids early p.	LRP5	p.His965Asp	missense_variant	0.225	0	457	407						FALSE	11	68183861	G	1	Clonal
Patient 2, Organoids early p.	SYTL2	p.Glu1611Val	missense_variant	0.418	0	79	26						FALSE	11	85411617	A	1	Clonal
Patient 2, Organoids early p.	ARHGEF12	p.Leu630Phe	missense_variant	0.457	0	210	76	TRUE					FALSE	11	120322267	T	1	Clonal
Patient 2, Organoids early p.	TASR30	p.Val125Leu	missense_variant	0.157	0	102	35						TRUE	12	11286471	G	0.63	Subclonal
Patient 2, Organoids early p.	HDAC7	p.Pro472Leu	missense_variant	0.792	0.013	72	76						TRUE	12	48188637	A	1	Clonal
Patient 2, Organoids early p.	KMT2D	p.Met1530Val	missense_variant	0.776	0	157	145	TRUE	TRUE	TRUE			TRUE	12	49439953	C	1	Clonal
Patient 2, Organoids early p.	C12orf42	p.Gly270Arg	missense_variant	0.198	0	96	30						TRUE	12	103696161	T	0.99	Clonal
Patient 2, Organoids early p.	SVOP	p.Asp79Asn	missense_variant	0.164	0	63	29						TRUE	12	109366201	T	0.79	Clonal
Patient 2, Organoids early p.	ANKLE2	p.Gly46Gly	synonymous_variant	0.385	0	13	13						TRUE	12	133338247	T	1	Clonal
Patient 2, Organoids early p.	KPNA3	p.Leu323Leu	synonymous_variant	0.388	0	103	36						TRUE	13	50283771	A	1	Clonal
Patient 2, Organoids early p.	SALL2	p.Pro365Leu	missense_variant	0.625	0	96	95						TRUE	14	21992768	A	1	Clonal
Patient 2, Organoids early p.	TRAV36DV7	p.Gly103Arg	missense_variant	0.078	0	51	23						TRUE	14	22695116	A	0.31	Subclonal
Patient 2, Organoids early p.	SRSF5	p.Ser90Gly	missense_variant	0.517	0	145	72						FALSE	14	70235585	G	1	Clonal
Patient 2, Organoids early p.	GOLGA5	p.Asn522Asp	missense_variant	0.439	0.012	198	86	TRUE					FALSE	14	93286126	A	1	Clonal
Patient 2, Organoids early p.	DPH6	p.Leu45Gln	missense_variant	1	0	53	22						TRUE	15	35830653	T	1	Clonal
Patient 2, Organoids early p.	SRRM2	p.Trp513*	stop_gained	0.442	0	86	84						FALSE	16	2812068	A	1	Clonal
Patient 2, Organoids early p.	C16orf89	p.Leu128Leu	synonymous_variant	0.541	0	74	46						FALSE	16	5112516	A	1	Clonal
Patient 2, Organoids early p.	ZNF843	p.Glu264Glu	synonymous_variant	0.146	0	41	21						FALSE	16	31447379	T	0.73	Clonal
Patient 2, Organoids early p.	CDH11	p.Glu391Asp	missense_variant	0.111	0	54	17	TRUE					FALSE	16	65016031	A	0.56	Subclonal
Patient 2, Organoids early p.	DPEP3	p.Arg3Trp	missense_variant	0.321	0	28	25						FALSE	16	68014352	A	1	Clonal
Patient 2, Organoids early p.	ZNF469	p.Thr3815Met	missense_variant	0.205	0	88	83						FALSE	16	88505322	T	1	Clonal
Patient 2, Organoids early p.	TP53	p.Arg209fs	frameshift_variant	0.92381	0	105	81	TRUE	TRUE	TRUE	TRUE		TRUE	17	7578221	T	1	Clonal
Patient 2, Organoids early p.	RARA	p.Asp449Asp	synonymous_variant	0.142857	0	70	48	TRUE					TRUE	17	38512388	T	0.71	Clonal
Patient 2, Organoids early p.	KRTAP4-11	p.Arg51Lys	missense_variant	0.0952381	0	105	38						TRUE	17	39274416	T	0.48	Subclonal
Patient 2, Organoids early p.	HOXB5	p.Arg224Leu	missense_variant	0.189	0	95	74						TRUE	17	46669710	A	0.95	Clonal
Patient 2, Organoids early p.	AKAP1	p.Leu832Val	missense_variant	0.205	0	44	32						TRUE	17	55194282	G	1	Clonal
Patient 2, Organoids early p.	USH1G	p.Thr100Lys	missense_variant	0.182	0	198	165						TRUE	17	72916632	T	0.91	Clonal
Patient 2, Organoids early p.	DOC8	p.Gln416*	stop_gained	0.254	0	142	100						TRUE	17	76887340	A	1	Clonal
Patient 2, Organoids early p.	FASN	p.Leu1826fs	frameshift_variant	0.190476	0	168	142						TRUE	17	80041170	G	0.95	Clonal
Patient 2, Organoids early p.	GALNT1	p.Arg426Cys	missense_variant	0.429	0	21	12						FALSE	18	33272261	T	1	Clonal
Patient 2, Organoids early p.	FHOD3	p.Leu261Leu	synonymous_variant	0.383	0	115	61						FALSE	18	34182699	T	1	Clonal
Patient 2, Organoids early p.	FHOD3	p.Arg1568His	missense_variant	0.503	0	183	94						FALSE	18	34349306	A	1	Clonal
Patient 2, Organoids early p.	SMAD7	p.Pro215Leu	missense_variant	0.47	0	66	49						FALSE	18	46474777	A	1	Clonal
Patient 2, Organoids early p.	DOT1L	p.Ile1251Ile	synonymous_variant	1	0.007519	125	134						TRUE	19	2226273	T	1	Clonal
Patient 2, Organoids early p.	ZNF414	p.Leu257Phe	missense_variant	0.226	0	31	32						TRUE	19	8576604	G	0.68	Clonal
Patient 2, Organoids early p.	ADAMTS10	p.Val904Val	synonymous_variant	0.582	0.011	79	94						TRUE	19	8650493	T	1	Clonal
Patient 2, Organoids early p.	MUC16	p.Leu12735Pro	missense_variant&splice_region_variant	0.255	0	47	48						TRUE	19	9015384	G	0.77	Clonal
Patient 2, Organoids early p.	ZNF561	p.Arg441Pro	missense_variant	1	0	125	110						TRUE	19	9721015	G	1	Clonal
Patient 2, Organoids early p.	RAVER1	p.Ala477Ala	synonymous_variant	1	0	8	16						TRUE	19	10431817	A	1	Clonal
Patient 2, Organoids early p.	CAPN12	p.His686Arg	missense_variant	1	0	23	33						TRUE	19	39221764	C	1	Clonal
Patient 2, Organoids early p.	ERCC1	p.Gly133Gly	synonymous_variant	1	0	101	147						TRUE	19	45923608	A	1	Clonal
Patient 2, Organoids early p.	RTN2	p.Ser211Ser	synonymous_variant	0.962	0	105	153						TRUE	19	45997605	C	1	Clonal
Patient 2, Organoids early p.	GPR4	p.Pro359Pro	synonymous_variant	0.00980392	0	102	128						TRUE	19	46094048	T	0.03	Subclonal
Patient 2, Organoids early p.	PLCB4	p.Val86Phe	missense_variant	0.714	0	84	30						TRUE	20	9319571	T	1	Clonal
Patient 2, Organoids early p.	MYH7B	p.Ser797*	stop_gained	0.356	0	90	90						FALSE	20	33580985	A	1	Clonal
Patient 2, Organoids early p.	CNKSR2	p.Glu480Gly	missense_variant	0.052	0	77	18						TRUE	X	21581401	G		Did not evaluate
Patient 2, Organoids early p.	PPP1R3F	p.Asn345Asn	synonymous_variant	1	0	28	23						TRUE	X	49137899	T		Did not evaluate
Patient 2, Organoids early p.	FGF13	p.Glu54Lys	missense_variant	1	0	45	15						TRUE	X	137939731	T		Did not evaluate
Patient 2, Organoids late p.	C1orf159	p.Thr26Met	missense_variant	0.391	0	46	61						FALSE	1	1026359	A	1	Clonal
Patient 2, Organoids late p.	ACTL8	p.Val6Ile	missense_variant	0.094	0	64	70						FALSE	1	18149519	A	0.29	Subclonal
Patient 2, Organoids late p.	TMCO4	p.Ala211Ser	missense_variant	0.583	0	36	27						FALSE	1	20073075	A	1	Clonal
Patient 2, Organoids late p.	HIVEP3	p.Met265fs	frameshift_variant	0.357143	0	98	91						FALSE	1	42049671	C	1	Clonal
Patient 2, Organoids late p.	LEPRE1	p.Asp253Val	missense_variant	0.549	0	175	147						FALSE	1	43224922	A	1	Clonal
Patient 2, Organoids late p.	KIF2C	p.Arg258Thr	missense_variant	0.2	0	20	24						FALSE	1	45221614	C	0.62	Subclonal
Patient 2, Organoids late p.	HPDL	p.Gly61Arg	missense_variant	0.16	0	94	84						FALSE	1	45793001	A	0.49	Subclonal
Patient 2, Organoids late p.	ELTD1	p.Ile30Ile	synonymous_variant	0.514	0	37	13						FALSE	1	79470822	A	1	Clonal
Patient 2, Organoids late p.	LRRC8C	p.Phe667Phe	synonymous_variant	0.405	0.019	116	53						FALSE	1	90180130	C	1	Clonal
Patient 2, Organoids late p.	GJA5	p.Lys233del	disruptive_inframe_deletion	0.0888889	0	315	82						FALSE	1	147230646	A	0.81	Clonal
Patient 2, Organoids late p.	CA14	p.Ser215Trp	missense_variant	0.115	0	252	112						FALSE	1	150235522	G	1	Clonal
Patient 2, Organoids late p.	APOA2	p.Met34fs	frameshift_variant	0.0527638	0	398	188						FALSE	1	161193173	T	0.48	Subclonal
Patient 2, Organoids late p.	GJC2	p.Leu353Pro	missense_variant	0.227	0	22	22						TRUE	1	228346517	C	0.93	Clonal
Patient 2, Organoids late p.	OTX1	p.His260Gln	missense_variant	0.177	0	198	86						FALSE	2	63283166	G	0.9	Clonal
Patient 2, Organoids late p.	PROM2	p.Leu119Leu	synonymous_variant	0.195	0	77	68						FALSE	2	95941736	T	0.99	Clonal
Patient 2, Organoids late p.	CYP27C1	p.Pro243Pro	synonymous_variant	0.186	0	70	64						FALSE	2	127951434	G	0.94	Clonal
Patient 2, Organoids late p.	NEB	p.Ile3069Thr	missense_variant	0.324	0	438	222						FALSE	2	152490376	G	1	Clonal
Patient 2, Organoids late p.	NBEAL1	p.Trp1775Cys	missense_variant	0.09	0	89	21						FALSE	2	204013821	T	0.46	Subclonal
Patient 2, Organoids late p.	FASTKD2	p.Asn663Ser	missense_variant	0.336	0	143	46						FALSE	2	207655385	G	1	Clonal
Patient 2, Organoids late p.	PIKFYVE	p.Asn383Asn	synonymous_variant	0.311	0	132	37						FALSE	2	209165759	T	1	Clonal
Patient 2, Organoids late p.	NCL	p.Asp200_Asp201del	disruptive_inframe_deletion	0.166667	0	150	40						FALSE	2	232326258	C	0.85	Clonal
Patient 2, Organoids late p.	COL6A3	p.Ser2202Ser	synonymous_variant	0.201	0	334	126						FALSE	2	238302279	T	1	Clonal
Patient 2, Organoids late p.	SNED1	p.Ala316Val	missense_variant	0.607	0	183	92						FALSE	2	241976672	T	1	Clonal
Patient 2, Organoids late p.	ATG4B	p.Arg201Arg	synonymous_variant	0.732	0	149	108						FALSE	2	242606124	A	1	Clonal
Patient 2, Organoids late p.	C3orf20	p.Ile46Leu	missense_variant	0.049	0	122	60						FALSE	3	14724356	C	0.2	Subclonal
Patient 2, Organoids late p.	SQOL1	p.Asp380Asp	synonymous_variant	0.073	0	137	57						FALSE	3	20215883	A	0.3	Subclonal
Patient 2, Organoids late p.	KIAA1143	p.Gln136Lys	missense_variant	0.215	0	65	30						FALSE	3	44794892	T	0.88	Clonal
Patient 2, Organoids late p.	TMF1	p.Cys318Ser	missense_variant	0.543	0	35	24						FALSE	3	69096903	G	1	Clonal
Patient 2, Organoids late p.	PPP4R2	p.Ser146Arg	missense_variant	0.182	0	22	9						FALSE	3	73112842	A	0.56	Subclonal
Patient 2, Organoids late p.	SPICE1	p.Leu419fs	frameshift_variant	0.292035	0	113	61						FALSE	3	113184532	G	0.9	Clonal
Patient 2, Organoids late p.	ITGB5	p.Asp640Yis	missense_variant&splice_region_variant	0.591	0	22	31						FALSE	3	124487959	G	1	Clonal
Patient 2, Organoids late p.	MSL2	p.Arg344Lys	missense_variant	0.351	0	111	46						FALSE	3	135870692	T	1	Clonal
Patient 2, Organoids late p.	PHC3	p.Trp937*	stop_gained	0.162	0	143	19						FALSE	3	169820290	T	0.82	Clonal
Patient 2, Organoids late p.	EPHB3	p.Gln509Lys	missense_variant	0.159	0	63	64						FALSE	3	184295491	A	0.81	Clonal
Patient 2, Organoids late p.	TMEM41A	p.Phe44Phe	synonymous_variant	0.409	0	22	22						FALSE	3	185214757	A	1	Clonal
Patient 2, Organoids late p.	ADH1A	p.Glu253Glu	synonymous_variant	0.037	0	134	84						TRUE	4	100203572	T	0.08	Subclonal
Patient 2, Organoids late p.	DNAJB14	p.Tyr38Cys	missense_variant	0.578	0	45	29						FALSE	4	100867616	C	1	Clonal
Patient 2, Organoids late p.	ADAMTS16	p.Val68Val	synonymous_variant	0.056	0	107	63						TRUE	5	5146271	G	0.23	Subclonal
Patient 2, Organoids late p.	BDP1	p.Ala932fs	frameshift_variant	0.701031	0	97	56						TRUE	5	70805704	T	1	Clonal
Patient 2, Organoids late p.	SLC22A4	p.Leu347_Leu348del	disruptive_inframe_deletion	0.258621	0	58	72						TRUE	5	131667533	T	0.8	Clonal
Patient 2, Organoids late p.	CFB	p.Ile744Val	missense_variant	0.791	0	110	115						FALSE	6	31915584	G	1	Clonal
Patient 2, Organoids late p.	DNAH8	p.Ser1436Arg	missense_variant	0.103	0	58	15						FALSE	6	38802396	G	0.53	Subclonal
Patient 2, Organoids late p.	RIMS1	p.Lys718Asn	missense_variant	0.149	0	87	16						FALSE	6	72957743	T	0.76	Clonal
Patient 2, Organoids late p.	ASCC3	c.6075+2T>G	splice_donor_variant&intron_variant	0.188	0	48	9						FALSE	6	100964054	C	0.95	Clonal
Patient 2, Organoids late p.	KIAA1919	p.Gln415Pro	missense_variant	0.186	0	118	65						FALSE	6	111588009	C	0.95	Clonal
Patient 2, Organoids late p.	AGPAT4	p.Glu149Gln	missense_variant	0.213	0	221	189						FALSE	6	161575246	G	1	Clonal
Patient 2, Organoids late p.	SDIM1	p.Arg56Gly	missense_variant	0.045	0	89	64						FALSE	6	166307988	C	0.23	Subclonal
Patient 2, Organoids late p.	POU6F2	p.Gly132Val	missense_variant	0.26	0	97	45						TRUE	7	39247103	T	1	Clonal
Patient 2, Organoids late p.	COPS8	p.Phe168Leu	missense_variant	0.488	0	43	54						TRUE	7	99688542	A	1	Clonal
Patient 2, Organoids late p.	CREB3L2	p.Lys325Glu	missense_variant&splice_region_variant	1	0	40	26	TRUE					TRUE	7	137588706	C	1	Clonal
Patient 2, Organoids late p.	MGAM	p.Ser1292Ser	synonymous_variant	0.175	0	40	38						TRUE	7	141759328	T	0.71	Clonal
Patient 2, Organoids late p.	MGAM	p.Ser2188Ser	synonymous_variant	0.083	0	168	74						TRUE	7	141785689	T	0.34	Subclonal
Patient 2, Organoids late p.	NOS3	p.Ala181Thr	missense_variant	0.333	0.026	30	38						TRUE	7	150693972	A	1	Clonal
Patient 2, Organoids late p.	NUGGC	p.Thr176Thr	synonymous_variant	0.154	0	39	24						FALSE	8	27925214	T	0.63	Subclonal
Patient 2, Organoids late p.	WRN	p.Ala1179Ser	missense_variant	0.304	0	92	28	TRUE					FALSE	8	31004955	T	1	Clonal
Patient 2, Organoids late p.	NSMAF	p.Glu12*	stop_gained	0.395	0	39	23						FALSE	8	59571872	A	1	Clonal
Patient 2, Organoids late p.	CA8	p.Pro63Pro	synonymous_variant	0.056	0	269	79						FALSE	8	61192351	A	0.34	Subclonal
Patient 2, Organoids late p.	CSMD3	p.Asp293Asn	missense_variant	0.232	0	194	25						FALSE	8	114111025	T	1	Clonal
Patient 2, Organoids late p.	ADCY8	p.His239Asn	missense_variant	0.093	0	172	22						FALSE	8	132051865	T	1	Clonal
Patient 2, Organoids late p.	CNTLN	p.Lys862Thr	missense_variant	1	0	53	21						TRUE	9	17395037	C	1	Clonal
Patient 2, Organoids late p.	TRMT10B	p.Thr195Thr	synonymous_variant	1	0	116	71						TRUE	9	37769949	C	1	Clonal
Patient 2, Organoids late p.	C9orf64	p.Ile114Met	missense_variant	0.978	0	46	32						TRUE	9	86570551	C	1	Clonal
Patient 2, Organoids late p.	TSC1	p.Gln767*	stop_gained	0.99	0	202	173	TRUE		TRUE			TRUE	9	135778084	A	1	Clonal
Patient 2, Organoids late p.	PRKCQ	p.Asn462Asn	synonymous_variant	0.734	0	244	79						FALSE	10	6506334	A	1	Clonal
Patient 2, Organoids late p.	MASTL	p.Arg793fs	frameshift_variant	0.0522193	0	383	91						FALSE	10	27469988	G	0.42	Subclonal
Patient 2, Organoids late p.	HK1	c.2481-1G>A	splice_acceptor_variant&intron_variant	1	0	55	73						FALSE	10	71158350	A	1	Clonal
Patient 2, Organoids late p.	SFXN3	p.Val222Val	synonymous_variant	0.967	0	30	50						TRUE	10	102796893	T	1	Clonal
Patient 2, Organoids late p.	EPS8L2	p.Asp172Tyr	missense_variant	0.742	0	62	84						FALSE	11	720735	T	1	Clonal
Patient 2, Organoids late p.	HPX	p.Ser288Gly	missense_variant	0.814	0	43	60						FALSE	11	6453221	C	1	Clonal
Patient 2, Organoids late p.	DCHS1	p.Leu644Gln	missense_variant	0.656	0	160	168						FALSE	11	6655404	T	1	Clonal
Patient 2, Organoids late p.	NELL1	p.Val349Leu	missense_variant	0.2	0	50	23						FALSE	11	20949989	C	0.82	Clonal
Patient 2, Organoids late p.	KIAA1549L	p.Gly1602Gly	synonymous_variant	0.522	0	23	17						FALSE	11	33667501	A	1	Clonal
Patient 2, Organoids late p.	OR8K5	p.Pro283Ser	missense_variant	0.185185	0	108	22						FALSE	11	55926947	A	0.76	Clonal
Patient 2, Organoids late p.	OR9Q1	p.Thr278Ala	missense_variant	0.43	0	79	40						FALSE	11	57947748	G	1	Clonal
Patient 2, Organoids late p.	MS4A12	p.Pro255Pro	synonymous_variant	0.445	0	209	82						FALSE	11	60274558	A	1	Clonal

Patient 2, Organoids late p.	LRP5	p.His965Asp	missense_variant	0.208	0	448	407	.	.	.	.	.	FALSE	11	68183861	G	0.85	Clonal
Patient 2, Organoids late p.	SYTL2	p.Glu1611Val	missense_variant	0.484	0	63	26	.	.	.	.	.	FALSE	11	85411617	A	1	Clonal
Patient 2, Organoids late p.	ARHGEF12	p.Leu830Phe	missense_variant	0.584	0	166	76	TRUE	.	.	.	.	FALSE	11	120322267	T	1	Clonal
Patient 2, Organoids late p.	TAS2R30	p.Val125Leu	missense_variant	0.272	0	103	35	.	.	.	.	.	TRUE	12	11286471	G	0.84	Clonal
Patient 2, Organoids late p.	HDAC7	p.Pro472Leu	missense_variant	0.792	0.013	77	76	.	.	.	.	.	TRUE	12	48188637	A	1	Clonal
Patient 2, Organoids late p.	KMT2D	p.Met1530Val	missense_variant	0.769	0	134	145	TRUE	TRUE	TRUE	.	.	TRUE	12	49439953	C	1	Clonal
Patient 2, Organoids late p.	C12orf42	p.Gly270Arg	missense_variant	0.205	0	78	30	.	.	.	.	.	TRUE	12	103696161	T	0.84	Clonal
Patient 2, Organoids late p.	SVOP	p.Asp79Asn	missense_variant	0.237	0	59	29	.	.	.	.	.	TRUE	12	109366201	T	0.97	Clonal
Patient 2, Organoids late p.	ANKLE2	p.Gly46Gly	synonymous_variant	0.166667	0	18	17	.	.	.	.	.	TRUE	12	133338247	T	0.68	Clonal
Patient 2, Organoids late p.	KPNA3	p.Leu323Leu	synonymous_variant	0.5	0	94	36	.	.	.	.	.	TRUE	13	50283771	A	1	Clonal
Patient 2, Organoids late p.	MYCBP2	p.Met3453Val	missense_variant	0.087	0	126	29	.	.	.	.	.	TRUE	13	77667310	C	0.36	Subclonal
Patient 2, Organoids late p.	MBNL2	p.Lys178Asn	missense_variant	0.143	0	21	11	.	.	.	.	.	TRUE	13	97995464	T	0.58	Subclonal
Patient 2, Organoids late p.	SALL2	p.Pro365Leu	missense_variant	0.767	0	91	95	.	.	.	.	.	FALSE	14	21992768	A	1	Clonal
Patient 2, Organoids late p.	AKAP6	p.Arg509*	stop_gained	0.00806452	0	124	41	.	.	.	.	.	FALSE	14	33015384	T	0.03	Subclonal
Patient 2, Organoids late p.	SRSF5	p.Ser90Gly	missense_variant	0.6	0	115	72	.	.	.	.	.	FALSE	14	70235585	G	1	Clonal
Patient 2, Organoids late p.	GOLGA5	p.Ala522Asp	missense_variant	0.288	0.012	156	86	TRUE	.	.	.	.	FALSE	14	93286126	A	0.89	Clonal
Patient 2, Organoids late p.	DPH6	p.Leu45Gln	missense_variant	1	0	67	22	.	.	.	.	.	TRUE	15	35830653	T	1	Clonal
Patient 2, Organoids late p.	PLA2G4E	p.Cys505Phe	missense_variant	0.2	0	25	21	.	.	.	.	.	TRUE	15	42282390	A	0.82	Clonal
Patient 2, Organoids late p.	SRRM2	p.Trp513*	stop_gained	0.529	0	87	84	.	.	.	.	.	FALSE	16	2812068	A	1	Clonal
Patient 2, Organoids late p.	SLX4	p.Pro198Gln	missense_variant	0.085	0.004926	176	203	.	.	.	.	.	FALSE	16	3656642	T	0.35	Subclonal
Patient 2, Organoids late p.	C16orf71	p.Glu92Gln	missense_variant	0.281	0	57	49	.	.	.	.	.	FALSE	16	4787945	C	1	Clonal
Patient 2, Organoids late p.	C16orf89	p.Leu128Leu	synonymous_variant	0.412	0	51	46	.	.	.	.	.	FALSE	16	5112516	A	1	Clonal
Patient 2, Organoids late p.	CDH11	p.Glu391Asp	missense_variant	0.191	0	68	17	TRUE	.	.	.	.	FALSE	16	65016031	A	0.97	Clonal
Patient 2, Organoids late p.	DPEP3	p.Arg3Trp	missense_variant	0.55	0	20	25	.	.	.	.	.	FALSE	16	68014352	A	1	Clonal
Patient 2, Organoids late p.	ZNF469	p.Thr3815Met	missense_variant	0.132	0	76	83	.	.	.	.	.	FALSE	16	88505322	T	0.67	Subclonal
Patient 2, Organoids late p.	TP53	p.Arg209fs	frameshift_variant	0.931373	0	102	81	TRUE	TRUE	TRUE	TRUE	.	TRUE	17	7578221	T	1	Clonal
Patient 2, Organoids late p.	MFAP4	p.Pro33Leu	missense_variant	0.181	0	116	74	.	.	.	.	.	TRUE	17	19290135	A	0.74	Subclonal
Patient 2, Organoids late p.	RARA	p.Asp449Asp	synonymous_variant	0.25	0	32	40	TRUE	.	.	.	.	TRUE	17	38512388	T	1	Clonal
Patient 2, Organoids late p.	KRTAP4-11	p.Arg51Lys	missense_variant	0.063	0	80	31	.	.	.	.	.	TRUE	17	39274416	T	0.32	Subclonal
Patient 2, Organoids late p.	HOXB5	p.Arg224Leu	missense_variant	0.173	0	81	74	.	.	.	.	.	TRUE	17	46669710	A	0.88	Clonal
Patient 2, Organoids late p.	AKAP1	p.Leu832Val	missense_variant	0.255	0	51	32	.	.	.	.	.	TRUE	17	55194282	G	1	Clonal
Patient 2, Organoids late p.	USH1G	p.Thr100Lys	missense_variant	0.147	0	231	165	.	.	.	.	.	TRUE	17	72916632	T	0.75	Subclonal
Patient 2, Organoids late p.	DDC8	p.Gln416*	stop_gained	0.123	0	138	100	.	.	.	.	.	TRUE	17	76887340	A	0.63	Subclonal
Patient 2, Organoids late p.	FASN	p.Leu1826fs	frameshift_variant	0.19898	0	196	142	.	.	.	.	.	TRUE	17	80041170	G	1	Clonal
Patient 2, Organoids late p.	GALNT1	p.Arg426Cys	missense_variant	0.6	0	15	12	.	.	.	.	.	FALSE	18	33272261	T	1	Clonal
Patient 2, Organoids late p.	FHOD3	p.Leu261Leu	synonymous_variant	0.61	0	82	61	.	.	.	.	.	FALSE	18	34182699	T	1	Clonal
Patient 2, Organoids late p.	FHOD3	p.Arg1568His	missense_variant	0.601	0	143	94	.	.	.	.	.	FALSE	18	34349306	A	1	Clonal
Patient 2, Organoids late p.	SMAD7	p.Pro215Leu	missense_variant	0.536	0	28	49	.	.	.	.	.	FALSE	18	46474777	A	1	Clonal
Patient 2, Organoids late p.	DOT1L	p.Ile1251Ile	synonymous_variant	1	0.007519	95	134	.	.	.	.	.	TRUE	19	2226273	T	1	Clonal
Patient 2, Organoids late p.	ZNF414	p.Leu257Phe	missense_variant	0.4	0	25	32	.	.	.	.	.	TRUE	19	8576604	G	1	Clonal
Patient 2, Organoids late p.	ADAMTS10	p.Val904Val	synonymous_variant	0.667	0.011	69	94	.	.	.	.	.	TRUE	19	8650493	T	1	Clonal
Patient 2, Organoids late p.	MUC16	p.Leu12735Pro	missense_variant&splice_region_variant	0.38	0	50	48	.	.	.	.	.	TRUE	19	9015384	G	1	Clonal
Patient 2, Organoids late p.	ZNF561	p.Arg441Pro	missense_variant	0.985	0	133	110	.	.	.	.	.	TRUE	19	9721015	G	1	Clonal
Patient 2, Organoids late p.	RAVER1	p.Ala477Ala	synonymous_variant	1	0	9	16	.	.	.	.	.	TRUE	19	10431817	A	1	Clonal
Patient 2, Organoids late p.	CAPN12	p.His686Arg	missense_variant	1	0	25	33	.	.	.	.	.	TRUE	19	39221764	C	1	Clonal
Patient 2, Organoids late p.	MARK4	p.Gly258Gly	synonymous_variant	0.064	0	48	75	.	.	.	.	.	TRUE	19	45774954	A	0.19	Subclonal
Patient 2, Organoids late p.	ERCC1	p.Gly133Gly	synonymous_variant	1	0	118	147	.	.	.	.	.	TRUE	19	45923608	A	1	Clonal
Patient 2, Organoids late p.	RTN2	p.Ser211Ser	synonymous_variant	0.373	0	118	153	.	.	.	.	.	TRUE	19	45997605	C	1	Clonal
Patient 2, Organoids late p.	GPR4	p.Pro359Pro	synonymous_variant	0.38	0	92	106	.	.	.	.	.	TRUE	19	46094048	T	1	Clonal
Patient 2, Organoids late p.	PLCB4	p.Val869Phe	missense_variant	0.75	0	76	30	.	.	.	.	.	FALSE	20	9319571	T	1	Clonal
Patient 2, Organoids late p.	MYH7B	p.Ser797*	stop_gained	0.417	0	103	90	.	.	.	.	.	FALSE	20	33580985	A	1	Clonal
Patient 2, Organoids late p.	SMTN	p.Gln325Lys	missense_variant	0.164	0	128	183	.	.	.	.	.	FALSE	22	31486982	A	0.51	Subclonal
Patient 2, Organoids late p.	SCML2	p.Thr408Ser	missense_variant	0.058	0	69	12	.	.	.	.	.	TRUE	X	18276215	A		Did not evaluate
Patient 2, Organoids late p.	PPP1R3F	p.Asn345Asn	synonymous_variant	1	0	29	23	.	.	.	.	.	TRUE	X	49137899	T		Did not evaluate
Patient 2, Organoids late p.	HEPH	p.Ala382Ser	missense_variant	0.087	0	104	30	.	.	.	.	.	TRUE	X	65409699	T		Did not evaluate
Patient 2, Organoids late p.	FGF13	p.Glu54Lys	missense_variant	1	0	29	15	.	.	.	.	.	TRUE	X	137939731	T		Did not evaluate

Table S4. Lists of Somatic Single Nucleotide Variants, Insertions and Deletions Identified by Whole Exome Sequencing in the Samples Included in the Study. Note: only data for patient 2 is shown here. The whole data list accessible at the journal's webpage[142].

Table S5

Upregulated

p-value	term ID	t name
4.4900E-09	GO:0048285	organelle fission
4.5000E-08	GO:0000280	nuclear division
5.5700E-07	GO:0007049	cell cycle
2.5600E-06	GO:0022402	cell cycle process
4.2100E-04	GO:0000278	mitotic cell cycle
4.8600E-02	GO:1903047	mitotic cell cycle process
3.7800E-08	GO:0051321	meiotic cell cycle
1.0700E-09	GO:1903046	meiotic cell cycle process
2.7300E-09	GO:0140013	meiotic nuclear division
1.1400E-06	GO:0007127	meiosis I
1.4800E-02	GO:0007140	male meiotic nuclear division
5.6000E-05	GO:0070192	chromosome organization involved in meiotic cell cycle
3.4900E-03	GO:0007059	chromosome segregation
1.7800E-03	GO:0098813	nuclear chromosome segregation
8.9800E-04	GO:0045132	meiotic chromosome segregation
2.0100E-02	GO:0045143	homologous chromosome segregation
3.7100E-02	GO:0007129	synapsis
5.4900E-04	GO:0006259	DNA metabolic process
2.8900E-03	GO:0006310	DNA recombination
4.2700E-02	GO:0035825	homologous recombination
4.2700E-02	GO:0007131	reciprocal meiotic recombination
2.3200E-02	GO:0000725	recombinational repair
2.8000E-02	GO:0006260	DNA replication
3.2500E-03	GO:0006261	DNA-dependent DNA replication
6.8300E-03	GO:0006302	double-strand break repair
2.1200E-02	GO:0000724	double-strand break repair via homologous recombination
4.9000E-02	GO:0033260	nuclear DNA replication
4.0200E-02	GO:1902969	mitotic DNA replication
3.8600E-02	GO:0007292	female gamete generation
9.6700E-03	GO:0000793	condensed chromosome
1.9800E-02	GO:0097159	organic cyclic compound binding
3.7700E-02	GO:0016887	ATPase activity
1.1900E-02	GO:0003677	DNA binding
1.5200E-02	GO:1901363	heterocyclic compound binding
4.3500E-02	KEGG:03440	Homologous recombination
3.2900E-05	REAC:176187	Activation of ATR in response to replication stress
3.4700E-03	REAC:68962	Activation of the pre-replicative complex
2.0900E-02	REAC:69306	DNA Replication
2.5100E-03	REAC:1640170	Cell Cycle
3.1400E-02	REAC:69278	Cell Cycle, Mitotic
6.1000E-03	REAC:69620	Cell Cycle Checkpoints

Downregulated

p-value	term ID	t name
4.7700E-02	GO:0070563	negative regulation of vitamin D receptor signaling pathway
2.1700E-02	KEGG:03320	PPAR signaling pathway

Table S5. Pathway Analysis on HCC Biopsies Used for Organoid Generation.